SIXTH FRAMEWORK PROGRAMME

Project contract no. 043363

ManMade

Diagnosing vulnerability, emergent phenomena and volatility in man-made networks

SPECIFIC TARGETED PROJECT

NEST PATHFINDER

Sub-Priority Tackling Complexity in Science

Work Package 5 – D5.5

Analysis of the divergence operator for the assessment of the stability of a microgrid weakly connected to the power system or islanded

Due date of delivery: Month 36
Actual submission date: 22nd December 2009

Start date of project: 1st of January 2007 Duration: 36 months

Lead authors for this deliverable: [D. Falabretti , M. Merlo, M. Delfanti (Milan Polytechnic), J.M. Zaldívar, (JRC), F. Strozzi (LIUC)]

	Project co-funded by the European Commission within the Sixth Framework Programme (2002-2006)	
	Dissemination Level	
PU	Public	X
PP	Restricted to other programme participants (including the Commission Services)	
RE	Restricted to a group specified by the consortium (including the Commission Services)	
CO	Confidential, only for members of the consortium (including the Commission Services)	

Executive Summary

In this report we have developed a realistic but still tractable model of an electrical system made up of a medium voltage microgrid connected to the high voltage network. The model has been implemented and different scenarios have been evaluated. Furthermore, this model has allowed us to calculate analytically the divergence of the system and to compare with the one obtained using the time series through state space reconstruction.

Due to recent developments during the project, instead of using the divergence as an early warning system for detecting malfunctioning in an electrical system, we have studied the application of the divergence for the control of electrical systems. The results and the comparison with a local regulation have shown that the use of this approach ensures better performances to the overall system. Whereas traditional local controllers are able to stabilize locally the sub-system they are controlling, without taking into account what happens to the rest of the grid, the divergence is able to act at a global level and, hence, it is able to avoid actions that could affect the entire system.

Finally, the reconstruction of the divergence using non-linear time series analysis has been performed. The results obtained open the door for the application of this type of control to real electrical systems by measuring the time evolution of selected state variables.

CONTENTS

1. INTRODUCTION 4
2. GENERATORS MODELIZATION 6
3. LOAD MODELIZATION 8
4. HV NETWORK AND SUBSTATION'S TRANSFORMER MODELIZATION 9
5. MV NETWORK MODELIZATION 10
6. PRELIMINARY OPERATIONS 12
7. SOLVING PROCESS 13
8. SIMULATIONS IN ABSENCE OF THE REGULATOR 18
9. DIVERGENCE 38
10. SIMULATIONS USING AN ENERGY STORAGE DEVICE DRIVEN BY THE DIVERGENCE 42
11. SIMULATIONS WITH A STORAGE DEVICE DRIVEN BY LOCAL QUANTITIES 50
12. PHASE SPACE DIVERGENCE RECONSTRUCTION 57
13. CONCLUSIONS 61
14. APPENDIX A 63
15. BIBLIOGRAPHY 74

1. INTRODUCTION

This study aims at assessing the stability of a medium voltage (MV) power grid in which one or more dispersed generators are connected (Figure 1). The network under consideration is of radial type and is connected to the high voltage (HV) system through the interposition of an HV/MV transformer, placed in the HV substation to which the MV network refers.

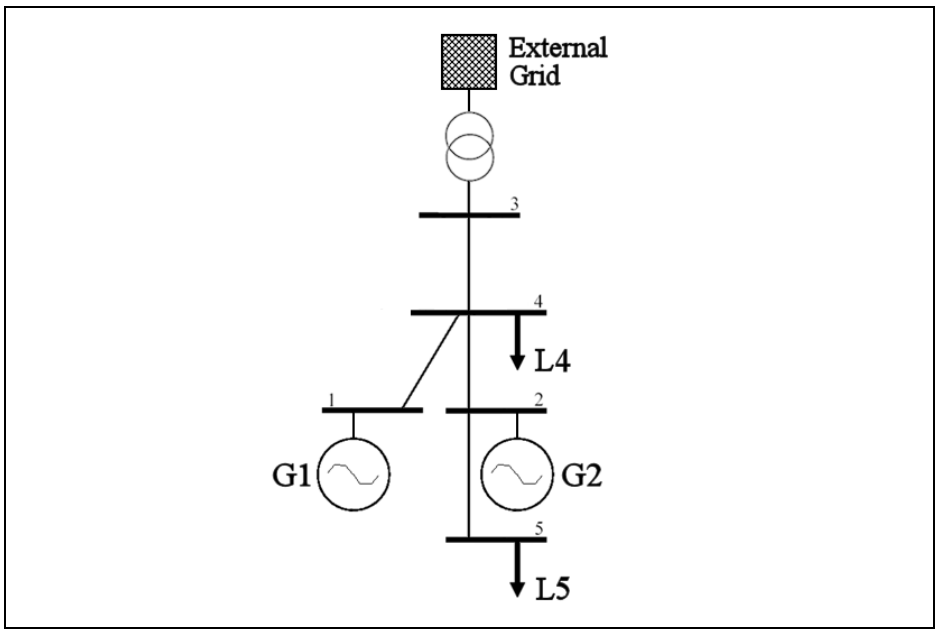

Figure 1
The MV network studied.

The presented situation is a case where the appearance of stability problems for the electric system is most likely. The fact that the network is at medium voltage, and is only weakly related to the transmission system, does not guarantee that its busses have enough short-circuit power to cope with high disturbances on generators. Since dispersed generators considered are wind turbines, changes in torque applied to their blades can be frequent, as dictated by the stochastic behavior of wind. The definition of a control device capable of increasing the dynamic performance of this system would therefore be of interest.

It is assumed to have two wind generators (G1 and G2) connected to the network through two ideal voltage transformers $^{20}\!/_{1.8}\,kV$. These generators are composed of a wind turbine and a Synchronous Machine (SM), which realizes the conversion of the mechanical energy supplied by the wind at the turbine blades into electric energy.

It is assumed that there are two loads (L4 and L5) which absorb a constant amount of power, also when the voltage at their supply terminals varies.

The lines forming the MV electric grid are then modeled through their longitudinal parameters, in terms of resistance and reactance, whilst the shunt parameters are neglected.

The modeling process of each electric component under analysis is described in detail in the following, along with the complete dynamic system. Based on this model, several simulations are

then carried out to evaluate the performance of the electrical and mechanical properties of interest, in the presence of disturbances acting on the mechanical torque supplied to the generators' shaft.

Then, the evaluation of the divergence is used, as an indicator of the stability of the power system, to drive a regulator to improve the dynamic behavior of the SMs. Also for this case, several simulations are given, in order to highlight the possible advantages introduced by the use of this approach.

Finally, a comparison between the action of the regulator just mentioned and a regulator controlled only by local quantities is presented.

2. GENERATORS MODELIZATION

Two wind generators are used in the realization of the model, in order to represent a generic renewable energy source, with a rated power equal to *3 MW* . It is assumed that they are coupled directly to the network without the interposition of either inverter or gearbox, and that SMs are equipped with permanent magnets.

The use of relatively high power electric machines (in the wind generators context) makes it necessary to highlight the effects that they induce on the overall power system. The assumption of small size generators, due to the prevalent electric power of the medium voltage network would, in fact, reduce the analysis to the study of one or more generators connected to a network with infinite short circuit power (ideal network). In the latter case the electric network would be negligibly affected by the behavior of generators and thus the analysis would lose significance.

The design of the machines, directly coupling to the network and permanent magnets, although typical of smaller generators, has been adopted for simplicity, and also to highlight the issues related to dynamic stability of the system following a disturbance.

The SMs are assumed equipped with damper windings, modeled by algebraic equations (again for simplicity, we preferred to avoid the introduction of two additional dynamic equations for each machine). In fact, in wind generators of the size considered, these windings are typically present; furthermore, in case of disturbance, their presence is necessary to allow the damping of mechanical oscillations that could trigger (in reality the friction helps to lessen them).

For both generators we assumed the following electrical and mechanical parameters:

- Rated voltage: $V_n = 1.8\ kV$
- Rated real power: $P_n = 3\ MW$
- Stator resistance: $R_S = 22\ m\Omega$
- Direct-axis inductance: $L_d = 2.28\ mH$
- Quadrature-axis inductance: $L_q = 2.28\ mH$
- Number of polar pairs: $n = 56$
- Moment of inertia: $I = 10^6\ kg \cdot m^2$
- Flux of permanent magnets: $\psi_{MP} = 8.44\ Wb$
- Damping coefficient: $k_{sm} = 5347.6061\ N \cdot m \cdot s$

As mentioned above, the coupling transformers to the MV network are assumed ideal (infinite shunt parameters and longitudinal parameters equal to zero) and with a transformation ratio $^{20}\!/_{1.8}\,kV$.

The adoption of permanent magnet generators (constant excitation flow) and the absence of dynamic equations of the damper windings, lead to a dynamic model of the 4th order for each of the machines (Krause, Wasynczuk, & Sudhoff, 2002).

To simplify the modeling of the electric machines, the Park transformation is applied to both the electrical and the constructive parameters (Marconato, 2002); hence the expressions "direct-axis" and "quadrature-axis" previously used.

$$\begin{cases} \dfrac{di_d^r}{dt} = \dfrac{1}{L_d}\left(v_d^r - R_s i_d^r + \omega_m L_q i_q^r\right) \\ \dfrac{di_q^r}{dt} = \dfrac{1}{L_q}\left(v_q^r - R_s i_q^r + \omega_m L_d i_d^r - \psi_{MP}\omega_m\right) \\ \dfrac{d\delta}{dt} = \omega - \omega_m \\ \dfrac{d\omega_m}{dt} = \dfrac{n}{J}\left(i_q^r \psi_{MP} - C_m - k_{sm}(\omega_m - \omega_0)\right) \end{cases} \quad (1)$$

In the above equations:

- i_d^r is the direct-axis current on rotor axes *[A]*;
- i_q^r is the quadrature-axis current on rotor axes *[A];*
- v_d^r is the direct-axis voltage on rotor axes *[V];*
- v_q^r is the quadrature-axis voltage on rotor axes *[V];*
- Ψ_{MP} is the flux of permanent magnets *[Wb];*
- ω_m is the rotational speed of the rotor *[*rad s^{-1}*];*
- ω is the actual pulsation of the network *[*rad s^{-1}*];*
- ω_0 is the nominal pulsation of the network, equal to $2 \cdot \pi \cdot 50$ rad s^{-1} *;*
- C_m is the mechanical torque applied to machine's shaft (negative if the machine is operating as generator) *[N·m];*
- δ is the load angle of the generator *[rad].*

The ordinary differential equations (ode) from Eq. (1) are integrated by calculating the derivatives and using the numerical algorithms (solvers) from MATLAB to calculate their magnitudes at the next time step:

$$\begin{cases} i_d^r(t+\Delta t) = \left.\dfrac{di_d^r}{dt}\right|_t \cdot \Delta t + i_d^r(t) \\ i_q^r(t+\Delta t) = \left.\dfrac{di_q^r}{dt}\right|_t \cdot \Delta t + i_q^r(t) \\ \delta(t+\Delta t) = \left.\dfrac{d\delta}{dt}\right|_t \cdot \Delta t + \delta(t) \\ \omega_m(t+\Delta t) = \left.\dfrac{d\omega_m}{dt}\right|_t \cdot \Delta t + \omega_m(t) \end{cases} \quad (2)$$

3. LOAD MODELIZATION

The loads are characterized by the active and reactive powers absorbed at their terminals. They are assumed constant (Kundur, 1994) and equal to:

- $P_{L4} = P_{L5} = 4\ MW$
- $Q_{L4} = Q_{L5} = 2\ Mvar$

The values mentioned above are equivalent to an inductive $cos\varphi \cong 0.9$. Therefore, it is assumed that the loads absorb electricity with an optimal power factor, consistently with the practice of avoiding additional charges applied by the distributor when $cos\varphi$ is too low.

Through the active and reactive power that characterizes the load, and its voltage, it is possible to determine, by the following expression, the equivalent admittance (Figure 2):

$$\overline{Y_L} = \frac{P_L - jQ_L}{|\overline{V_L}|^2} \qquad (3)$$

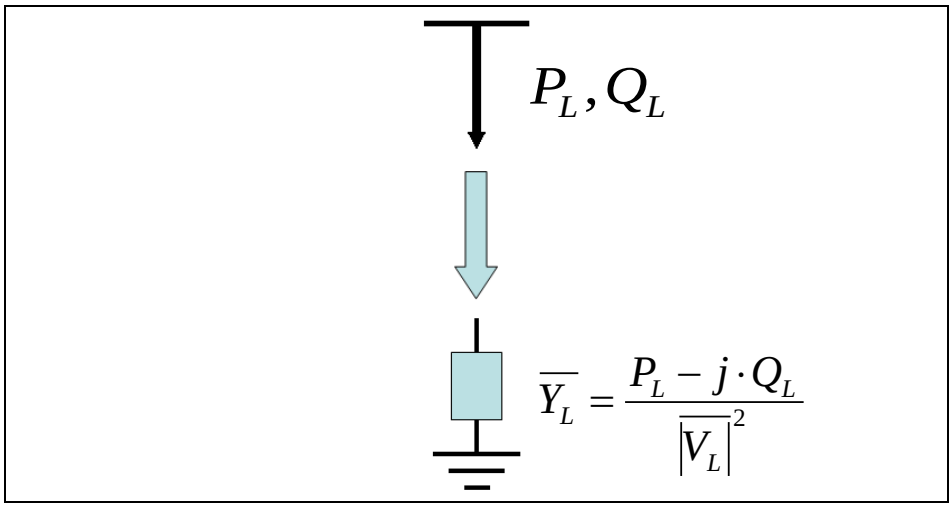

Figure 2
Modelization of the grid's loads.

The admittance found by the algebraic equation (3) is then used to perform the so-called load flow calculations, which allow evaluating the profile of the network voltage, once the potential on the HV side of the HV/MV transformer is given, along with the active and reactive injections/consumptions of power of generators/loads.

4. HV NETWORK AND SUBSTATION'S TRANSFORMER MODELIZATION

The medium voltage network in analysis is connected to a high voltage network (*130 kV*, Figure 3) by means of an HV/MV transformer, located into the substation, with the following characteristics:

- Rated voltage: $V_n = 130/20\ kV$
- Rated power: $A_n = 16\ MVA$
- Short-circuit voltage: $V_{cc} = 0.13\ p.u.$

It is assumed that the short-circuit power of the HV network is infinite; downstream the substation's transformer, it is limited by the longitudinal reactance of the transformer itself.

A short-circuit voltage of the transformer equal to *0.13 p.u.* is equivalent, according to the nominal voltage, to a reactance of *3.25 Ω* (on MV side).

In addition, it is assumed that, under the conditions of initial operation of the network, the on-load tap-changer (OLTC) will adjust the voltage on the MV side in order to keep it close to the rated value (*20 kV*). Since the dynamics of the OLTC are considerably slower than the duration of the phenomena investigated, we can consider the transformer's ratio constant (no regulation); therefore, as a result of disturbances, the voltage on MV bus may be subject to changes.

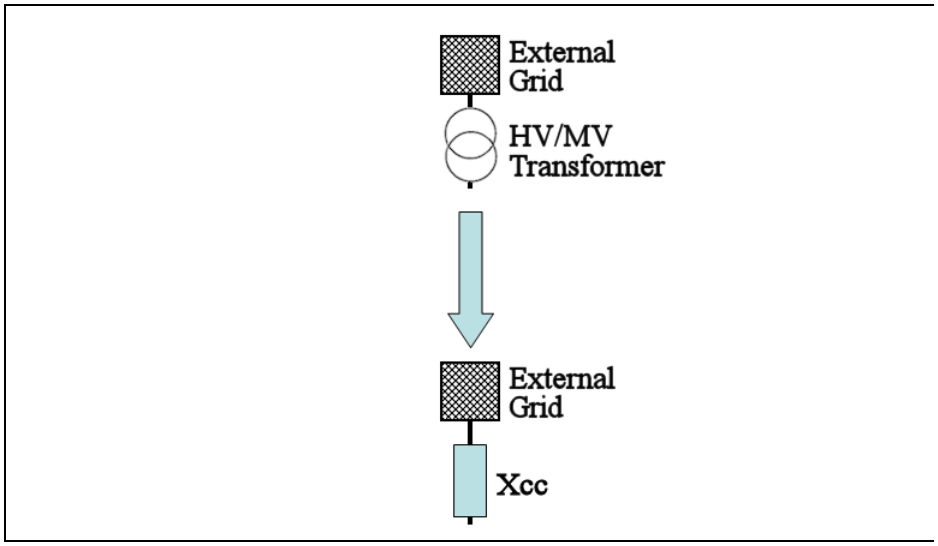

Figure 3
Modelization of the external grid and substation's MV/HV transformer.

5. MV NETWORK MODELIZATION

The medium voltage network is a *20 kV* radial network. It is characterized by its longitudinal impedances, whilst the shunt parameters are neglected.

The impedances of each line section are:

- $\overline{z_{14}} = 0.05 + j0.08$
- $\overline{z_{24}} = 0.09 + j0.07$
- $\overline{z_{25}} = 0.1 + j0.09$
- $\overline{z_{34}} = 0.03 + j0.05$

The impedances' notation refers to Figure 4:

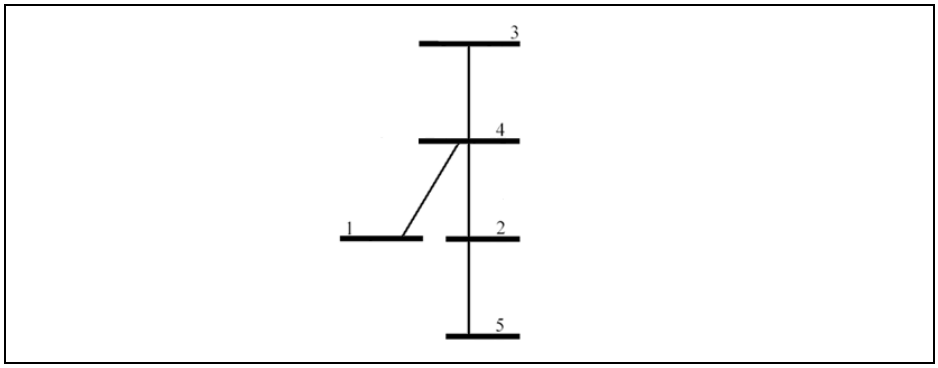

Figure 4
Topology of the MV network under examination.

The impedances are expressed in per unit and not in physical values for convenience, so as to apply the load flow equations reported in the literature. They are convertible to physical values using the expression:

$$\overline{Z_{fisica}} = \overline{Z_{pu}} \cdot \frac{V_{rif}^2}{A_{rif}} \qquad (4)$$

where:

- $\overline{Z_{fisica}}$ is the impedance in physical value [Ω];
- $\overline{Z_{pu}}$ is the impedance in per unit to convert in physical value [*p.u.*];
- V_{rif} is the reference voltage for the conversion (equal to *20 kV*);
- A_{rif} is the reference power for the conversion (equal to *3 MVA*).

The branch impedances are necessary to evaluate the so-called nodal admittance matrix which will be used in the load flow calculations, as explained below. Therefore, it is necessary to calculate the branch admittance in *p.u.* from each branch impedance:

- $\overline{y_{14}} = 5.6180 - j8.9888$
- $\overline{y_{24}} = 6.9231 - j5.3846$

- $\overline{y_{25}} = 5.5249 - j4.9724$
- $\overline{y_{34}} = 8.8235 - j14.7059$

As already discussed for the impedances, these admittances are convertible to physical values using the equation:

$$\overline{Y_{fisica}} = \overline{Y_{pu}} \cdot \frac{A_{rif}}{V_{rif}^2} \tag{5}$$

where:

- $\overline{Y_{fisica}}$ is the admittance in physical value $[S]$;
- $\overline{Y_{pu}}$ is admittance in per unit which to convert in physical value $[p.u.]$.

Through a direct inspection (for further information refer to specific literature about electric systems (Marconato, 2002)) it is possible to get the nodal admittance matrix from the analysis of network topology (Figure 4):

$$\overline{Y_N} = \begin{bmatrix} \overline{y_{14}} & 0 & 0 & -\overline{y_{14}} & 0 \\ 0 & \overline{y_{24}} + \overline{y_{25}} & 0 & -\overline{y_{24}} & -\overline{y_{25}} \\ 0 & 0 & \overline{y_{34}} & -\overline{y_{34}} & 0 \\ -\overline{y_{14}} & -\overline{y_{24}} & -\overline{y_{34}} & \overline{y_{14}} + \overline{y_{24}} + \overline{y_{34}} & 0 \\ 0 & -\overline{y_{25}} & 0 & 0 & \overline{y_{25}} \end{bmatrix} \tag{6}$$

6. PRELIMINARY OPERATIONS

The 5 busses network in analysis (Figure 1) is first converted into a 6 busses network, by explicitly representing the HV bars of the substation transformer (Figure 5). This procedure allows to assign to the HV bars the role of slack in the load flow calculations, and permits to the MV bars to vary their voltage amplitude and phase as a function of the transit on the HV/MV transformer.

In the traditional way to allocate the known and unknown electrical quantities of load flow, the load (4 and 5) and transit (3) busses of the network are of *(P,Q)* type, i.e. the value of active and reactive power injected in them are fixed. The connection busses of the generators are classified as busses of *(P,V)* type, in which the active power supplied by the generator and the voltage module are known. Finally, in the slack bus (the HV bars of substation's transformer) the voltage is supposed set in module and phase.

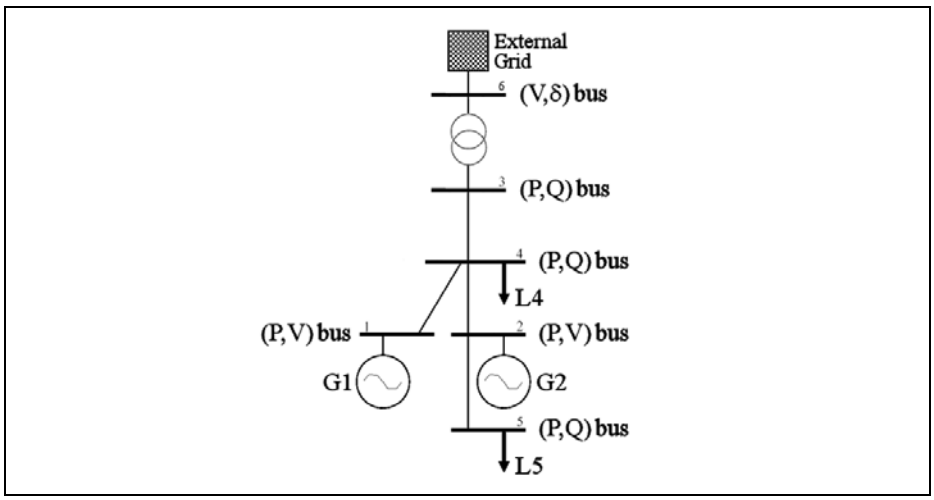

Figure 5
Network model: the bus of the substation's HV bars and the various types of busses are highlighted.

7. SOLVING PROCESS

The problem analyzed is the coupling between a set of differential equations characterizing dynamically the SMs and their interaction with the MV network, and a set of algebraic equations, consisting in the load flow equations (Stagg & El-Abiad, 1983).

At each iteration of the solution process, the network's voltage profile at a given instant is used to calculate, through the system of differential equations, the active and reactive power provided by each machine immediately after. These are transformed into equivalent admittances, through a process similar to the one depicted for loads, and integrated into a new nodal admittance matrix, which is then used in the load flow calculation to determine the new voltage profile of the network.

To convert from network quantities (in *p.u.*) to machine quantities (in physical values), it is also necessary to apply the Park transformation. On the other hand, it is not necessity to use the inverse Park transformation: in fact, the active and reactive power generated by the machines (that are the only output of interest of the dynamic system) are not affected by this transformation, due to the property of orthogonality. Eventually, the active and reactive power mentioned above can be introduced, after proper conversion in *p.u.*, in the load flow process.

To take into consideration the dynamic aspects of network's quantities, it is appropriate also to evaluate the actual pulsation of network itself, deriving it from the phase changes of voltages, rather than taking it constant and equal to $2 \cdot \pi \cdot 50$ *rad/s*.

The solution process is divided into the following phases (Figure 6):

1) The voltages at the terminals of the machines, in *p.u.*, calculated using the load flow at the instant t, are converted into physical values, and subsequently transformed with Park:

$$\begin{cases} \overline{V_1} = \dot{\overline{V}}_1 \cdot V_{rifMT} \\ \overline{V_2} = \dot{\overline{V}}_2 \cdot V_{rifMT} \end{cases} \tag{7}$$

   where:

   - $\overline{V_1}$ and $\overline{V_2}$ are the voltages at the terminals of the generators [*V*];
   - $\dot{\overline{V}}_1$ and $\dot{\overline{V}}_2$ are the voltages at the terminals of the generators [*p.u.*];
   - V_{rifMT} is the MV reference voltage, equal to *20 kV*.

$$\begin{cases} v_{d1}^r = |\overline{V_1}| sin\delta_1 \\ v_{q1}^r = |\overline{V_1}| cos\delta_1 \\ v_{d2}^r = |\overline{V_2}| sin\delta_2 \\ v_{q2}^r = |\overline{V_2}| cos\delta_2 \end{cases} \tag{8}$$

where:

- v_{d1}^r and v_{d2}^r are the direct-axis voltages at the terminals of the generators [*V*];
- v_{q1}^r and v_{q2}^r are the quadrature-axis voltages at the terminals of the generators [*V*];
- δ_1 and δ_2 are the load angles of the generators [*rad*];

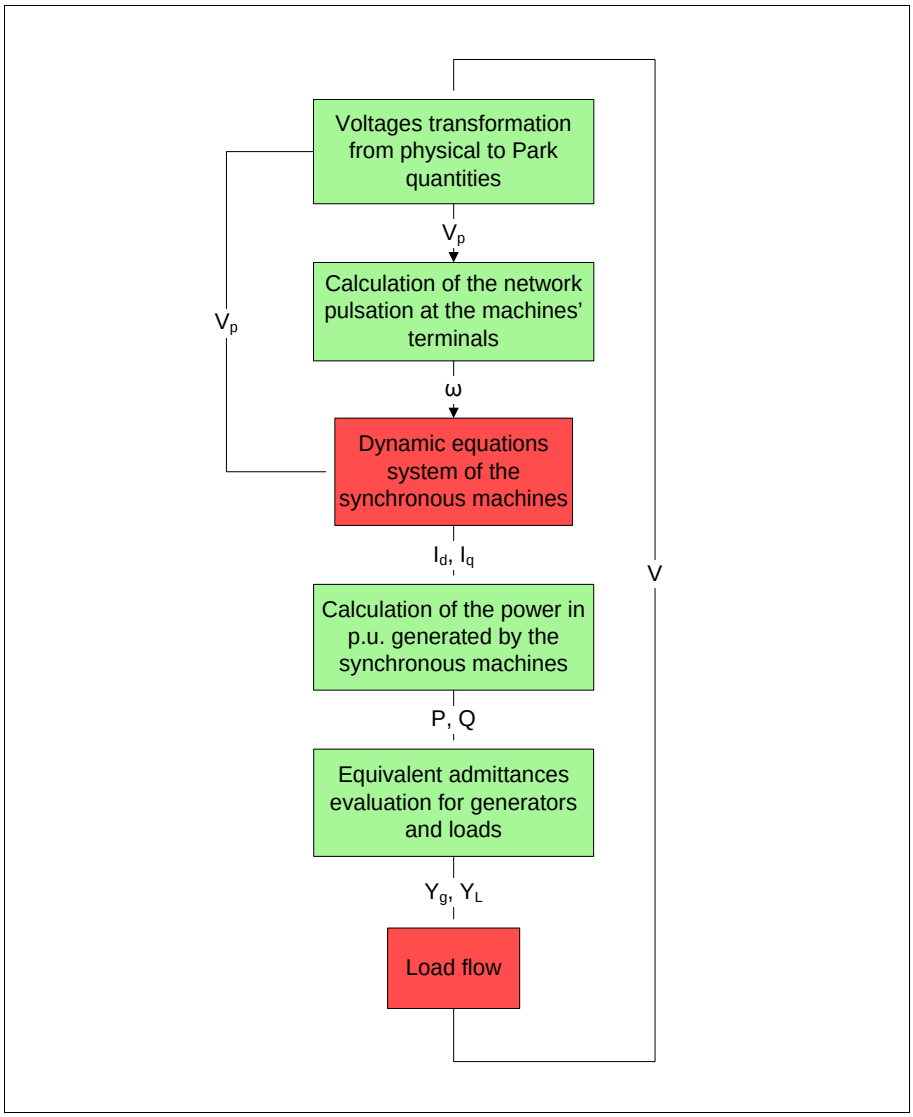

Figure 6
Solution process of the problem under analysis.

2) The variations of the voltage phase at the generators' terminals are then used to determine the variation of pulsation, and thus of frequency, of the voltage vectors themselves (the constants of the problem are highlighted in red):

$$\omega_1 = \frac{d\varphi_1}{dt} + \omega_0$$
$$\omega_2 = \frac{d\varphi_2}{dt} + \omega_0 \qquad (9)$$

where:

- ω_1 and ω_2 are the actual voltage pulsations at the generators' terminals [*rad/s*];

- φ_1 and φ_2 are the voltage phases at the terminals of the generators [*rad*];
- ω_0 is the rated pulsation of the grid, equal to $2 \cdot \pi \cdot 50$ *rad/s*.

3) The variables i_{d1}^r, i_{d2}^r, i_{q1}^r, i_{q2}^r, δ_1, δ_2, ω_{m1}, ω_{m1} are updated by the system of differential equations of the two generators (the variables of the problem are highlighted in red and the inputs in green):

$$\begin{cases} \frac{di_{d1}^r}{dt} = \frac{1}{L_{d1}}\left(v_{d1}^r - R_{s1} i_{d1}^r + \omega_{m1} L_{q1} i_{q1}^r\right) \\ \frac{di_{q1}^r}{dt} = \frac{1}{L_{q1}}\left(v_{q1}^r - R_{s1} i_{q1}^r + \omega_{m1} L_{d1} i_{d1}^r - \psi_{MP1}\omega_{m1}\right) \\ \frac{d\delta_1}{dt} = \omega_1 - \omega_{m1} \\ \frac{d\omega_{m1}}{dt} = \frac{n_1}{J_1}\left(i_{q1}^r \psi_{MP1} - C_{m1} - k_{sm}(\omega_{m1} - \omega_0)\right) \\ \frac{di_{d2}^r}{dt} = \frac{1}{L_{d2}}\left(v_{d2}^r - R_{s2} i_{d2}^r + \omega_{m2} L_{q2} i_{q2}^r\right) \\ \frac{di_{q2}^r}{dt} = \frac{1}{L_{q2}}\left(v_{q2}^r - R_{s2} i_{q2}^r + \omega_{m2} L_{d2} i_{d2}^r - \psi_{MP2}\omega_{m2}\right) \\ \frac{d\delta_2}{dt} = \omega_2 - \omega_{m2} \\ \frac{d\omega_{m2}}{dt} = \frac{n_2}{J_2}\left(i_{q2}^r \psi_{MP2} - C_{m2} - k_{sm}(\omega_{m2} - \omega_0)\right) \end{cases} \quad (10)$$

The same symbolism as in Eq. (1) has been used.

The motive torques C_m, imposed to the shafts of the machines, are the variables of interest . In particular, several time domain characteristics will be applied to achieve the various simulations. As the generators are wind turbines, these torques may vary over time depending on the force applied by the wind to the blades.

4) The direct and quadrature-axis currents are used, with the voltages previously calculated, to assess the active and reactive power provided by the machines:

$$\begin{aligned} \dot{P_{g1}} &= -\frac{\left(v_{d1}^r i_{d1}^r + v_{q1}^r i_{q1}^r\right)}{A_{rif}} \\ \dot{P_{g2}} &= -\frac{\left(v_{d2}^r i_{d2}^r + v_{q2}^r i_{q2}^r\right)}{A_{rif}} \\ \dot{Q_{g1}} &= -\frac{\left(v_{q1}^r i_{d1}^r - v_{d1}^r i_{q1}^r\right)}{A_{rif}} \\ \dot{Q_{g2}} &= -\frac{\left(v_{q2}^r i_{d2}^r - v_{d2}^r i_{q2}^r\right)}{A_{rif}} \end{aligned} \quad (11)$$

where:

- $\dot{P}_{g1}$ and $\dot{P}_{g2}$ are the active powers provided by the generators [*p.u.*];
- $\dot{Q}_{g1}$ and $\dot{Q}_{g2}$ are the reactive powers provided by the generators [*p.u.*];
- A_{rif} is the reference power, equal to *3 MW*.

5) Through the power values calculated by Eq. (11), it is now possible to obtain, with the same process used for the modelization of the loads, some "active" admittances equivalent to the generators. Unlike passive users of the network, the admittances obtained for active users (i.e. for generators) show typically a negative real part, since they enter active power in the network instead of absorbing it. As for the imaginary part of these admittances, its sign is dependent on the operating point of the generator (i.e., under or over-excitation). In the first case the machine acts as inductor, absorbing inductive reactive power, and hence the admittance has a negative imaginary part (similarly to loads); in the second case it acts as a capacitor, generating inductive reactive power, with a positive imaginary part. Although by a transformation of this kind the physical meaning vanishes (negative resistive multi-poles do not exist), it is formally correct and can easily match the set of equations related to the machines to that of load flow. The equivalent admittances of generators and loads obtained are:

$$\overline{y_{G1}} = -\frac{\dot{P}^{*}_{g1} - j\dot{Q}^{*}_{g1}}{|\dot{V}_1|^2}$$

$$\overline{y_{G2}} = -\frac{\dot{P}^{*}_{g2} - j\dot{Q}^{*}_{g2}}{|\dot{V}_2|^2}$$

$$\overline{y_{L4}} = \frac{\dot{P}^{*}_{L4} - j\dot{Q}^{*}_{L4}}{|\dot{V}_4|^2}$$

$$\overline{y_{L5}} = \frac{\dot{P}^{*}_{L5} - j\dot{Q}^{*}_{L5}}{|\dot{V}_5|^2} \qquad (12)$$

where:

- $\overline{y_{G1}}$ and $\overline{y_{G2}}$ are the equivalent admittances of generators [*p.u.*];
- $\overline{y_{L1}}$ and $\overline{y_{L2}}$ are the equivalent admittances of loads [*p.u.*];
- $\dot{V}_1$, $\dot{V}_2$, $\dot{V}_4$ and $\dot{V}_5$ are the voltages, in amplitude and phase, of the network's busses in which the generators or the loads in analysis are connected [*p.u.*].

6) The admittances obtained from the previous step are then used, using the inspection method again, to calculate the new nodal admittance matrix. A further equation, concerning the branch of the network between substation's MV and HV busses, is then added to the set of load flow equations:

$$\dot{\overline{E_{sl}}} = \dot{\overline{V_3}} + jx_t\dot{\overline{I_t}} \tag{13}$$

where:

- $\dot{\overline{E_{sl}}}$ is the voltage of the slack bus, constant and equal to *1 p.u.*;
- $\dot{\overline{V_3}}$ is the voltage of the bus 3 (MV bus of substation) [*p.u.*];
- x_t is the short-circuit impedance of the substation's transformer, equal to 0.*13 p.u.*;
- $\dot{\overline{I_t}}$ is the current flowing through the HV/MV transformer [*p.u.*].

Then the overall resulting system is:

$$\begin{bmatrix} 0 \\ 0 \\ 0 \\ 0 \\ 0 \\ \dot{\overline{E_{sl}}} \end{bmatrix} = \begin{bmatrix} \overline{y_{14}} + \overline{y_{G1}} & 0 & 0 & -\overline{y_{14}} & 0 & 0 \\ 0 & \overline{y_{24}} + \overline{y_{25}} + \overline{y_{G2}} & 0 & -\overline{y_{24}} & -\overline{y_{25}} & 0 \\ 0 & 0 & \overline{y_{34}} & -\overline{y_{34}} & 0 & -1 \\ -\overline{y_{14}} & -\overline{y_{24}} & -\overline{y_{34}} & \overline{y_{14}} + \overline{y_{24}} + \overline{y_{34}} + \overline{y_{L4}} & 0 & 0 \\ 0 & -\overline{y_{25}} & 0 & 0 & \overline{y_{25}} + \overline{y_{L5}} & 0 \\ 0 & 0 & 1 & 0 & 0 & jx_t \end{bmatrix} \begin{bmatrix} \dot{\overline{V_1}} \\ \dot{\overline{V_2}} \\ \dot{\overline{V_3}} \\ \dot{\overline{V_4}} \\ \dot{\overline{V_5}} \\ \dot{\overline{I_t}} \end{bmatrix} \tag{14}$$

This matrix, once inverted, allows the evaluation of the voltage profile of the network (load flow) and the identification of the current delivered to the HV bars:

$$\begin{bmatrix} \dot{\overline{V_1}} \\ \dot{\overline{V_2}} \\ \dot{\overline{V_3}} \\ \dot{\overline{V_4}} \\ \dot{\overline{V_5}} \\ \dot{\overline{I_t}} \end{bmatrix} = \begin{bmatrix} \overline{y_{14}} + \overline{y_{G1}} & 0 & 0 & -\overline{y_{14}} & 0 & 0 \\ 0 & \overline{y_{24}} + \overline{y_{25}} + \overline{y_{G2}} & 0 & -\overline{y_{24}} & -\overline{y_{25}} & 0 \\ 0 & 0 & \overline{y_{34}} & -\overline{y_{34}} & 0 & -1 \\ -\overline{y_{14}} & -\overline{y_{24}} & -\overline{y_{34}} & \overline{y_{14}} + \overline{y_{24}} + \overline{y_{34}} + \overline{y_{L4}} & 0 & 0 \\ 0 & -\overline{y_{25}} & 0 & 0 & \overline{y_{25}} + \overline{y_{L5}} & 0 \\ 0 & 0 & 1 & 0 & 0 & jx_t \end{bmatrix}^{-1} \begin{bmatrix} 0 \\ 0 \\ 0 \\ 0 \\ 0 \\ \dot{\overline{E_{sl}}} \end{bmatrix} \tag{15}$$

After determining voltages, the process is repeated: voltages are in fact used to calculate the state variables at the next time step.

8. SIMULATIONS IN ABSENCE OF THE REGULATOR

A series of tests has been performed on the developed model by varying the torque applied to the shaft of one or both generators. In each of these tests, all the electrical and mechanical quantities have been evaluated and stored.

The simulations performed in this phase aim at highlighting only the dynamic behavior of the developed model, therefore no regulation is introduced. In the next chapters the "divergence" operator will then be defined and eventually it will be applied in a regulation scheme.

The most significant simulations for the study of the system's behavior are shown in the Table 1; the results of further tests are also shown in Appendix A.

Table 1 – Tests carried out in absence of the regulator.

	Torque SM 1	Torque SM 2
Test 1	Constant, equal to C_n.	In $t = 5\ s$ it goes (by one step) from C_n to the 105% of C_n.
Test 2	Sinusoidal characteristic with amplitude equal to the 5% of C_n and mean value C_n.	In $t = 5\ s$ it goes (by one step) from C_n to the 105% of C_n.
Test 3	Sinusoidal characteristic with amplitude equal to the 5% of C_n and mean value C_n.	Sinusoidal characteristic with amplitude equal to the 5% of C_n and mean value C_n. In anti-phase with the torque applied to the SM 1.

To implement the simulations the following criteria are been adopted:

- in the initial condition of each simulation the machines have already reached the steady-state, with constant torque equal to the rated value ($5.3476061 \cdot 10^5\ Nm$);
- to highlight the system's response to particular disturbances, in some simulations the composition of more torque characteristics, such as step and sinusoidal or more sinusoidal characteristics, has been applied;
- unless otherwise specified noise is absent (Appendix A contains some simulations carried out by superimposing white noise of different intensity to the torque applied to the generators);
- the torque variation applied to one of two machines, or both, is introduced at the time $t = 5\ s$;
- in the simulations the numerical integration has been carried out up to $50\ s$ (considering it a reasonable time to correctly represent the dynamic behavior of the analyzed system);
- in the graphs related to the magnitudes and phases of the network's voltages, each color refers to a specific bus:
  - Bus 1: red
  - Bus 2: green
  - Bus 3: blue
  - Bus 4: magenta
  - Bus 5: black

TEST 1 IN ABSENCE OF THE REGULATOR

In this first simulation the torque in input to the SM 1 is kept constant and equal to the nominal value (*-5.348·10^5 Nm*) (Figure 7). Besides, a step disturbance is applied to the torque of the SM 2, increasing its magnitude of 5% (Figure 8).

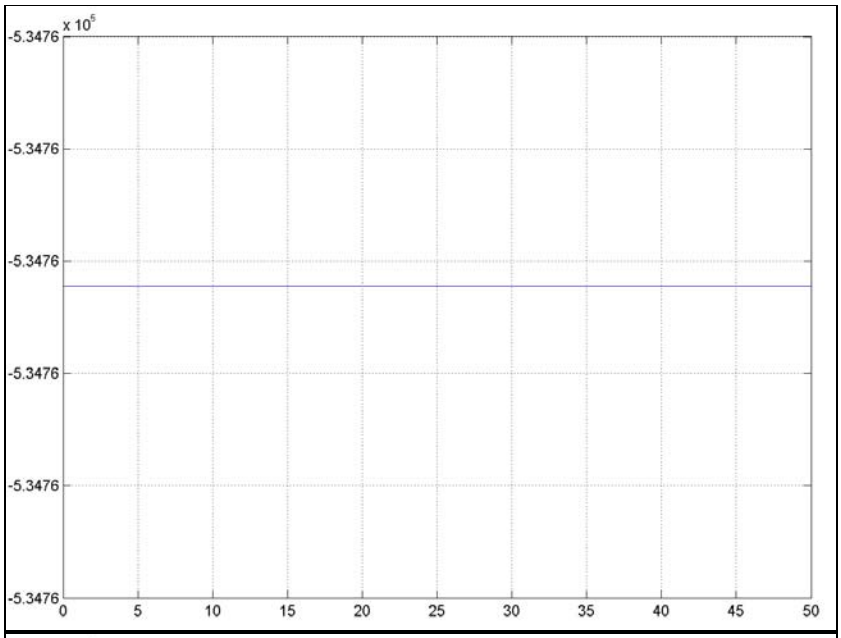

Figure 7
Torque applied to the SM 1 in the Test 1 in absence of the regulator [Nm].

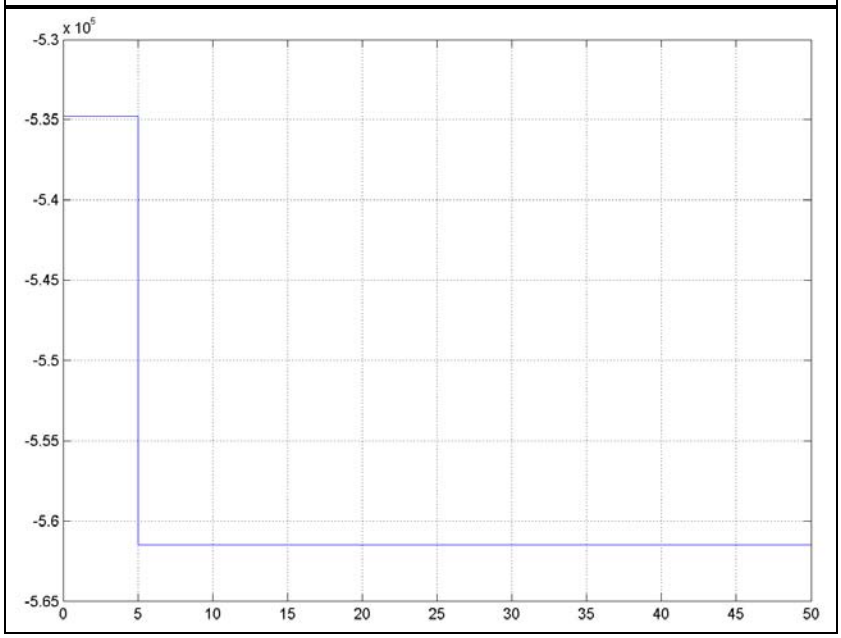

Figure 8
Torque applied to the SM 2 in the Test 1 in absence of the regulator [Nm].

From Figure 9 and Figure 10 it's possible to see how the rotational speed of the SM 2 suffers instantly the effects of the torque's change; also, how the SM 1 changes its rotational speed more slowly, and with less oscillations when compared to SM 2. The oscillations of the latter need more time to fade than in the first case. The delay in the dynamic behavior of the SM 1 is due to the fact that it does not react to the disturbance directly, but through the effects on the network's quantities of the SM 2. The wind generator introduces in fact a delay due to its internal dynamics.

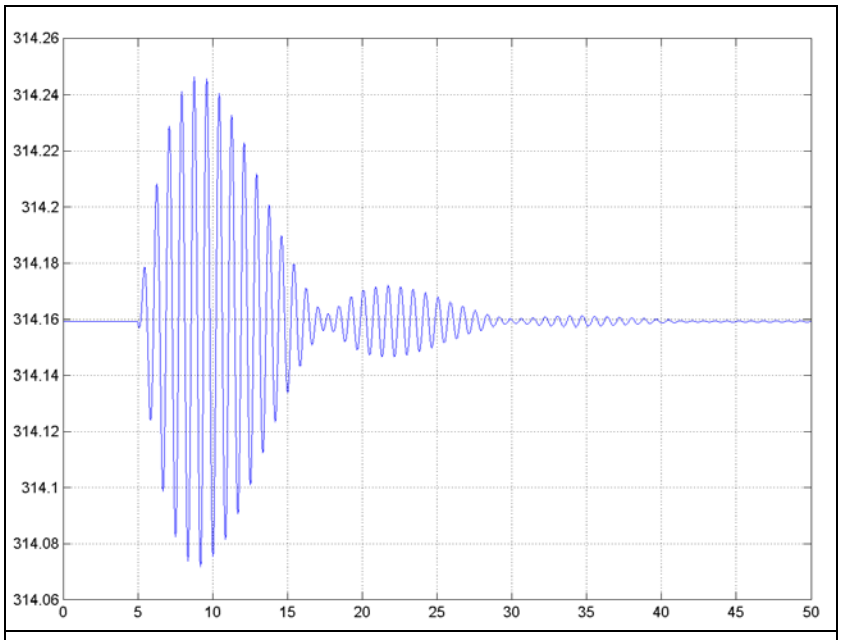

Figure 9
Rotational speed of the SM 1 in the Test 1 in absence of the regulator [rad s^{-1}].

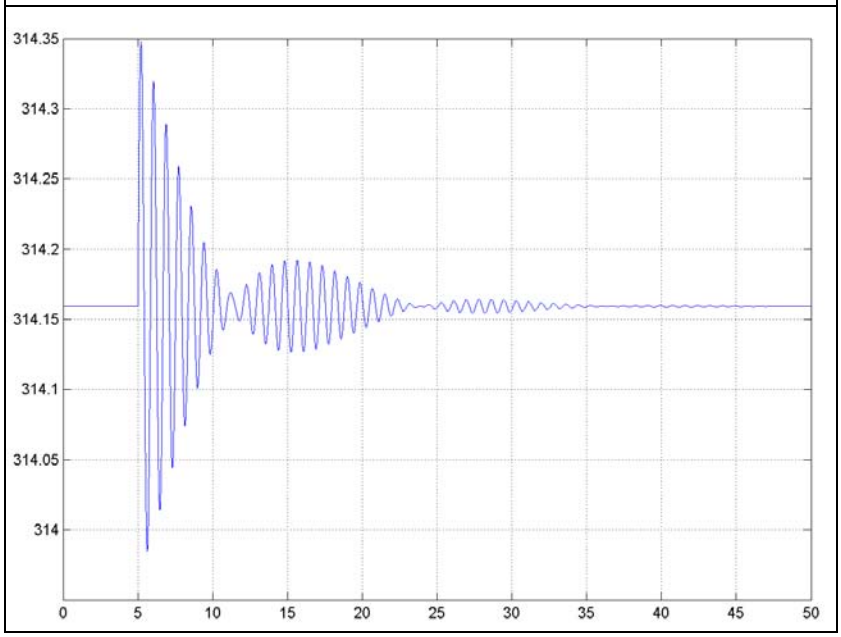

Figure 10
Rotational speed of the SM 2 in the Test 1 in absence of the regulator [rad s^{-1}].

After a series of oscillations very similar to those of its rotational speed, the electric torque generated by the SM 1 (Figure 11), returns to the initial value. In fact, in steady-state, each alternator must necessarily provide an electric torque equal to the mechanical torque applied to its shaft (neglecting losses). This fact is clearly observable in Figure 12 where the electric torque generated by the SM 2 realizes a step of amplitude equal to the mechanical torque.

The active power supplied must have the same trend of the electric torque, because it is the product of the electric torque and the rotational speed, and the latter is roughly constant. So, in the case of SM 1, after a series of initial fluctuations, the active power returns to the initial value (Figure 13); the active power of the SM 2 increases by 5%, as the mechanical torque (Figure 14).

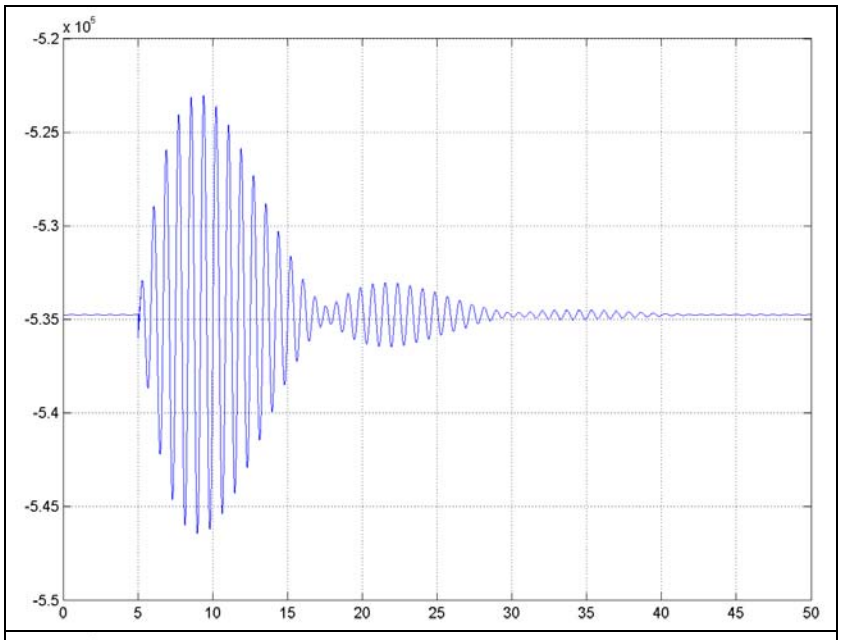

Figure 11
Electric torque absorbed by the SM 1 in the Test 1 in absence of the regulator [Nm].

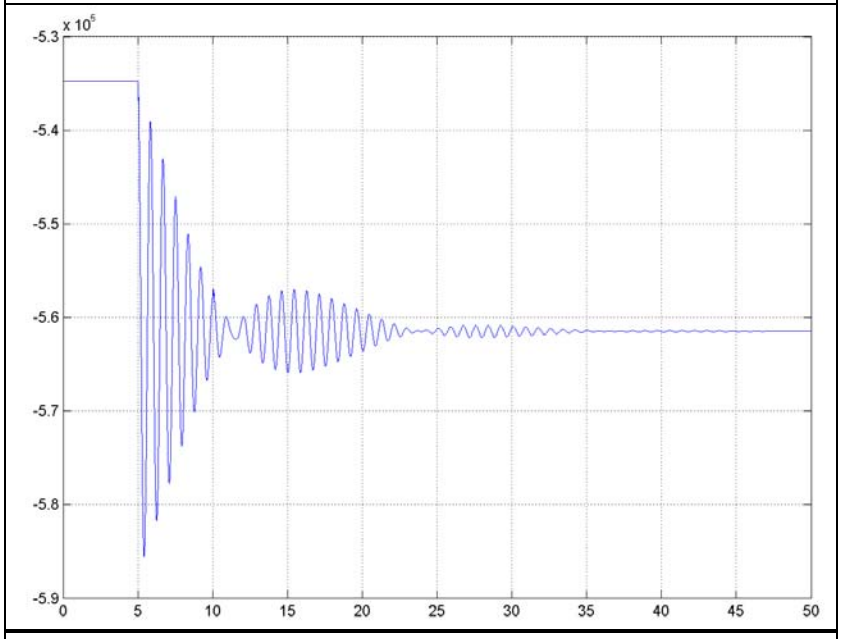

Figure 12
Electric torque absorbed by the SM 2 in the Test 1 in absence of the regulator [Nm].

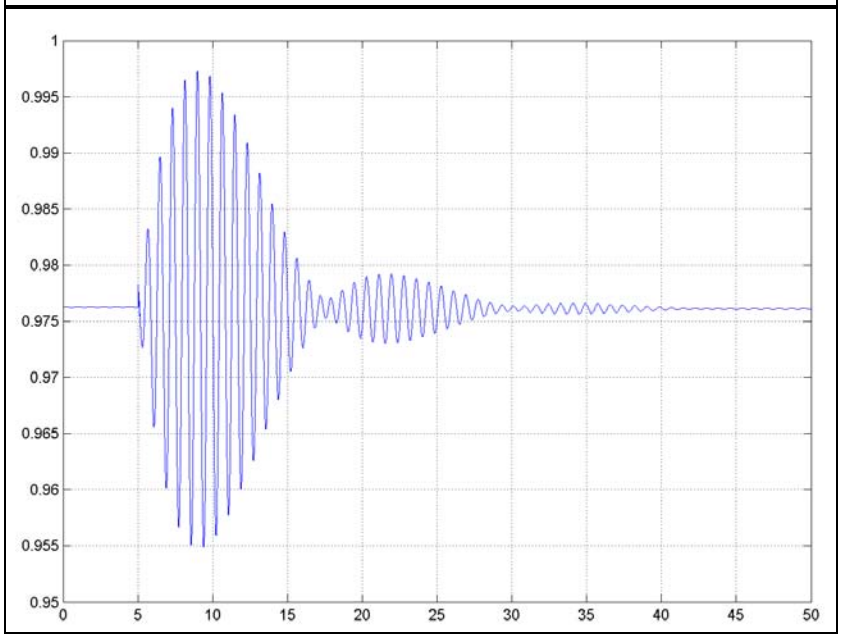

Figure 13
Active power supplied by the SM 1 in the Test 1 in absence of the regulator [p.u.].

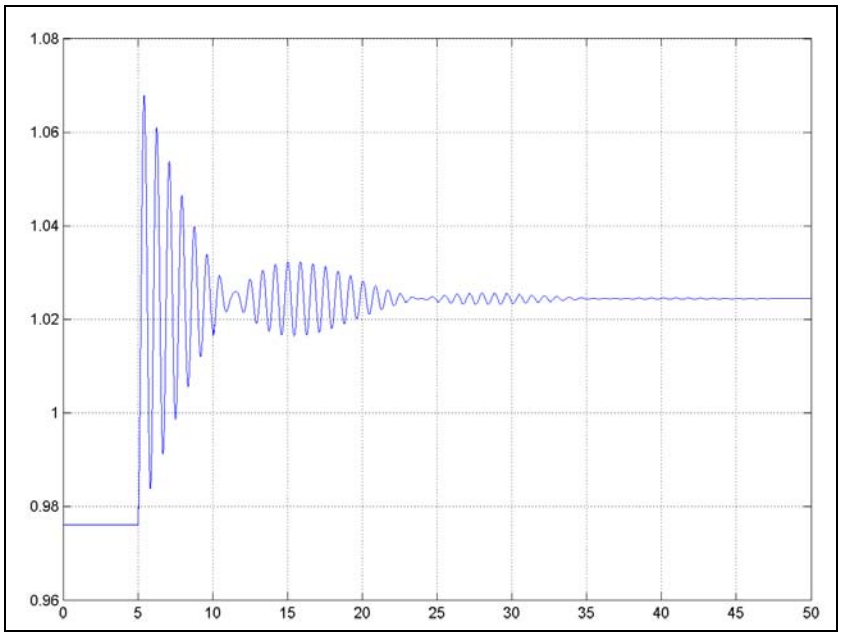

Figure 14
Active power supplied by the SM 2 in the Test 1 in absence of the regulator [p.u.].

Conversely, the interpretation of the values of the reactive power supplied is more complicated. In fact they depend, according to Eq. (11), both on the direct and quadrature-axis voltages, and on the currents. In turn, voltages are function of the network's transits, and currents generated depend on the machines dynamic Eqs. (10). While the consequences of the change in mechanical torque on the generator's direct-axis current (Figure 17 and Figure 18) are not easy to understand, those on the quadrature-axis current (Figure 19 and Figure 20) are more intuitive, because:

$$C_e = i_q^r \psi_{MP} \tag{16}$$

Given that the electric torque at rated speed must be equal to the mechanical torque and given that the permanent magnets flow is constant, the quadrature-axis current has the same variation of the mechanical torque applied to the shaft. This explains the greater variation of reactive power supplied by the SM 2 (Figure 16) compared to SM 1 (Figure 15).

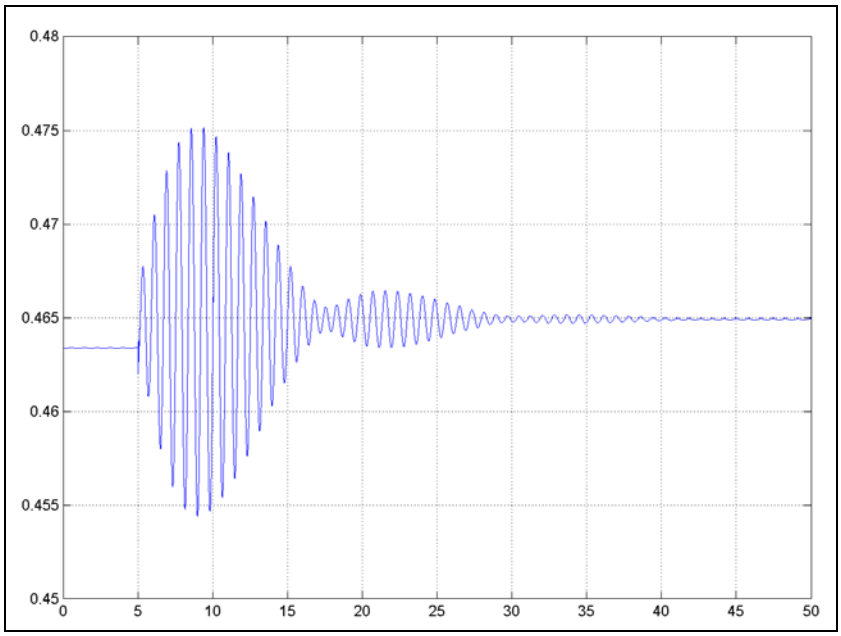

Figure 15
Reactive power supplied by the SM 1 in the Test 1 in absence of the regulator [p.u.].

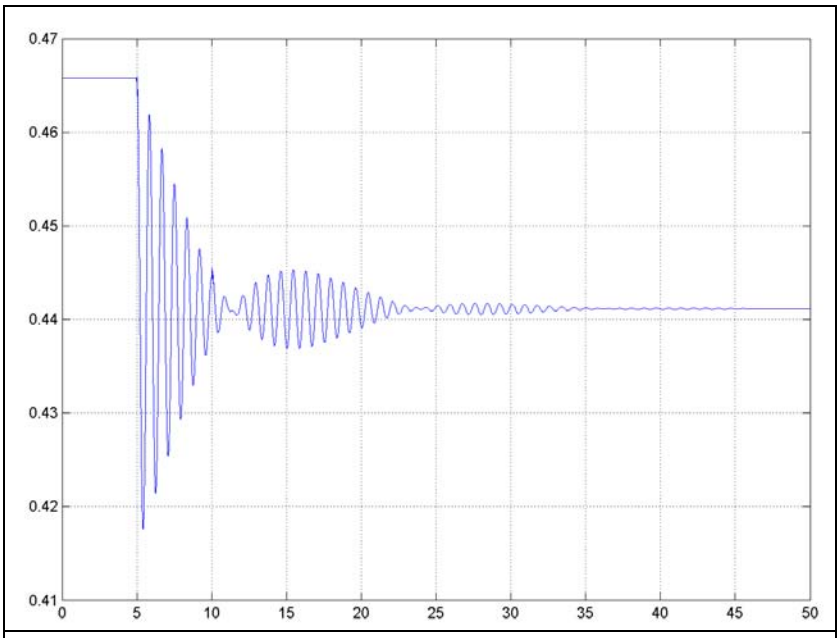

Figure 16
Reactive power supplied by the SM 2 in the Test 1 in absence of the regulator [p.u.].

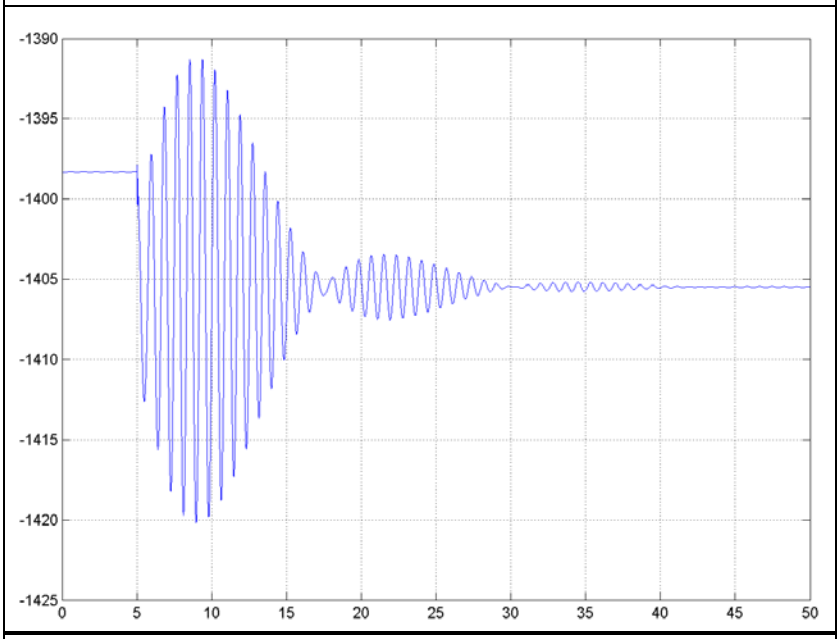

Figure 17
Direct-axis current absorbed by the SM 1 in the Test 1 in absence of the regulator [A].

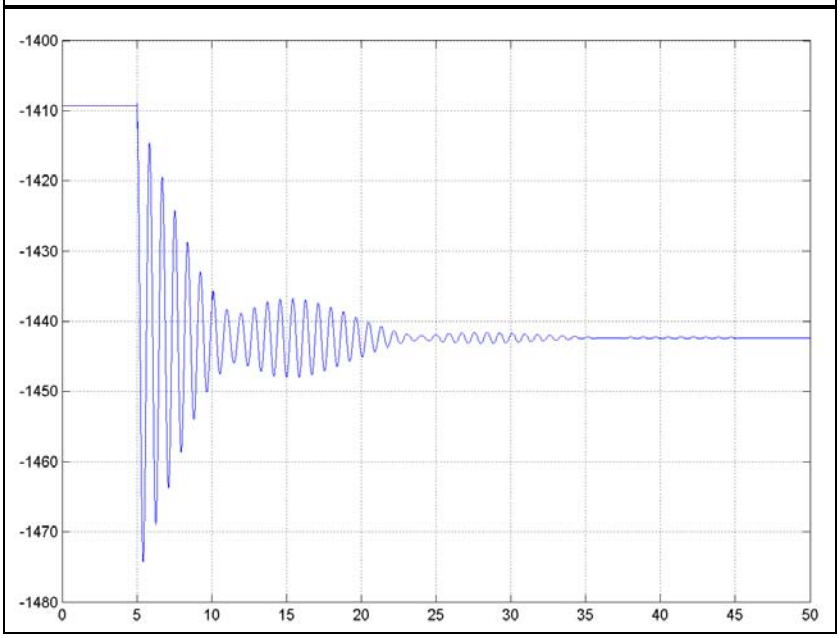

Figure 18
Direct-axis current absorbed by the SM 2 in the Test 1 in absence of the regulator [A].

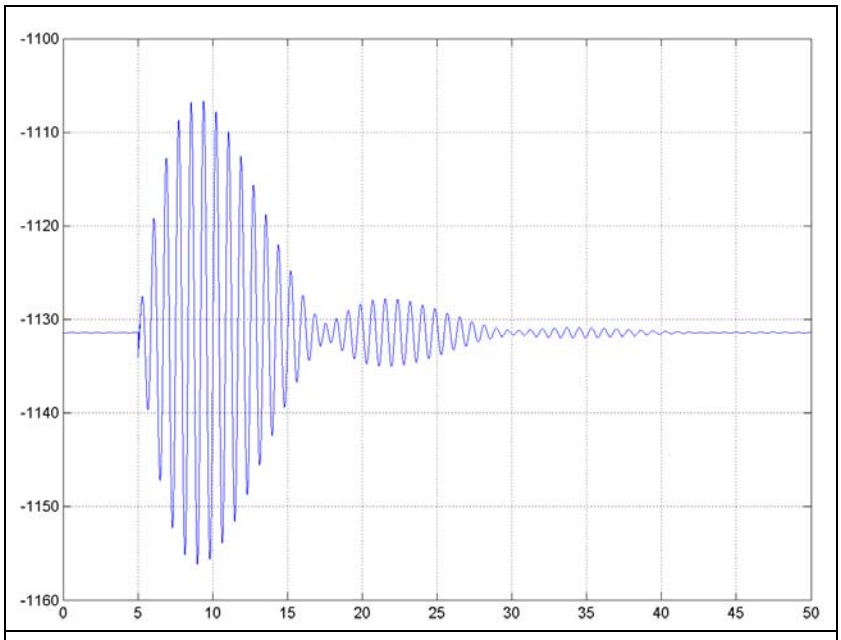

Figure 19
Quadrature-axis current absorbed by the SM 1 in the Test 1 in absence of the regulator [A].

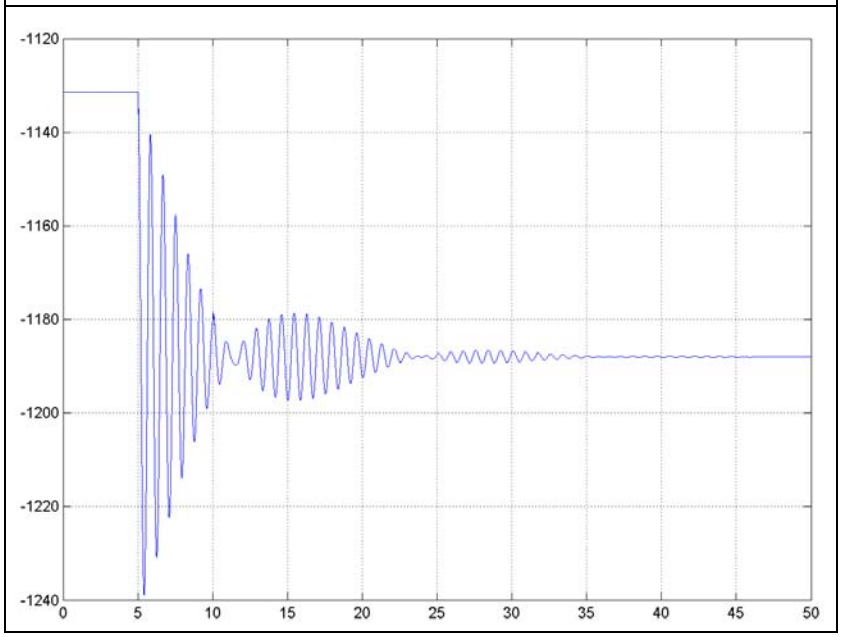

Figure 20
Quadrature-axis current absorbed by the SM 2 in the Test 1 in absence of the regulator [A].

The amplitudes of the network's voltages (Figure 21) lightly decrease. This is mostly dependent on the reactive power transits, which are affected by the reduction of its generation. The gap between the reactive power generated and that required by the loads, created after the disturbance, is filled by the contribution of the HV network. Therefore, increasing the transit of reactive power along the feeder, the voltage drops are increased, too.

It is also possible to observe that the connection bus of the SM 1, radial connected to the feeder, always presents a higher voltage than that of the substation's MV bars. This indicates the inversion of the reactive power flow on the branch between the bus 1 and the bus 4, which flows from the bus 1 (downstream) to the bus 4 (upstream). On the other hand, there is no reverse power flow between the bus 4 and the bus 2, since all the reactive power supplied by the SM 2 is absorbed by the load in the bus 5.

The voltage phases of the network's busses (Figure 22) are strongly dependent on the transits of active power along the lines. Due to the active power introduced into the network by the SM 2, the contribution of the HV network to feed the loads is reduced, in turn allowing a reduction of all the voltage phases of the network.

What stated earlier for the inversion of the reactive power flow can also be extended to the active power flows. In particular, the difference between the phase in the connection bus of SM 2 (green) and the bus immediately upstream (magenta) must be pointed. Before the increase of torque, there is a small but significant difference between the phases (the active power flows from the bus 4 to the bus 2 to supply the load in 5); after the disturbance the gap diminishes sharply (the SM 2 is supplying almost totally the load in the bus 5, so the active transit on the branch under consideration is strongly reduced).

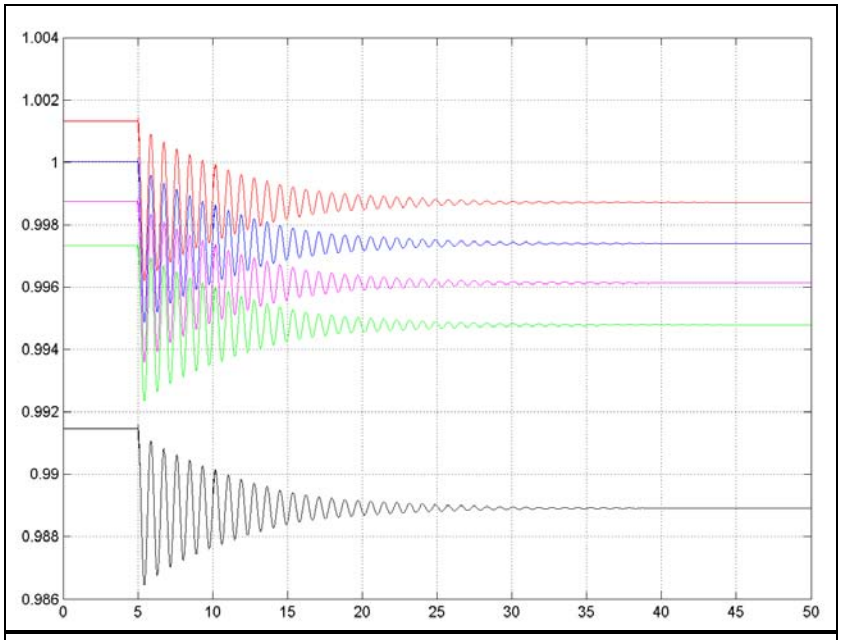

Figure 21
Amplitudes of the network's voltages in the Test 1 in absence of the regulator [p.u.].

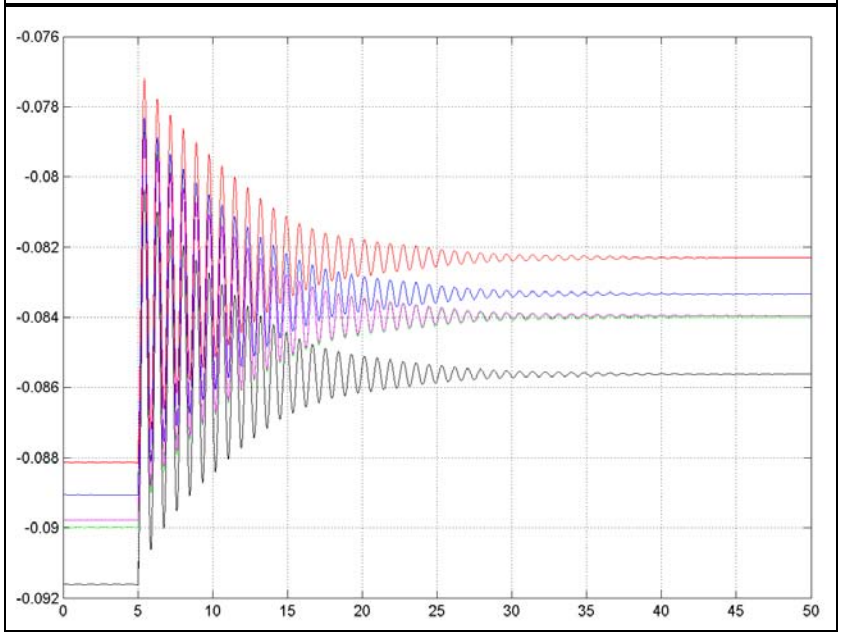

Figure 22
Phases of the network's voltages in the Test 1 in absence of the regulator [p.u.].

To guarantee stability, the load angle of the SMs should theoretically remain below 90°, but in practice it is advisable that it remains adequately bellow such limit. In the initial conditions, the SM 1 and the SM 2 have load angles respectively equal to 25.6° (Figure 23) and 25.7° (Figure 24); they are well below the limit just mentioned. After the increase of the torque applied to the SM 2, there is a slight grown of both the angles to approximately 25.7° and 27.2°: nevertheless, they remain at acceptable values.

For a synchronous isotropic generator, active power is given by:

$$P = \frac{VE}{X_S} sin\delta \tag{17}$$

where:

- P is the active power delivered by the generator [MW];
- V is the voltage at the terminals of the machine [kV];
- E is the excitation voltage [kV];
- X_s is the synchronous reactance of the generator [Ω];
- δ is the load angle of the machine [rad].

Assuming that the supply voltage and the excitation remain approximately constant, the active power variation in output is proportional to the sinus of the load angle. The sinus of 25.7° (load angle of the SM 2 before the disturbance) is about 0.434, while the sinus of 27.2° (load angle of the SM 2 after the increase of torque) is 0.457. So, it has been subject to an increase of 5.3%, in agreement with the increase of 5% of the torque at the shaft.

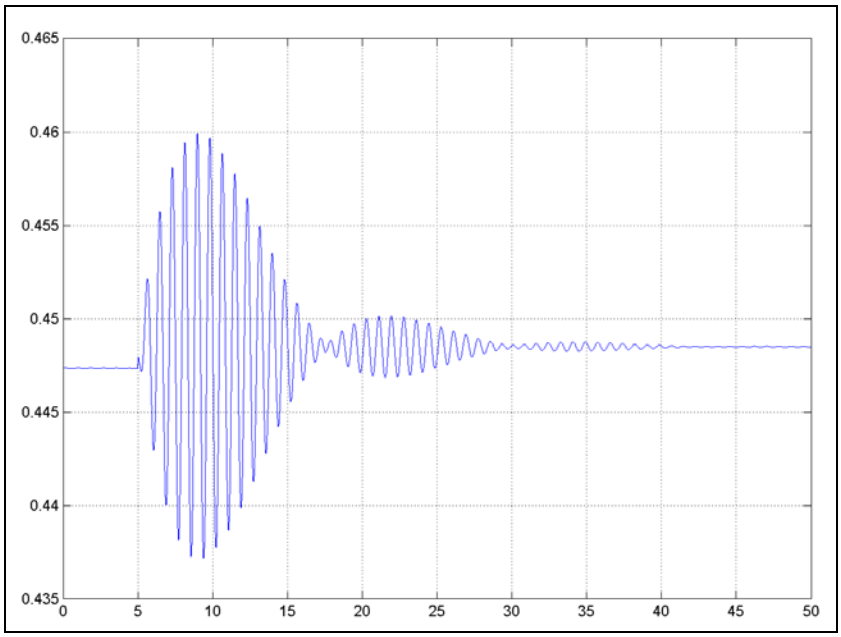

Figure 23
Load angle of the SM 1 in the Test 1 in absence of the regulator [rad].

The voltage pulsations at the terminals of the two SMs (Figure 25 and Figure 26) undergo impulsive changes because of the network dynamics, which are significantly faster than generators dynamics. The frequency of the network changes almost instantly, ensuring the variation of the mutual phase displacement between the voltage vectors.

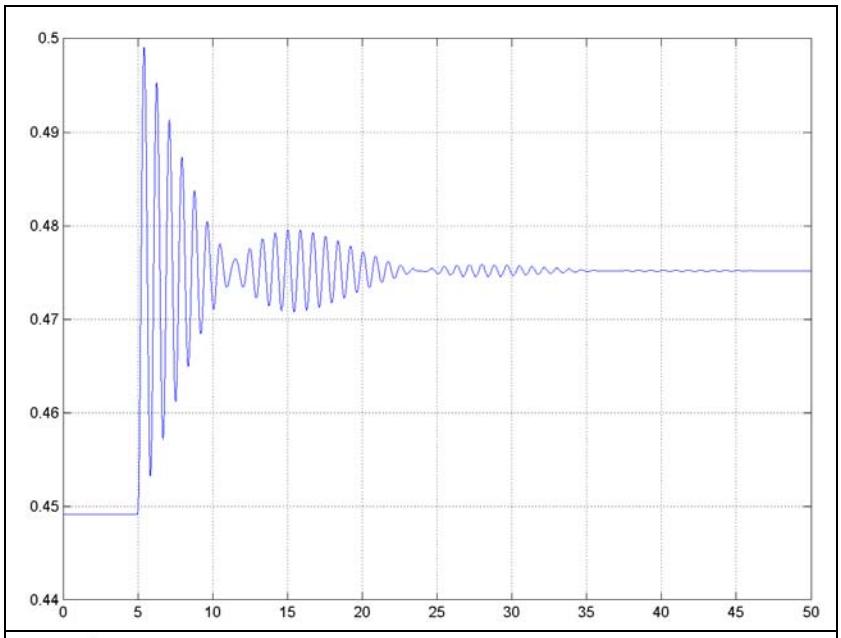

Figure 24
Load angle of the SM 2 in the Test 1 in absence of the regulator [rad].

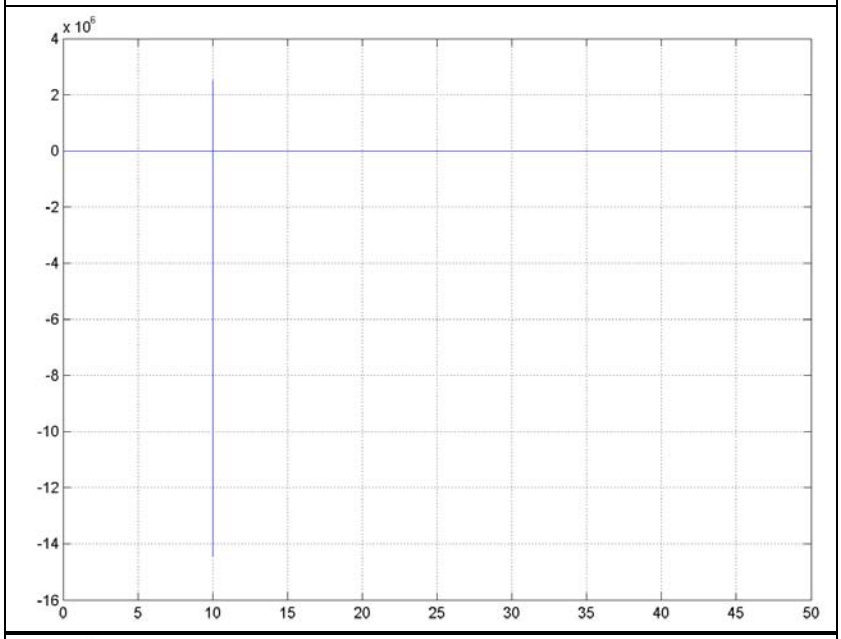

Figure 25
Pulsation of the voltage at the terminals of the SM 1 in the Test 1 in absence of the regulator [rad s^{-1}].

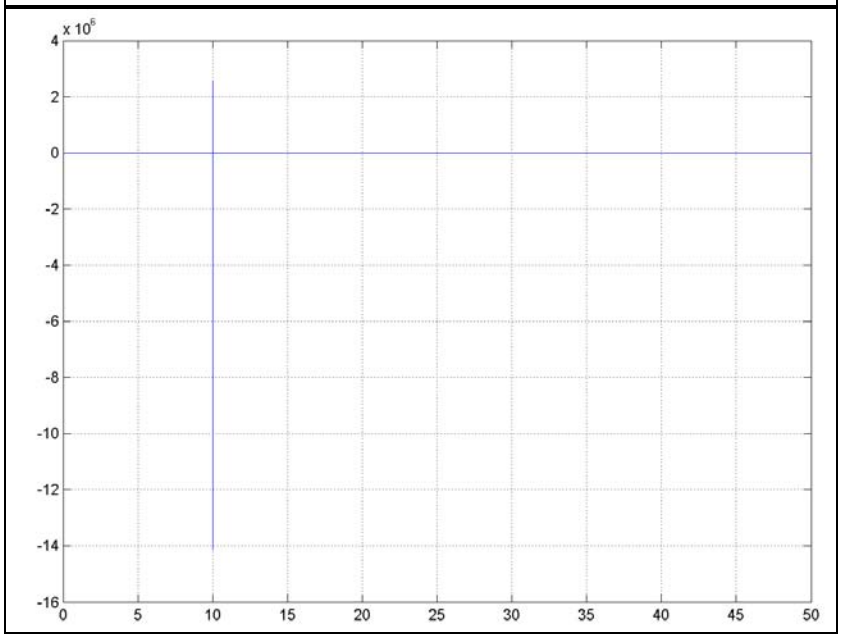

Figure 26
Pulsation of the voltage at the terminals of the SM 2 in the Test 1 in absence of the regulator [rad s^{-1}].

TEST 2 IN ABSENCE OF THE REGULATOR

In the second test studied, a step change in the torque applied to SM 2 (that increase in magnitude of 5%) is simulated (Figure 28). The torque applied to the SM 1 has a sinusoidal characteristic with amplitude again of the 5% of the rated torque and a frequency of *0.07 Hz* (Figure 27).

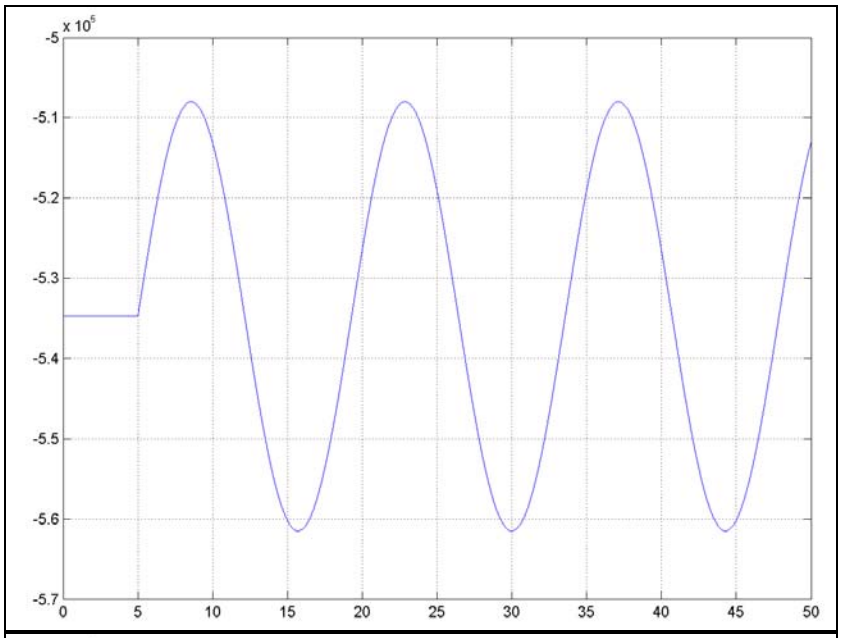

Figure 27
Torque applied to the SM 1 in the Test 2 in absence of the regulator [Nm].

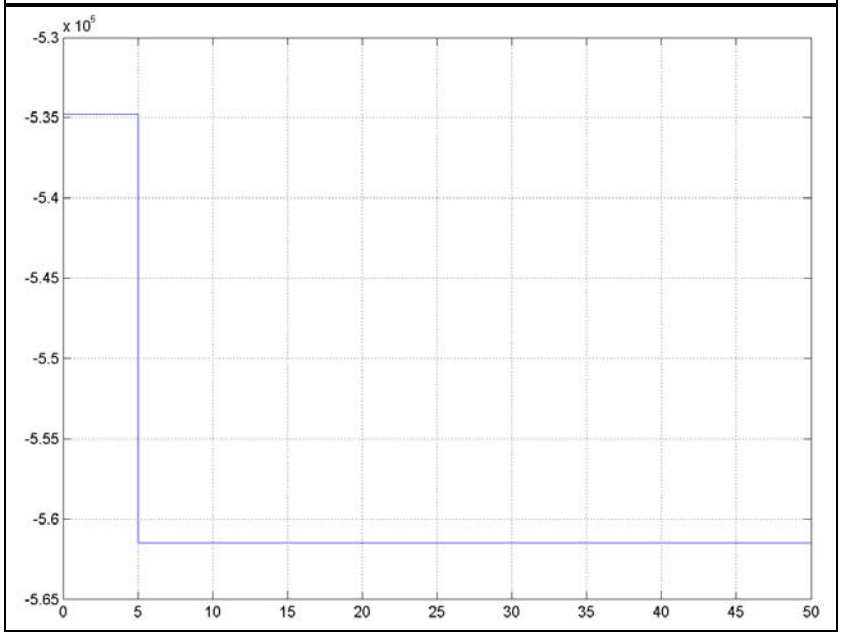

Figure 28
Torque applied to the SM 2 in the Test 2 in absence of the regulator [Nm].

Looking at the mechanical speeds of the two generators, the speed of SM 2 (Figure 30) presents the typical oscillations of the torque step, without being affected by the sinusoidal torque oscillations applied to the SM 1. On the other hand, the SM 1, instead, first is influenced by both the step on the other machine and the discontinuity introduced by the transition between constant and sinusoidal torque (Figure 29). Moreover, after an initial adjustment, the mechanical speed of the SM 1 chases perfectly the torque fluctuations. This happens thanks to the low frequency of the sine wave with respect to the generator dynamics.

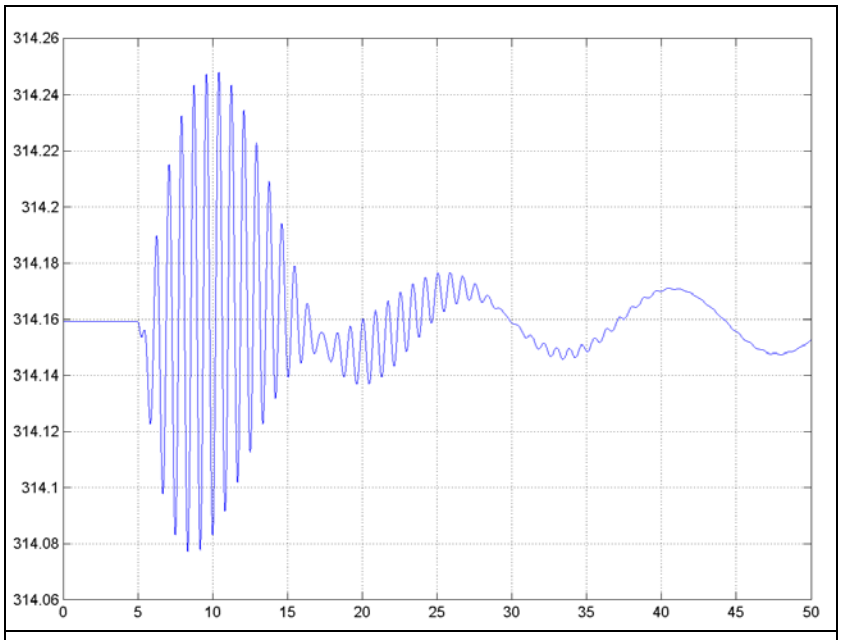

Figure 29
Rotational speed of the SM 1 in the Test 2 in absence of the regulator [rad s^{-1}].

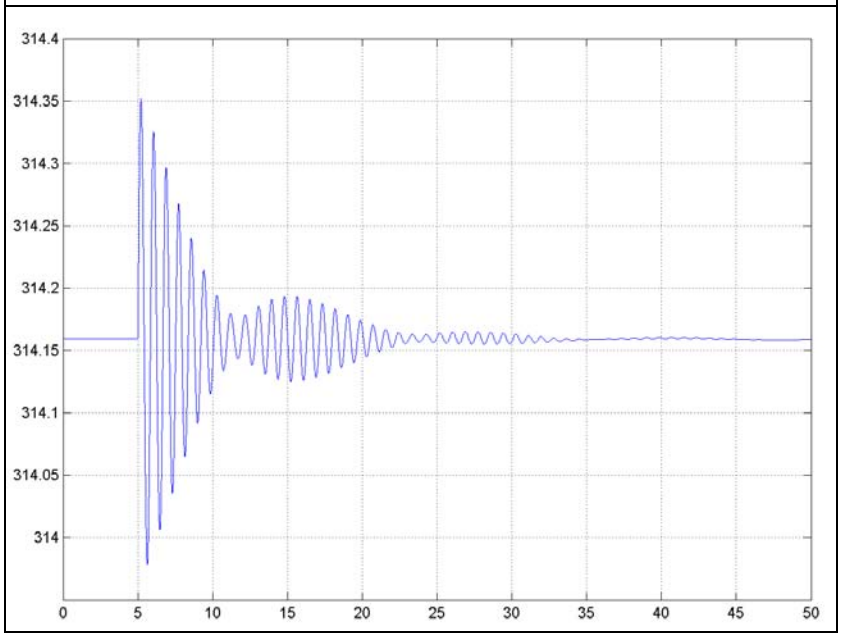

Figure 30
Rotational speed of the SM 2 in the Test 2 in absence of the regulator [rad s^{-1}].

The active (Figure 31 and Figure 32) and reactive (Figure 33 and Figure 34) power provided by the SM 1, being less affected by the initial discontinuity of the torque and by the disturbance on the other generator, chase at once the sinusoidal characteristic. Moreover, the reactive power generated by the SM 2 assumes, after the initial transient, a trend sinusoidal too. Indeed, it depends on the voltage and the latter is strongly influenced by the SM 1 generation; therefore, it is more affected by the disturbance on the other machine than by the active power supplied by itself, function almost solely of torque in input.

The trend of the voltage amplitude characteristics is the result of the superposition of the effects related to the disturbances acting on both SMs (Figure 35). The reduction of the reactive power generated by the SM 2 causes a downward shift of the sinusoidal voltage characteristic, which has not the initial potential as an average value. The downward shift is due to the fact that by reducing the generators reactive power inlet into the network, the reactive transits from the HV network increase, and the voltage drop also rises.

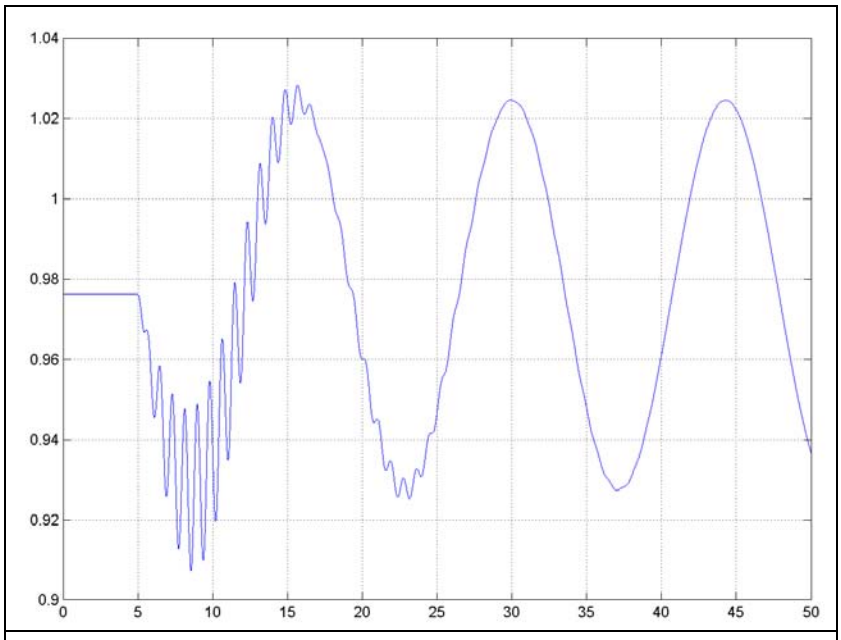

Figure 31
Active power supplied by the SM 1 in the Test 2 in absence of the regulator [p.u.].

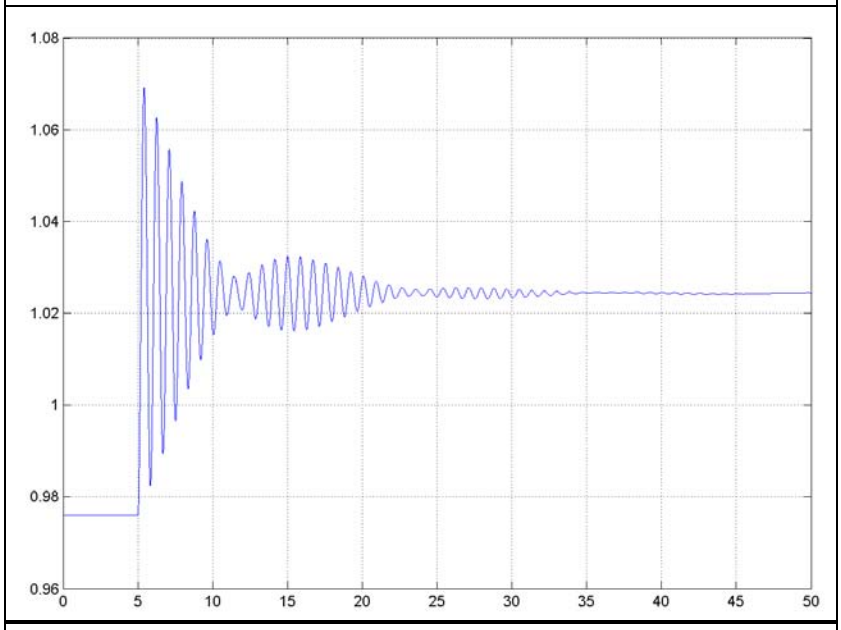

Figure 32
Active power supplied by the SM 2 in the Test 2 in absence of the regulator [p.u.].

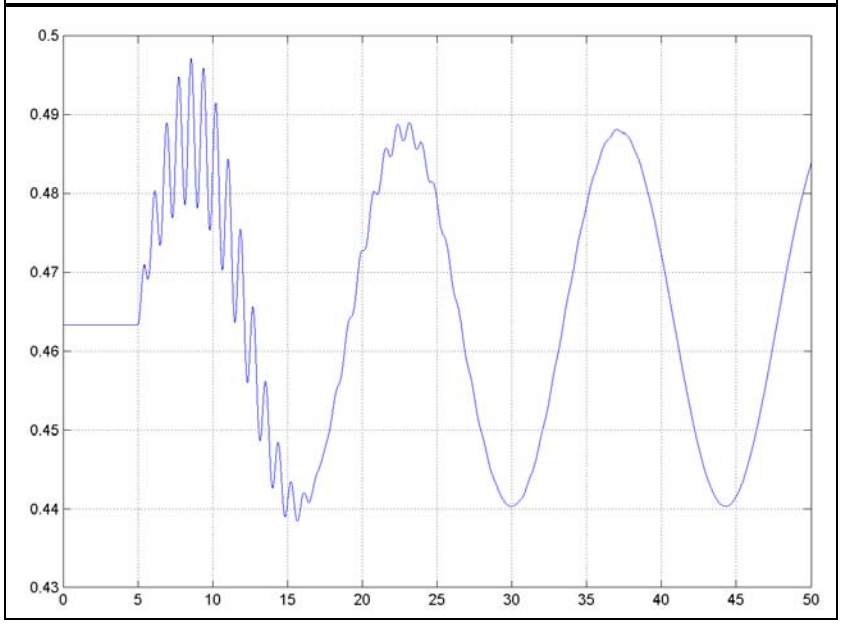

Figure 33
Reactive power supplied by the SM 1 in the Test 2 in absence of the regulator [p.u.].

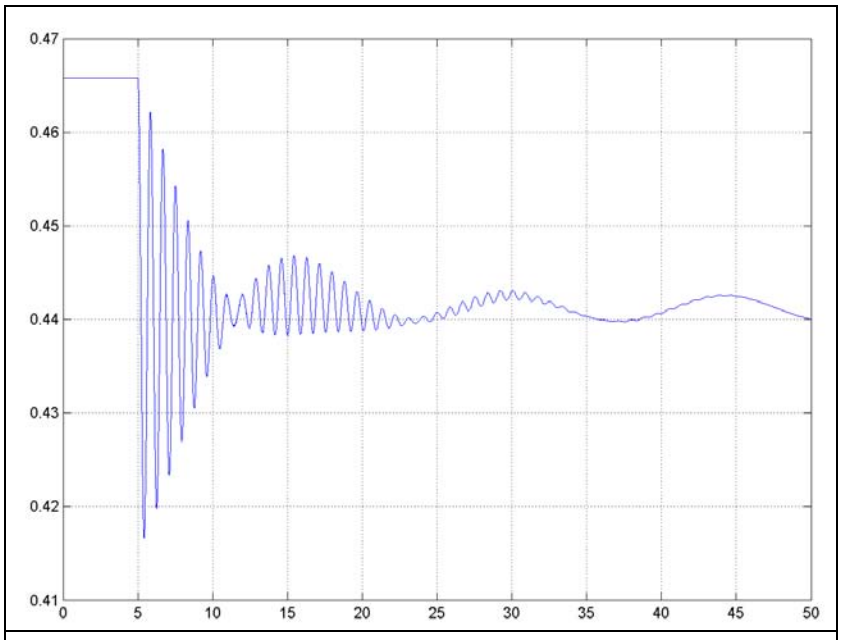

Figure 34
Reactive power supplied by the SM 2 in the Test 2 in absence of the regulator [p.u.].

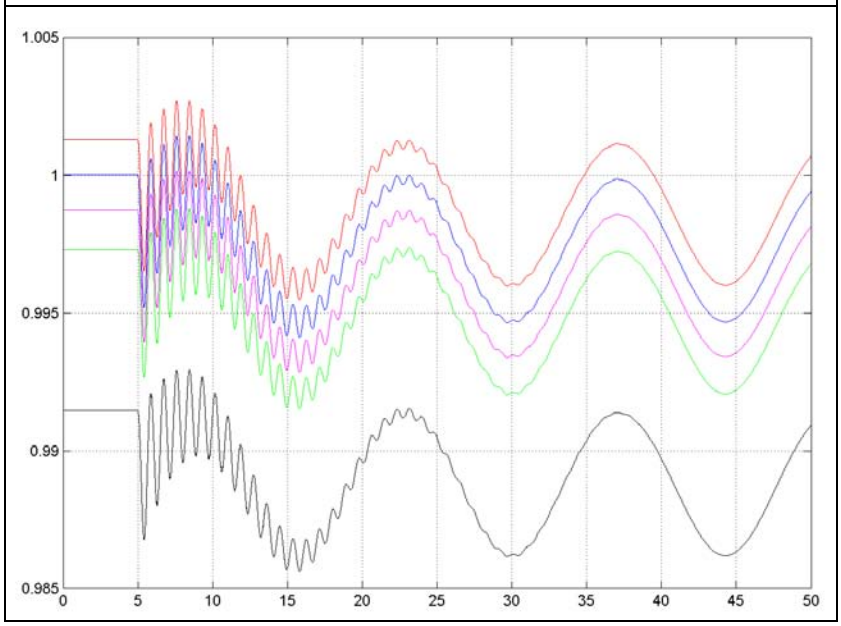

Figure 35
Amplitudes of the network's voltages in the Test 2 in absence of the regulator [p.u.].

The voltage phases are affected in a similar way by the active power generated by the SMs (Figure 36). Their characteristics are always sinusoidal, but in anti-phase with that of the amplitudes: the active power trend is opposite to the reactive one.

Finally, the load angles (Figure 37 and Figure 38), also in this case, remain in a widely accepted range, still less than 29°. The sinusoidal trend that the load angle of the SM 2 presents at steady-state is due, according to Eq. (17), to the voltage variation at the terminals of the machine.

Since the voltage at its terminals is sinusoidal and the load angle is in anti-phase with it, to maintain constant the active power output (the torque applied to the shaft of the machine is constant itself), it is necessary that the load angle causes a resulting effect equal and opposite to the effect of voltage.

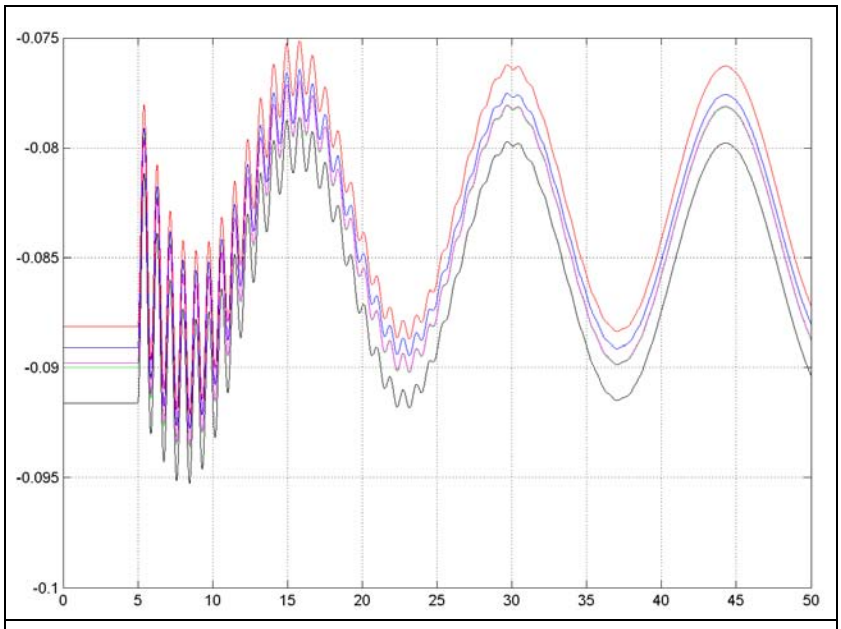

Figure 36
Phases of the network's voltages in the Test 2 in absence of the regulator [p.u.].

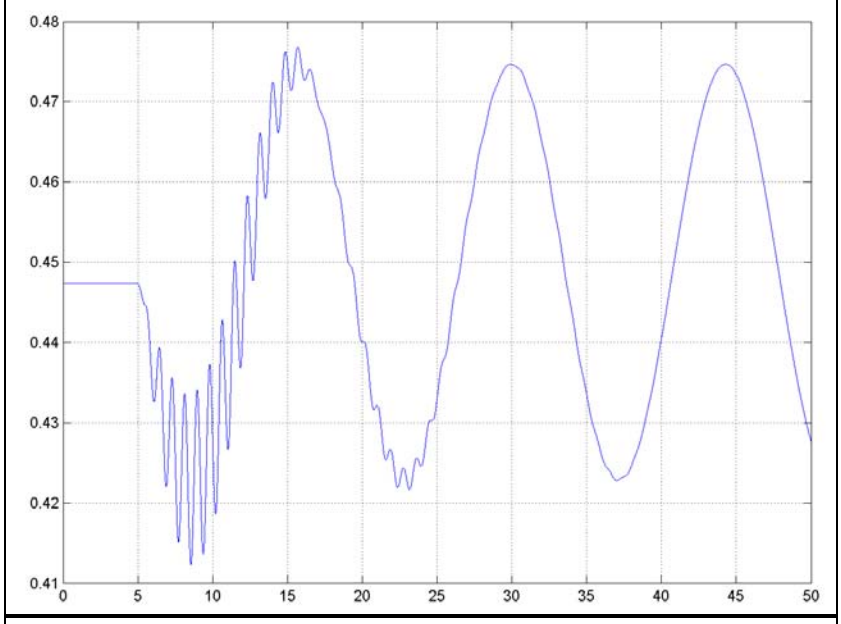

Figure 37
Load angle of the SM 1 in the Test 2 in absence of the regulator [rad].

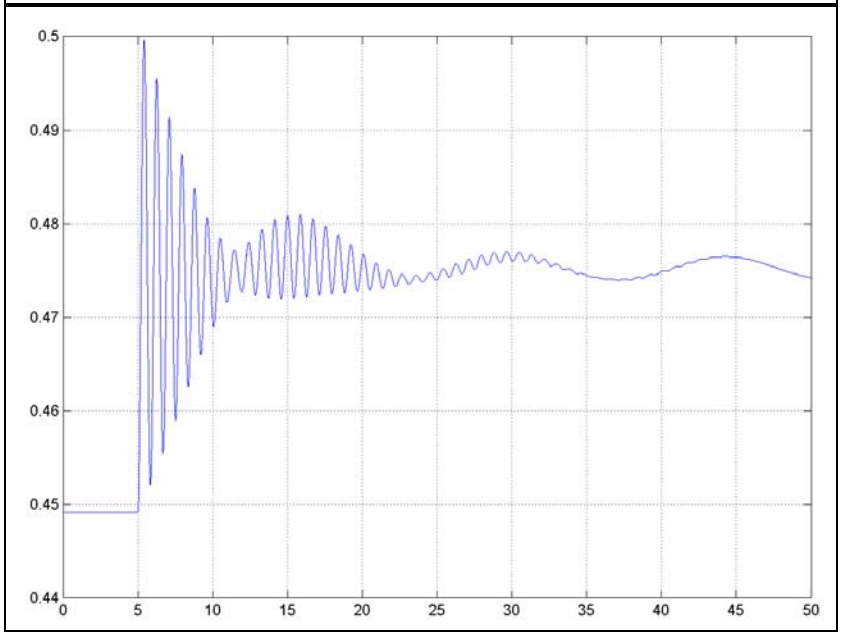

Figure 38
Load angle of the SM 2 in the Test 2 in absence of the regulator [rad].

TEST 3 IN ABSENCE OF THE REGULATOR

In this test, two sinusoidal torques with identical amplitudes, but in anti-phase have been applied to the machines (Figure 39 and Figure 40). The amplitude of these oscillations is still maintained at the 5% of the generators nominal torque and the frequency is set to *0.07 Hz*: which is slow enough to be caught by the generators dynamics.

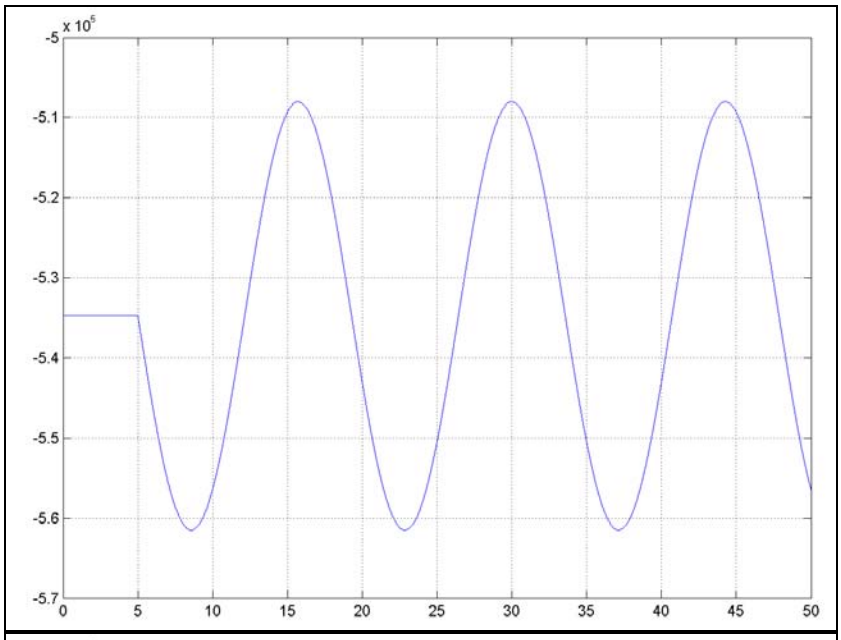

Figure 39
Torque applied to the SM 1 in the Test 3 in absence of the regulator [Nm].

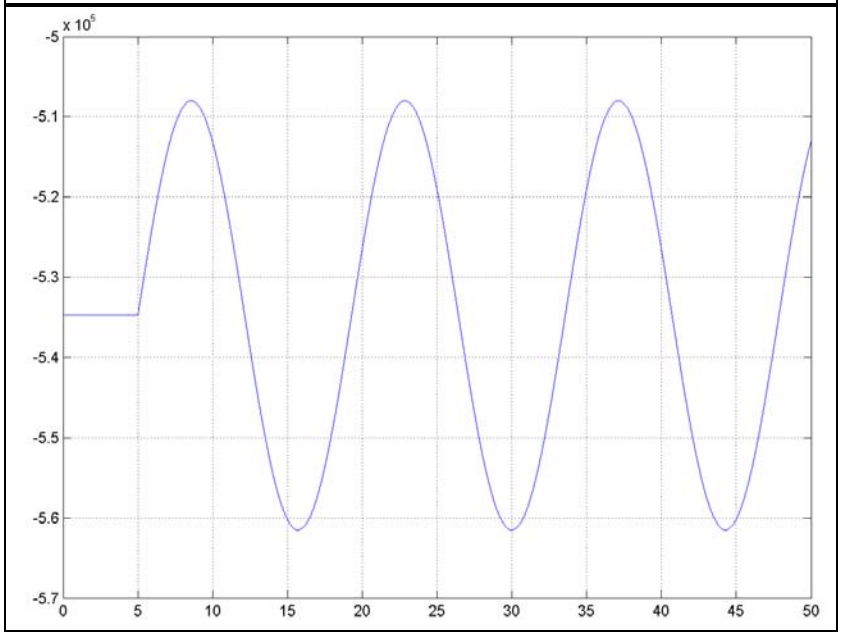

Figure 40
Torque applied to the SM 2 in the Test 3 in absence of the regulator [Nm].

In this case, the rotational speeds of the two generators are both sinusoidal and influenced mainly by the change in torque applied to the relevant shaft (Figure 41 and Figure 42). Also in this case, the initial discontinuity caused by the transition of the torque from a constant to a sinusoidal value triggers oscillations, but much smaller than those in the previous test. The trends of the mechanical speed of machines are not in phase with the disturbance torque, indeed the generators mechanical dynamics introduce a delay.

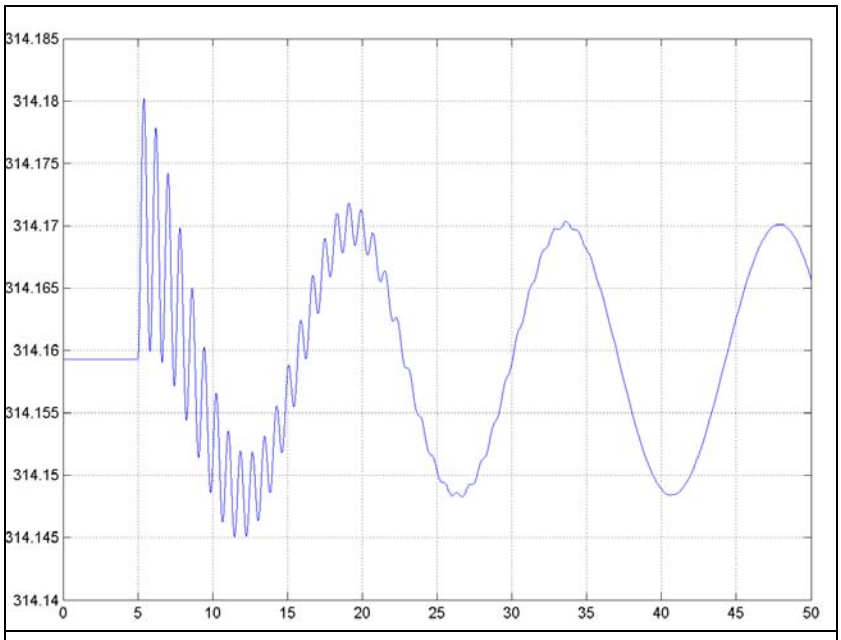

Figure 41
Rotational speed of the SM 1 in the Test 3 in absence of the regulator [rad/s].

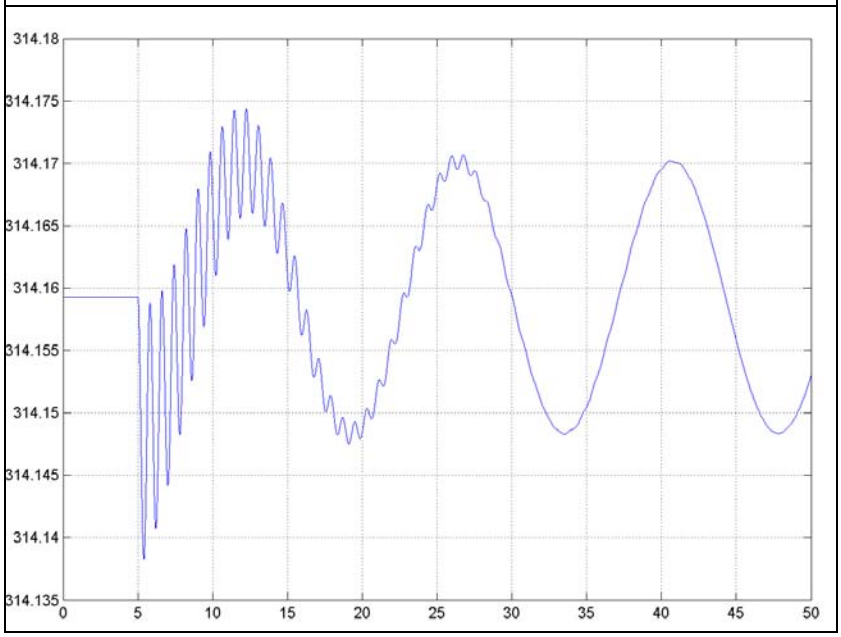

Figure 42
Rotational speed of the SM 2 in the Test 3 in absence of the regulator [rad/s].

The active (Figure 43 and Figure 44) and reactive (Figure 45 and Figure 46) powers have a sinusoidal characteristic almost with no fluctuations. They are, respectively, in phase and anti-phase with the torque applied to the SMs.

The amplitudes of network's voltages are in a negligible way influenced by torque disturbances (Figure 47). Their trends are sinusoidal with moderate amplitude and frequency double then the torque frequency. This indicates that the reactive power supplied by each machine tends on the whole to balance each other out.

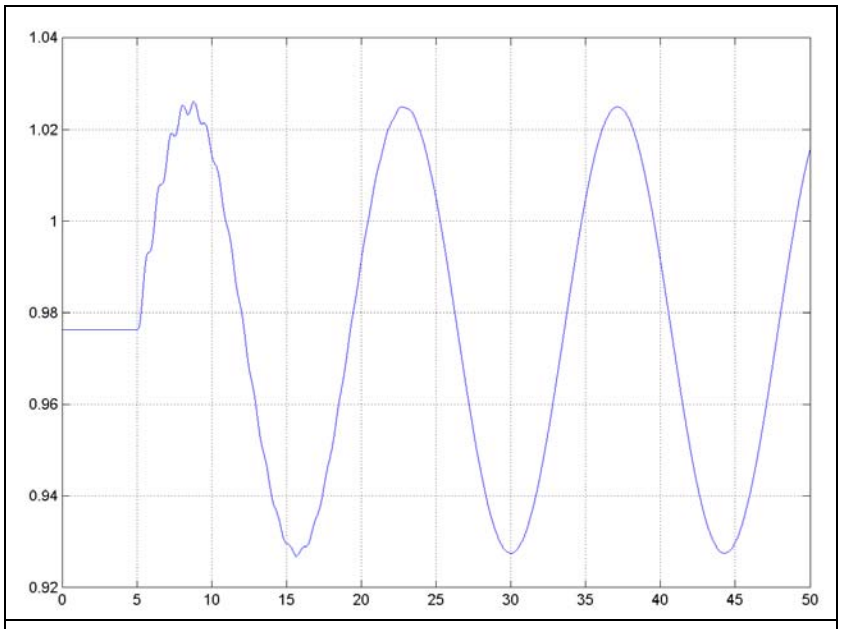

Figure 43
Active power supplied by the SM 1 in the Test 3 in absence of the regulator [p.u.].

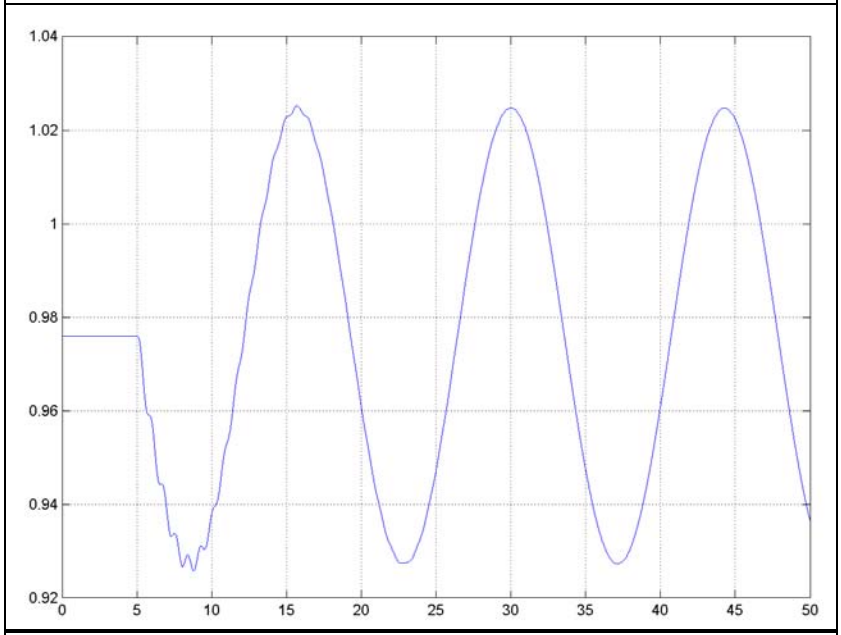

Figure 44
Active power supplied by the SM 2 in the Test 3 in absence of the regulator [p.u.].

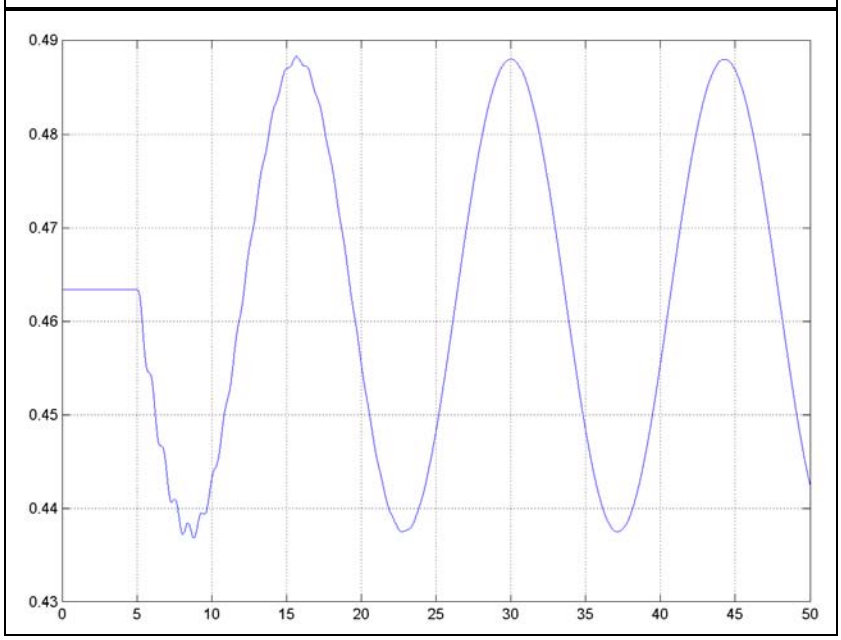

Figure 45
Reactive power supplied by the SM 1 in the Test 3 in absence of the regulator [p.u.].

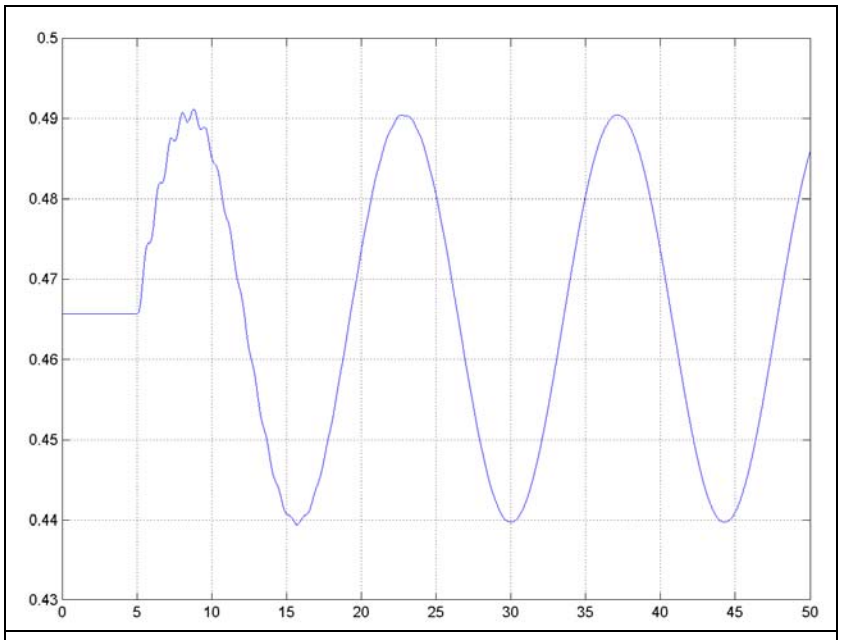

Figure 46
Reactive power supplied by the SM 2 in the Test 3 in absence of the regulator [p.u.].

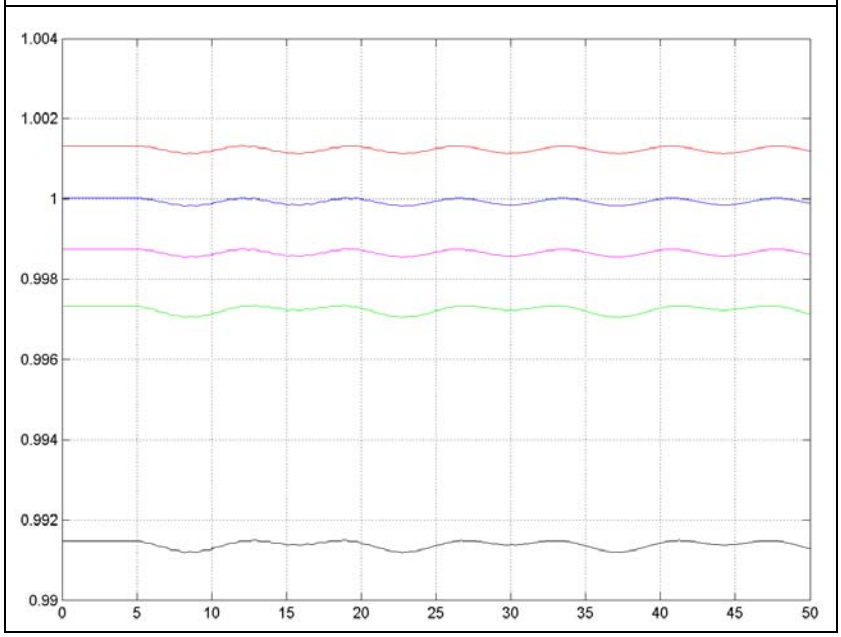

Figure 47
Amplitudes of the network's voltages in the Test 3 in absence of the regulator [p.u.].

The voltage phases suffer for the perturbations accordingly to which bus is considered (Figure 48). The voltages of the busses closest to the substation (blue and magenta) are almost constant. These busses in fact, due to the proximity to the infinite power network, have in turn a short-circuit power greater than that of the downstream busses (the latter are also located closer to the source of the disturbance) and are less affected by the voltage drop due to reactive transits. The voltage of the SM 1 connection bus is clearly influenced by the reactive power variation caused by the same generator. The bus of the SM 2 and the busses downstream are subject almost exclusively to the active power variation generated by the SM 2.

Finally, the load angles have trends similar to the active power generated: given the small amplitude of the torque variation, they remain, also in this case, within perfectly acceptable values (Figure 49 and Figure 50).

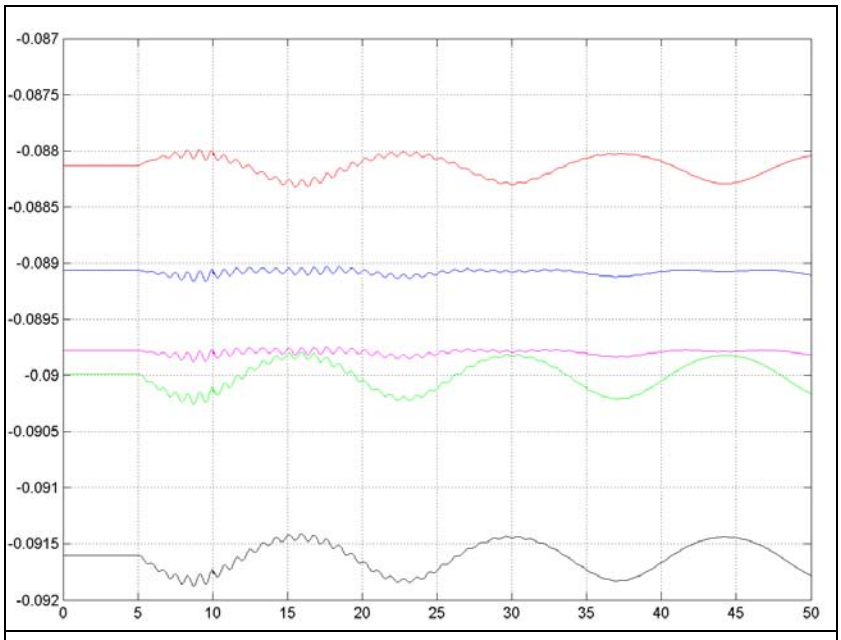

Figure 48
Phases of the network's voltages in the Test 3 in absence of the regulator [p.u.].

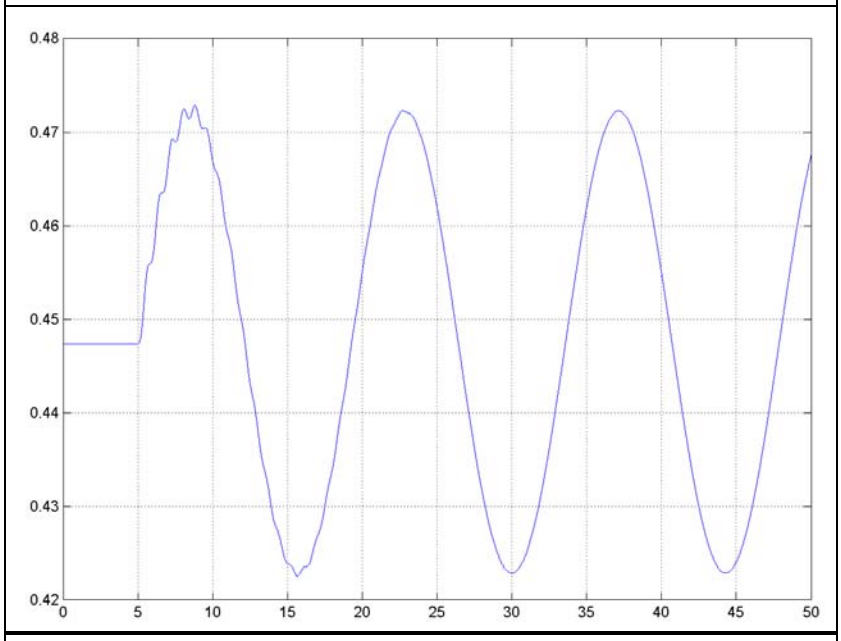

Figure 49
Load angle of the SM 1 in the Test 3 in absence of the regulator [rad].

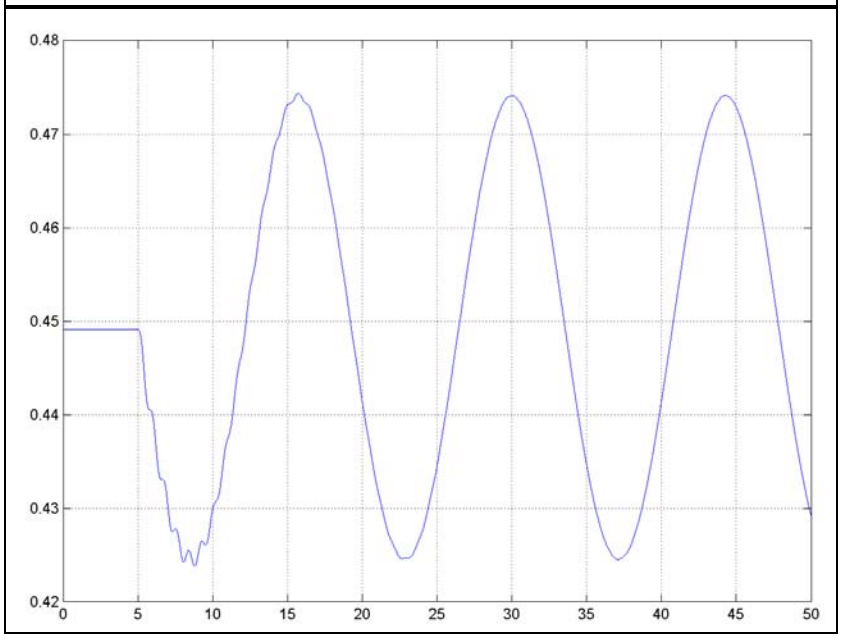

Figure 50
Load angle of the SM 2 in the Test 3 in absence of the regulator [rad].

9. DIVERGENCE

In this chapter the divergence of the developed electric system is introduced. The divergence is the trace of the Jacobian of the system of odes described previously. As explained above, the main objective is to obtain a stability index that can be employed in a regulator, with the aim of improving the dynamic behavior of the generators.

The total divergence is the sum of the divergence of each machine. It is reported in *p.u.* with respect to the "benchmark" divergence, i.e. the divergence that alternators show at the steady-state (rotational speed equal to ω_0):

$$|Div| = \left| \sum_n \frac{\sqrt{\left(\frac{R_{sn}}{L_{sn}}\right)^2 + (j\omega_n)^2}}{\sqrt{\left(\frac{R_{sn}}{L_{sn}}\right)^2 + (j\omega_0)^2}} \right| \tag{18}$$

In this equation the same symbolism as in Eq. (1) is employed.

From Eq. (18) it can be observed that, since the resistance and the inductance of the machine are constant, only the mechanical speed affects the divergence.

In the following, the divergence trends (calculated as above-mentioned) of the three simulations described in the previous chapter are shown.

TEST 1 IN ABSENCE OF THE REGULATOR – DIVERGENCE

In the first simulation the divergence is mostly affected by the angular velocity variation of the SM 2, which is larger than the one observed in SM 1 (Figure 51). After a few seconds from the onset of the disturbance; however, it supersedes the effects related to SM 1, because that machine has less attenuation of its ω_m oscillations.

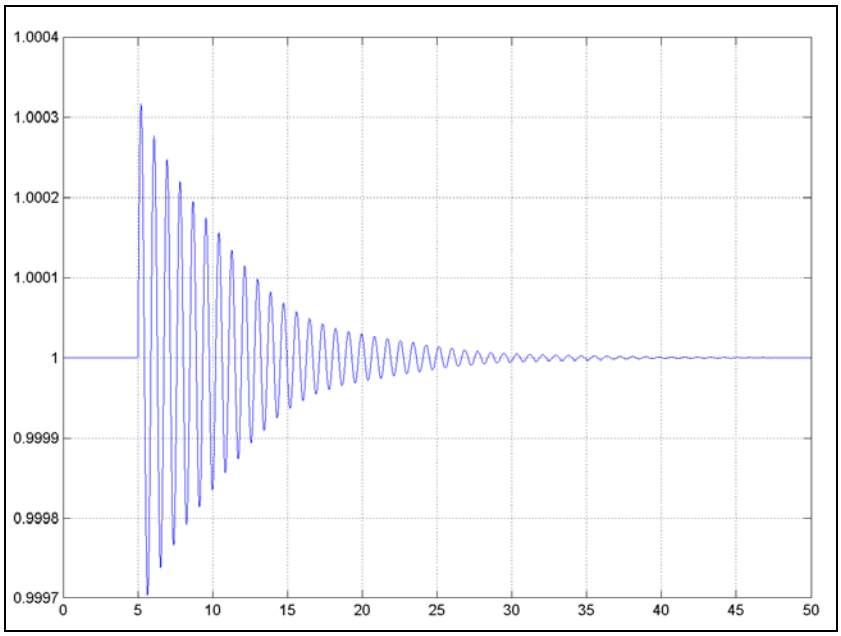

Figure 51
Divergence of the system in the Test 1 in absence of the regulator [p.u.].

TEST 2 IN ABSENCE OF THE REGULATOR – DIVERGENCE

In the second simulation the divergence has a highly oscillatory trend. This is due, in a first instance, to the strong fluctuations of the SM 2 caused by the step of the torque to which the generator is subject (Figure 52). After the first periods following the beginning of the oscillations, the disturbances related to the sinusoid applied to the SM 1 come into play. They are minor in amplitude, but more protracted in time; at the end of such oscillator phenomena, finally, the divergence takes a sinusoidal characteristic typical of the mechanical speed of the SM 1.

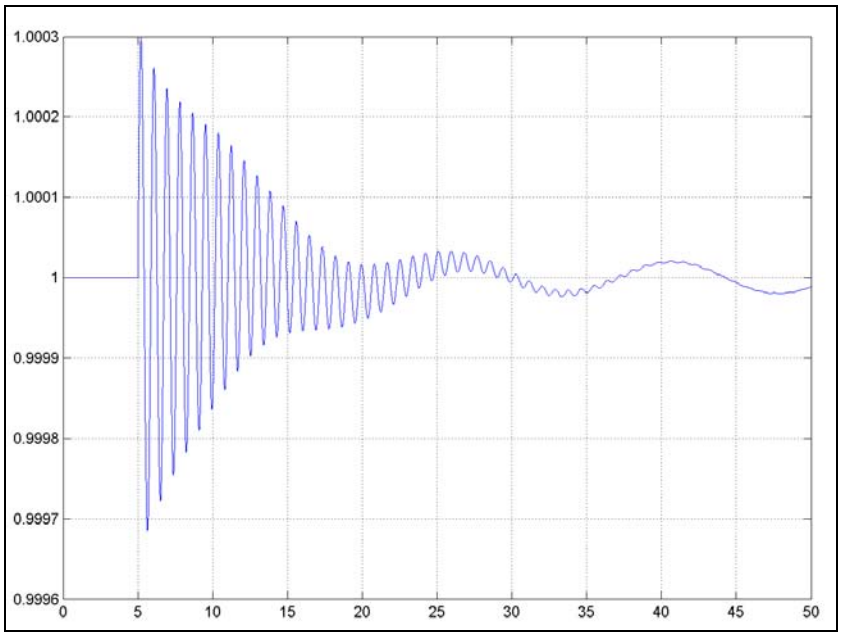

Figure 52
Divergence of the system in the Test 2 in absence of the regulator [p.u.].

TEST 3 IN ABSENCE OF THE REGULATOR – DIVERGENCE

The divergence, in this test, is the result of the equal and opposite effects of torque perturbations on the two generators. That explains why the software for the representation of the trends has approximated the entire y-axis to the value "1" (Figure 53). Despite the small amplitude of oscillations, a first period appears, in which the divergence is affected by the initial discontinuity of the torques (assuming a strongly oscillatory trend). Later on, the effects of the two machines tend to better compensate one each other, originating sinusoidal oscillations at double frequency (as regards the force) and of moderate amplitude.

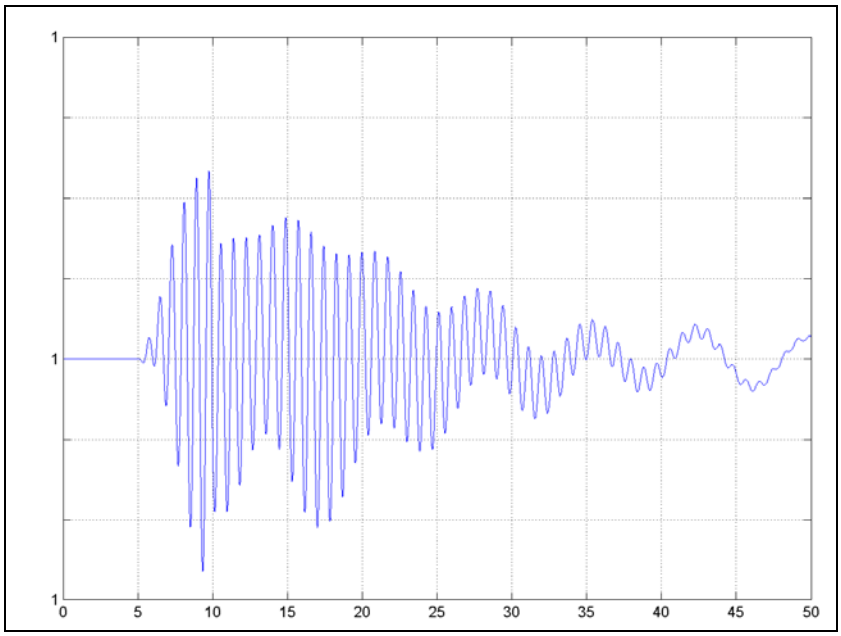

Figure 53
Divergence of the system in the Test 3 in absence of the regulator [p.u.].

10. SIMULATIONS USING AN ENERGY STORAGE DEVICE DRIVEN BY THE DIVERGENCE

Once analyzed the transient behaviour of the dynamical system after some types of disturbances on the mechanical torques of the SMs, it is now possible to evaluate some control alternatives for the oscillations' mitigation of the electrical and mechanical amplitudes that the torque variations induce.

Excluding for hypothesis the use of the voltage and frequency regulation devices (typically used in these machines), a possible solution is the use of a storage system (capacitor) capable to absorb and supply electricity as needed. The electric energy stored by a capacitor is equal to:

$$W = \frac{1}{2} C V^2 \tag{19}$$

where:

- W is the electrical energy stored [J];
- C is the capacity of the capacitor [F];
- V is the direct voltage applied to the capacitor [V].

The capacitor is coupled to the network through a DC – AC converter with the task to convert electrical magnitudes from continue to alternate and vice versa, and to adjust the DC side voltage to control the charging/discharging process of the capacitor. This process is ruled by a proportional – derivative regulator (Figure 54), with a rapid response when compared to the dynamics of the electromechanical system introduced in the previous Sections. This approach makes it possible to consider the time constants null and void.

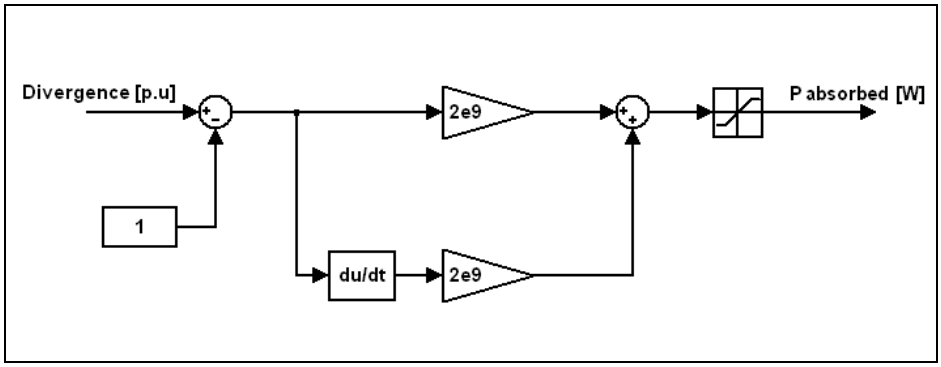

Figure 54
Principle scheme of the regulator based on the divergence.

The divergence of the system, in *p.u.*, is built with zero mean value, so that the proportional regulator provides an output amount not null only when it deviates from the nominal value. A divergence greater than the unity is indeed sign that, on the whole, the SMs took a rotational speed higher than the nominal: the storage system must absorb electrical power so as to create an imbalance between the power absorbed from the load and that generated by the SMs, in order to slow down the generators. Conversely, if the divergence is less than the unity, the storage system

must enter electric power into the network, covering the energy needs of the loads and thus prompting generators to accelerate.

In addition to the proportional block, the regulator is also equipped with a derivative controller, in order to absorb or generate more power when the system is rapidly changing its divergence. This improves the dynamic performances, providing substantial responses of the storage device even in the case of small deviations from the nominal value of the divergence that happen, however, very quickly (and are therefore more critical for the stability of the electric system).

Finally, it was assumed that the capacitor is able to deliver up to *±0.15 MW* (i.e. the ±5% of the power rating of each generator: beyond that threshold the regulator saturates) and that is installed on the same network's bus of the SM 2.

The simulations below refer to the same torque disturbances of the tests previously carried out. This allows a comparison between the dynamic behavior of the system with and without regulator.

TEST 1 WITH THE REGULATOR BASED ON THE DIVERGENCE

Subsequently to the step disturbance on the SM 2 torque, the strong fluctuations that trigger on the machines lead the regulator to provide the maximum allowable power, reaching the saturation (Figure 55). The mechanical speed oscillations of the SM 1 are positively affected by the action of the regulator (Figure 56), significantly reducing their peak amplitude (changing from *314.07 – 314.25 Hz* to *314.09 – 314.23 Hz*) with respect to the case without the storage system (Figure 9). Moreover, they damp down more regularly, ensuring a lesser amplitude also in the final stages of the disturbance.

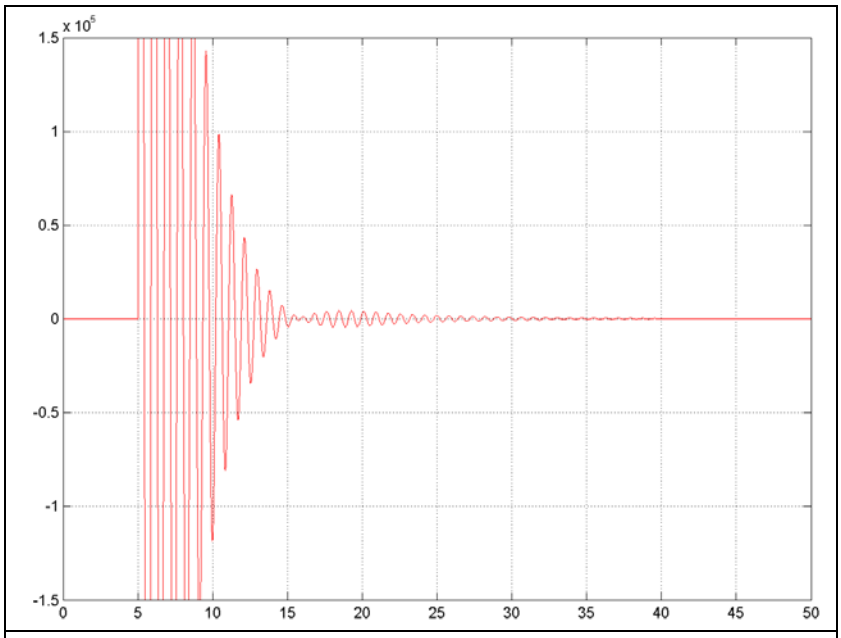

Figure 55
Power absorbed by the storage device in the Test 1 with the regulator based on the divergence [W].

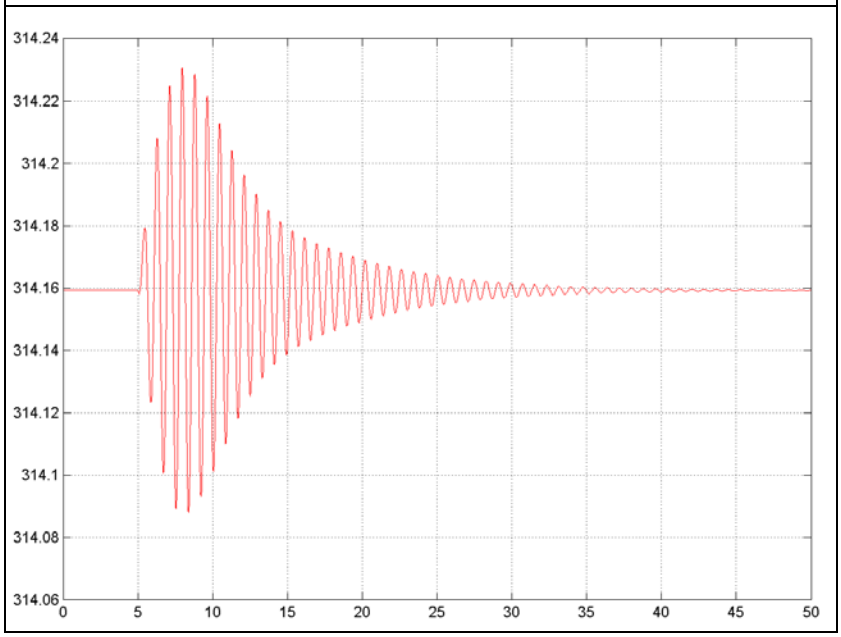

Figure 56
Rotational speed of the SM 1 in the Test 1 with the regulator based on the divergence [rad s^{-1}].

Despite the regulator is installed in the same connection bus of the SM 2, the speed variations of the latter do not benefit by the effects of the stabilizing device in a perceptible way (Figure 57). The peak value of oscillations remains in fact unchanged and only after some seconds from the

onset of the torque variation some improvements appear (compared to the case without regulator) (Figure 10).

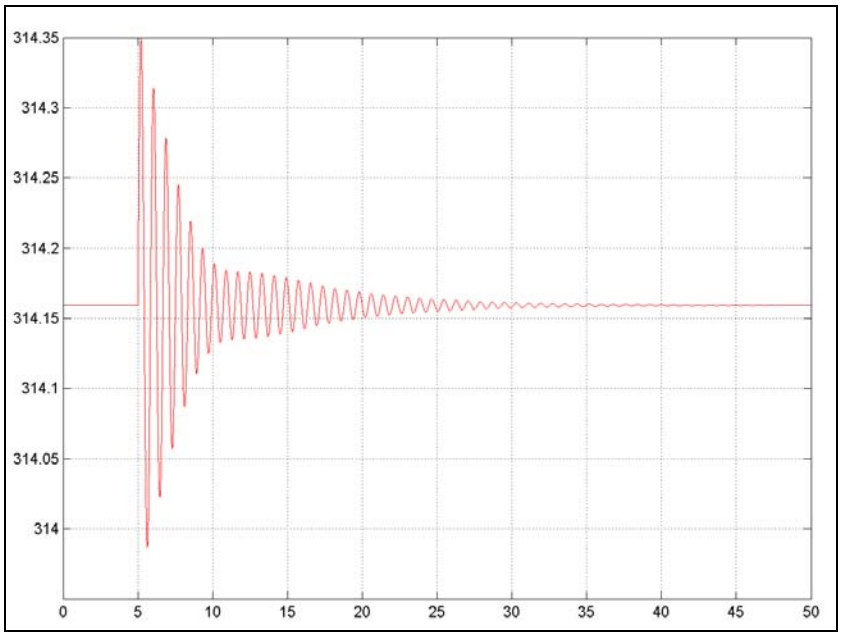

Figure 57
Rotational speed of the SM 2 in the Test 1 with the regulator based on the divergence [rad s^{-1}].

TEST 2 WITH THE REGULATOR BASED ON THE DIVERGENCE

Applying a sinusoidal perturbation to the SM 1 and a torque step to the SM 2, the oscillations generated (especially those due to the step) induce the regulator to initially supply/absorb the maximum allowed power (Figure 58). After a few seconds from the disturbance, such power takes a sinusoidal trend: the storage system absorbs energy when the SM 1 exceeds its synchronism speed, while it supplies energy when the generator is slowing down. Because of the reduced frequency of the disturbance, the derivative block of the regulator intervenes in a much moderated way, compared to the proportional block.

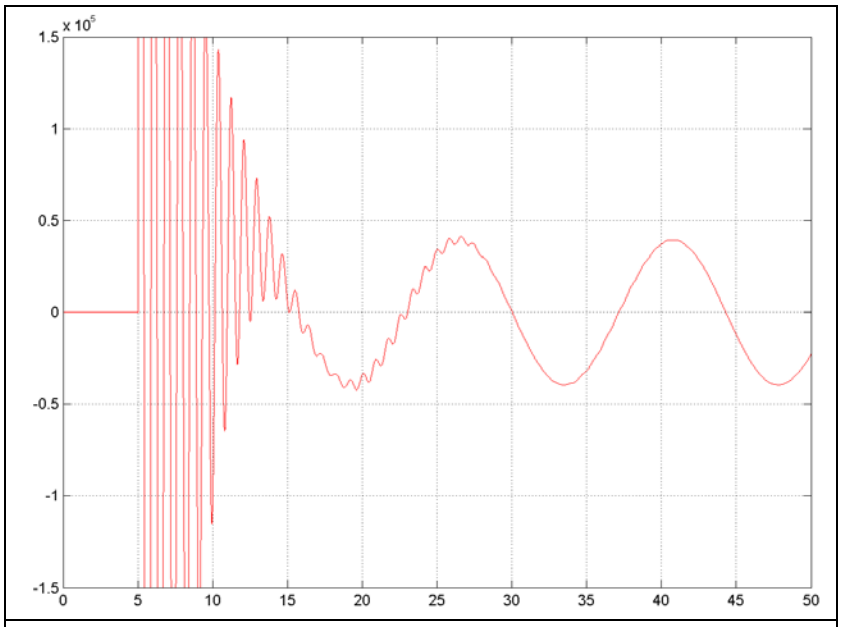

Figure 58
Power absorbed by the storage device in the Test 2 with the regulator based on the divergence [W].

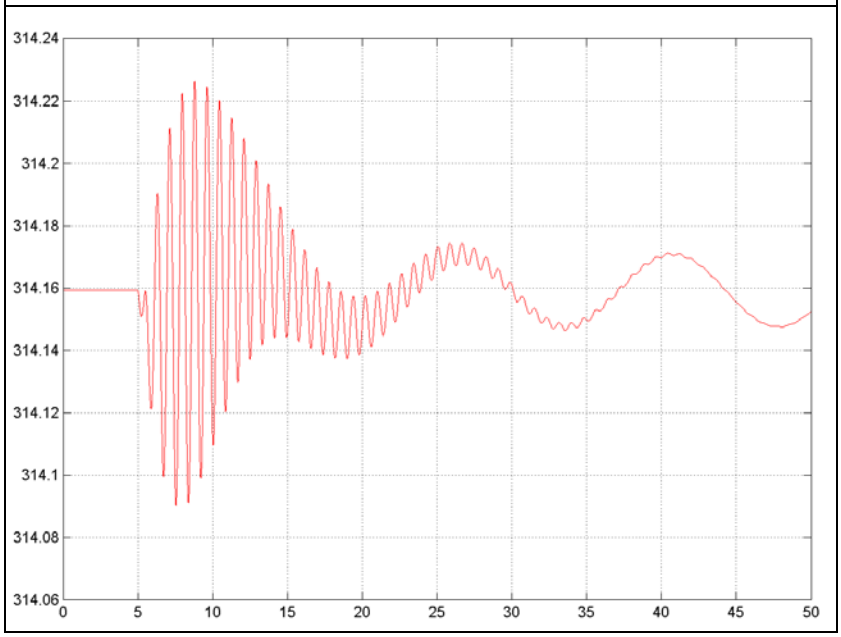

Figure 59
Rotational speed of the SM 1 in the Test 2 with the regulator based on the divergence [rad s^{-1}].

The speed of the SM 1 benefits in a substantial way of the storage system's action (Figure 59) as regards the case without the use of the latter (Figure 29), passing from an oscillatory trend included between *314.08* and *314.25 Hz* to one included between *314.09* and *314.23 Hz*. The time necessary to damp these oscillations remains practically unchanged.

As in the previous test, the peak value of the SM 2 oscillations will not show any benefit (Figure 60) compared to the case without regulator (Figure 30): however, the damping in the final stages of the disturbance improves.

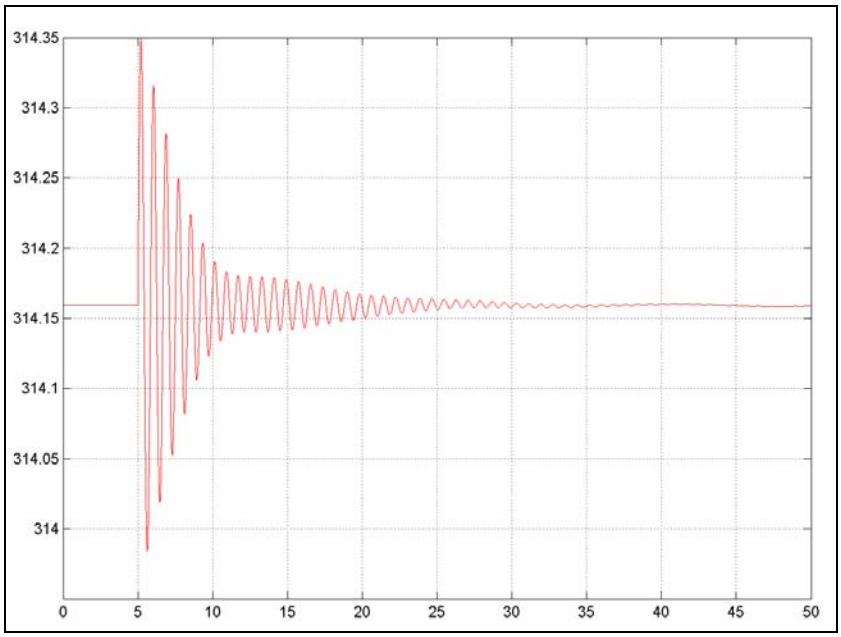

Figure 60
Rotational speed of the SM 2 in the Test 2 with the regulator based on the divergence [rad s^{-1}].

TEST 3 WITH THE REGULATOR BASED ON THE DIVERGENCE

In the test, the simulation previously carried out applying to the generators' torques two sinusoidal perturbations in anti-phase is reported. The regulator driven by the divergence is now introduced.

The rotational speed of the machines tends, as already seen, to be equal and opposite, so the resulting divergence of the system differs little from the nominal value and also the power output supplied by the storage device is limited (Figure 61). From the comparison between the speed trends of the two SMs with regulator (Figure 62 and Figure 63) and those without (Figure 41 and Figure 42), it is noticeable that such device does not introduce an appreciable improvement in the system's behavior.

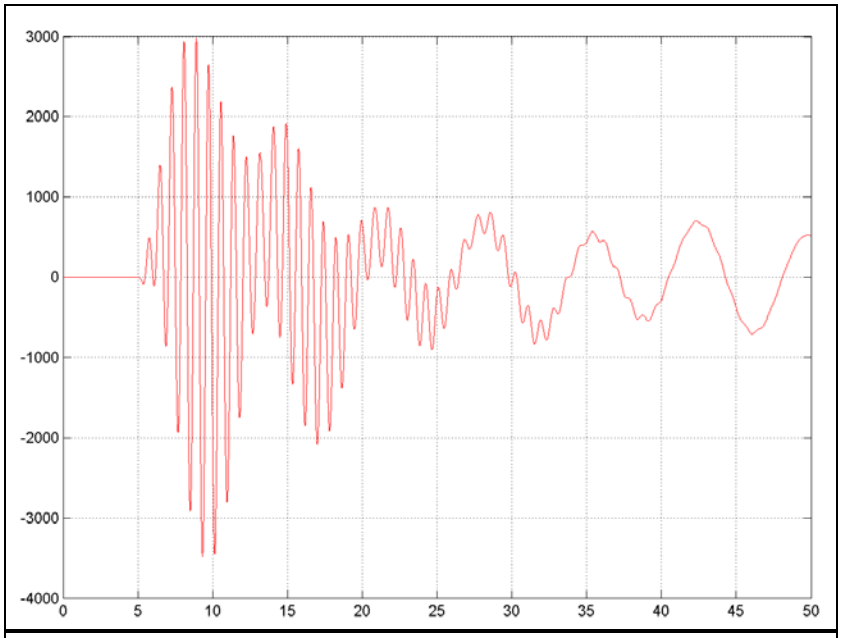

Figure 61
Power absorbed by the storage device in the Test 2 with the regulator based on the divergence [W].

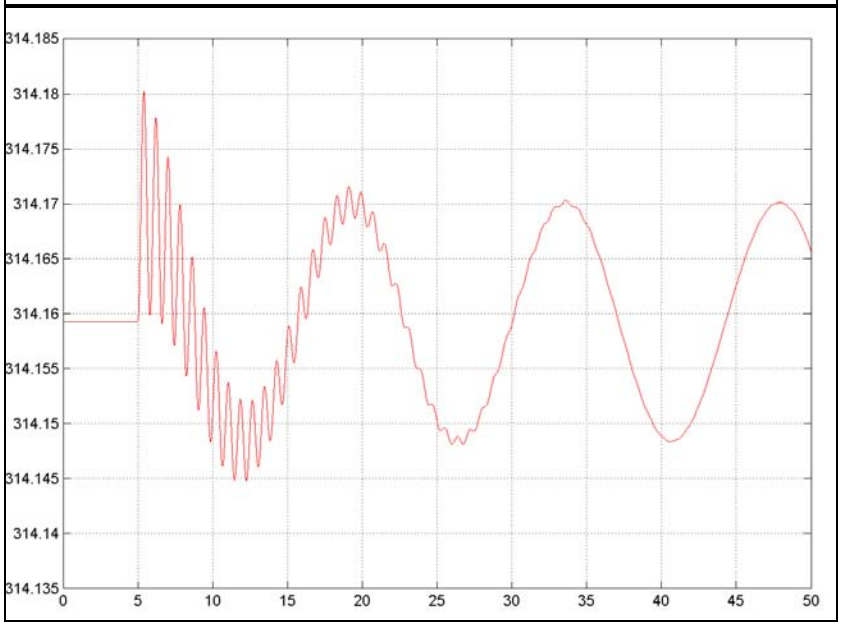

Figure 62
Rotational speed of the SM 1 in the Test 3 with the regulator based on the divergence [rad s^{-1}].

It should be noted that, in terms of divergence, the case with equal and opposite perturbations is the worst for the regulator. The fact that it does not introduce deterioration in the generators

dynamics should therefore be considered as a very positive outcome. Moreover, given the torques applied, the system does not require further injections/withdrawals of active power (the natural power exchange between the two SMs is exactly what is needed to both to damp their fluctuations), it is appropriate that the regulator is not unnecessary stressed by the introduction of energy into the network.

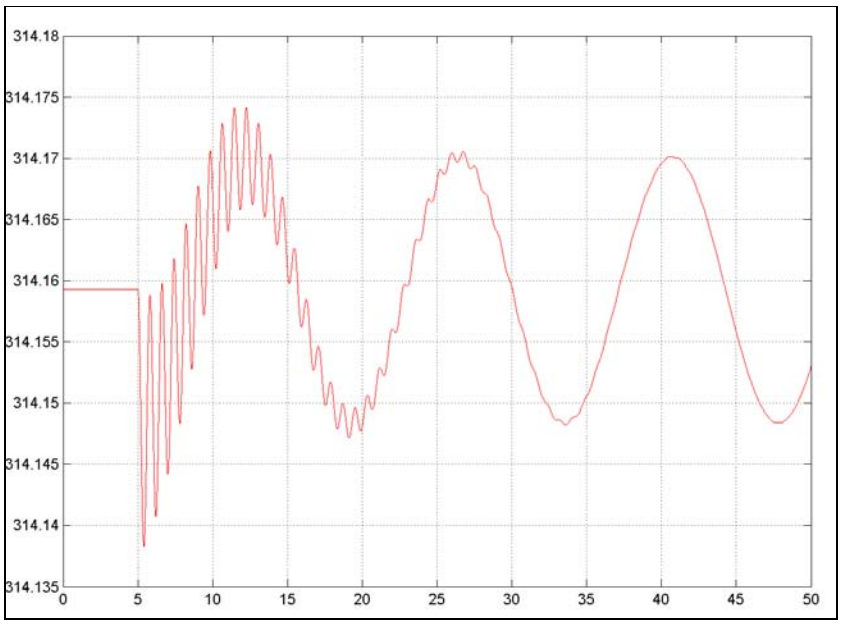

Figure 63
Rotational speed of the SM 2 in the Test 3 with the regulator based on the divergence [rad s^{-1}].

11. SIMULATIONS WITH A STORAGE DEVICE DRIVEN BY LOCAL QUANTITIES

A storage system not longer driven by the divergence, but driven only by local quantities, is now introduced. In particular, the only quantity used by the device is the rotational speed of the generator in the installation bus of the capacitor, i.e., of the SM 2.

For the realization of this regulator the ω_{m2} was converted in *p.u.* referring to its rated value:

$$\omega_{m2pu} = \frac{\omega_{m2}}{\omega_0} \tag{20}$$

It was then provided as input to a controller at all similar to the previous one (Figure 64).

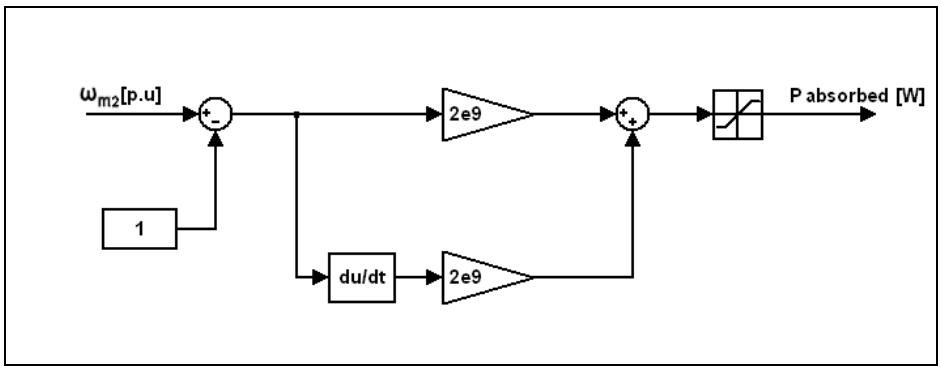

Figure 64
Principe scheme of the regulator based on local quantities.

It is expected that the use of a device like this may degrade the overall behavior of the system, being unable to consider the trend of the mechanical quantities of the other machine connected to the network. On the other hand, it is reasonable to expect an improvement of the situation for the SM 2, since now a dedicated storage system is in place. In fact, getting in input only the generator rotational speed, the regulation device should be more able to mitigate the effects of torque disturbances on it.

TEST 1 WITH THE REGULATOR BASED ON LOCAL QUANTITIES

Subsequently to a torque step on the SM 1, in the first phases after the disturbance, the storage device tends to provide/absorb all the power available (Figure 65). After that, the power it supplies to the network is reduced, but less rapidly than as occurred with the use of the divergence operator.

The mechanical speed of the SM 1 does not experience any improvement compared to the case without controller (Figure 9) and, indeed, it also requires now a longer transition before returns to the nominal value (after *45 s* from the step it is still oscillating in a non-negligible way) (Figure 66).

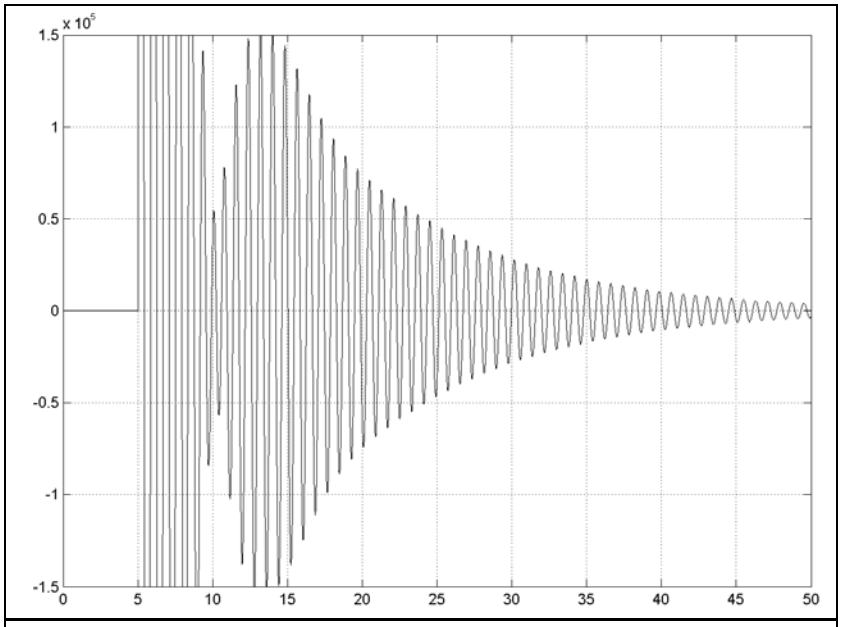

Figure 65
Power absorbed by the storage device in the Test 1 with the regulator based on local quantities [W].

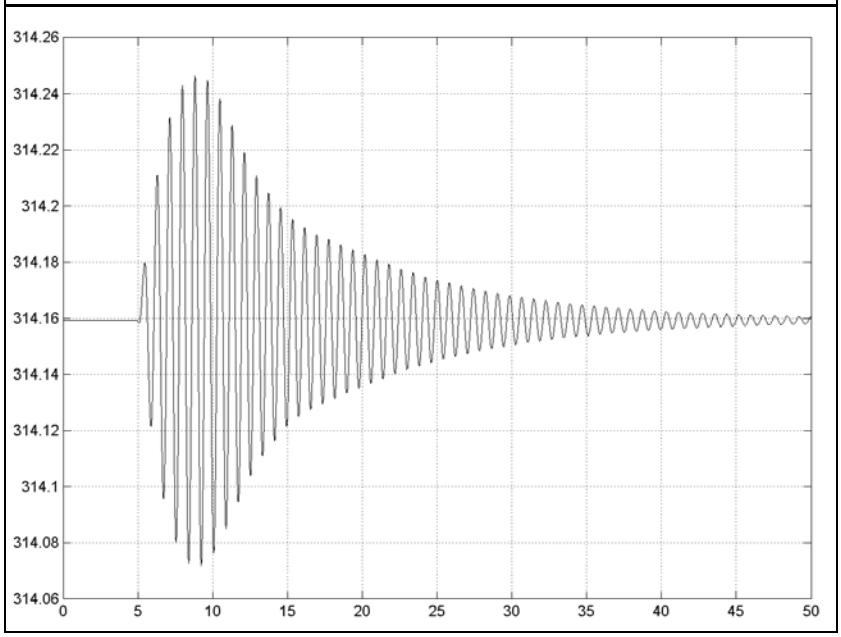

Figure 66
Rotational speed of the SM 1 in the Test 1 with the regulator based on local quantities [rad s^{-1}].

The SM 2 improves its behavior, but in a less significant way than expected (Figure 67). The peak value of the disturbance remains unchanged, whereas, after a few seconds from the disturbance, its amplitude is slightly decreased compared to the case without regulator (Figure 10).

Moreover, the simulations carried out with the storage system driven by the divergence highlighted better dynamics both for SM 1 (Figure 56) and for SM 2 (Figure 57). There was indeed a faster damping of the magnitudes, compared with this regulator.

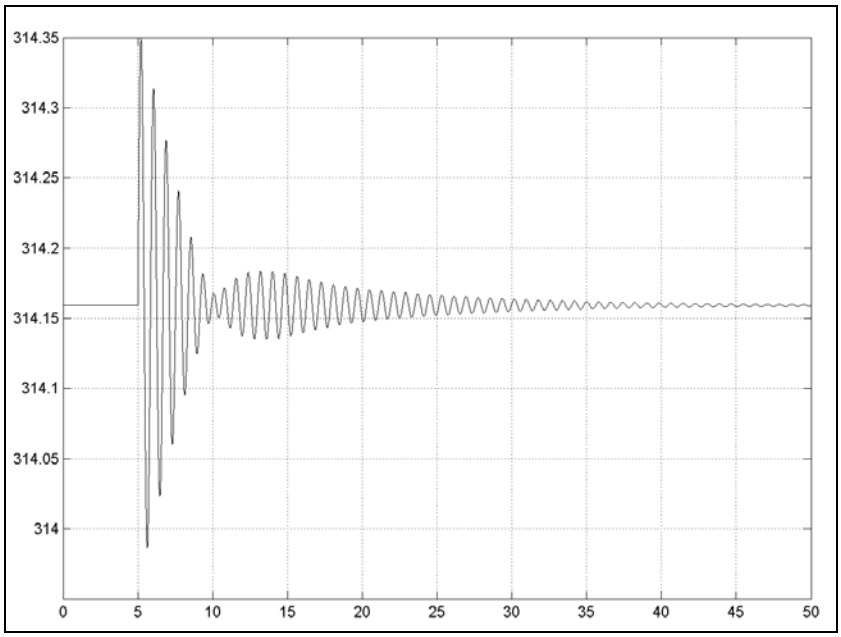

Figure 67
Rotational speed of the SM 2 in the Test 1 with the regulator based on local quantities [rad s^{-1}].

TEST 2 WITH THE REGULATOR BASED ON LOCAL QUANTITIES

Due to the torque step applied to the rotor of the machine connected to the same bus of the storage system, the system alternately absorbs and delivers the maximum available power (Figure 68). Contrary to what happens in the tests carried out using the divergence (Figure 58), in this case, the rebound of electrical energy takes a less sinusoidal characteristic (the sinusoidal torque is applied to the other machine and then the regulator perceives its effects indirectly), but with much strong and less damped oscillations.

The SM 1 engine speed characteristic (Figure 69) is in this case worsened, compared to both cases, i.e. to the situation without regulator (Figure 29) and to the situation with the regulator based on divergence (Figure 59).

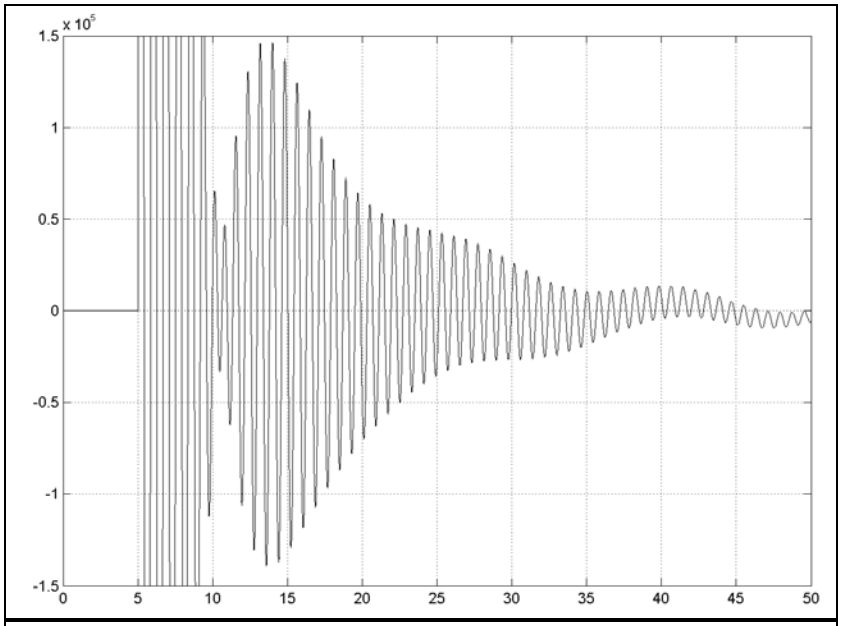

Figure 68
Power absorbed by the storage device in the Test 2 with the regulator based on local quantities [W].

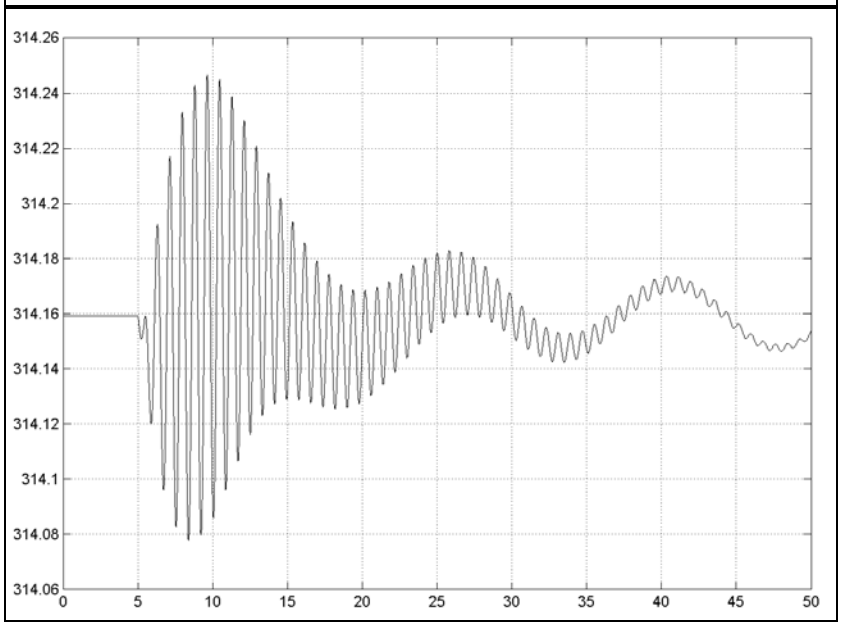

Figure 69
Rotational speed of the SM 1 in the Test 2 with the regulator based on local quantities [rad s^{-1}].

The SM 2 mechanical speed (Figure 70) retains its peak value again unchanged as regards to the previous cases (Figure 30 and Figure 60). The damping time is rather improved and comparable to the one achieved by the regulator based on divergence.

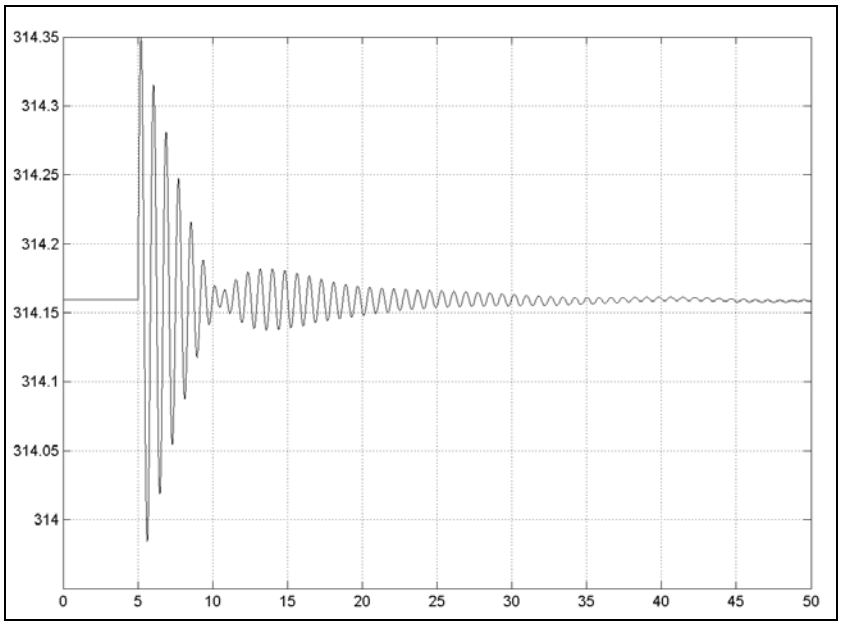

Figure 70
Rotational speed of the SM 2 in the Test 2 with the regulator based on local quantities [rad s^{-1}].

TEST 3 WITH THE REGULATOR BASED ON LOCAL QUANTITIES

In this simulation, during the first phases of the disturbance the storage device tends to absorb power (Figure 71) to slow down the SM 2. In fact, the only information available to the storage device is its rotational speed and the latter is subject to an initial increase caused by the sinusoidal torque applied. Subsequently, a not damped sinusoidal energy rebound between the generator and the network triggers. Comparing this simulation with the test based on divergence (Figure 61), the device is now unnecessarily subject to a much higher stress. As mentioned earlier, in this case the SMs exchange autonomously the electrical energy without any necessity of external interventions.

Also the engine speed characteristic of the SM 1 is worse using only local quantities (Figure 72), both as regards the case of the regulator based on the divergence (Figure 62), but even for the case without any stabilizing device (Figure 41). In the present test, in fact, there is a slight increase of the initial peak of the oscillations, but especially, they are less damped than those of the previous simulations.

Finally, the speed oscillations of the SM 2, being subject to a much better damping, improve (Figure 73) as regards the previous cases (Figure 42 and Figure 63).

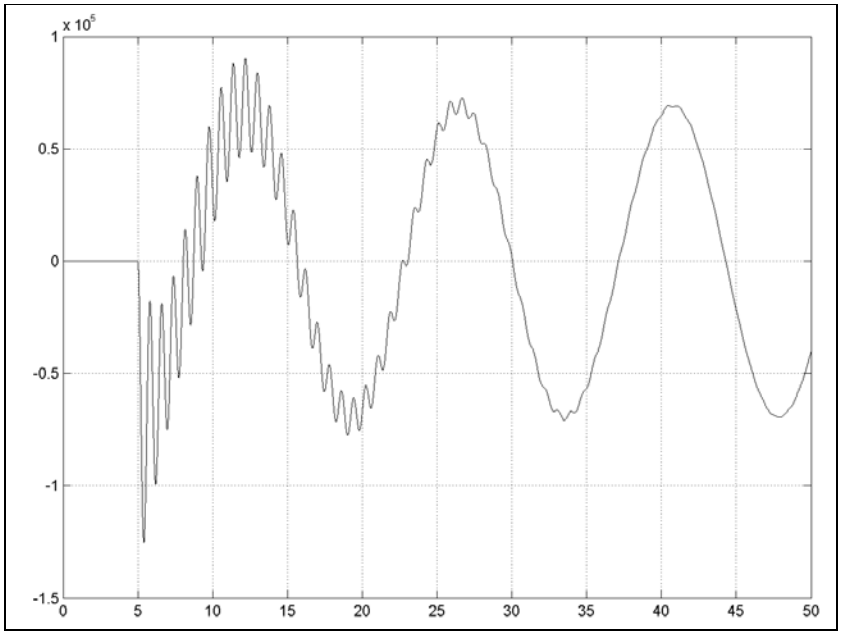

Figure 71
Power absorbed by the storage device in the Test 3 with the regulator based on local quantities [W].

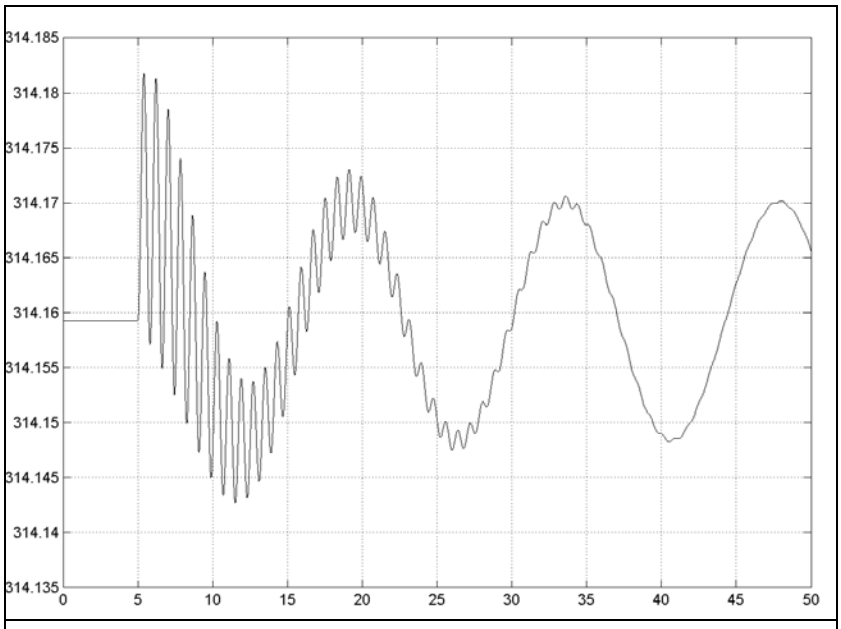

Figure 72
Rotational speed of the SM 1 in the Test 3 with the regulator based on local quantities [rad s^{-1}].

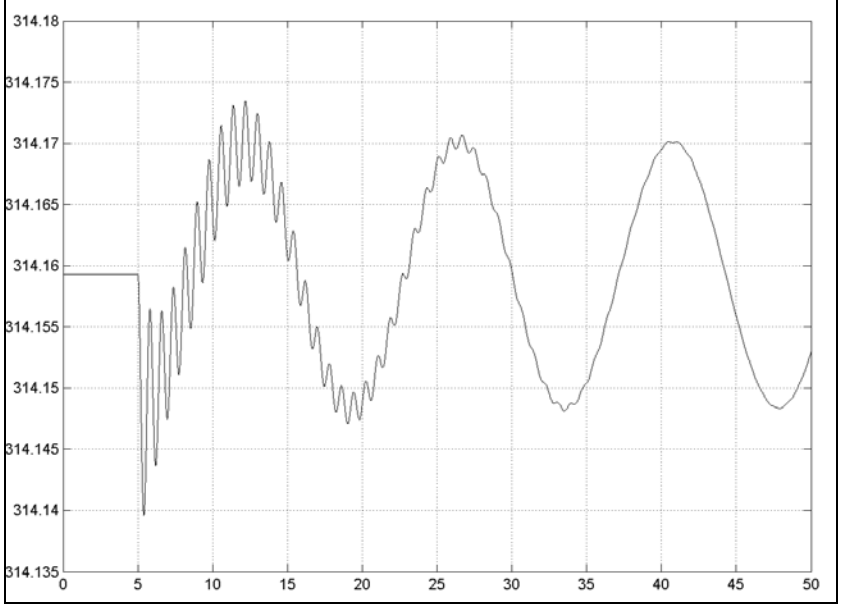

Figure 73
Rotational speed of the SM 2 in the Test 3 with the regulator based on local quantities [rad s^{-1}].

12. PHASE SPACE DIVERGENCE RECONSTRUCTION

Being the divergence a local property which is preserved under phase space reconstruction, it has several properties that make it particularly appropriate for transient dynamical systems, as electrical networks. Furthermore, it can be reconstructed from experimental data, without the need to know the differential equations of the system (Strozzi et al., 1999; Bosch et al., 2004a) using the embedding theory.

The divergence of the flow, which is the trace of the Jacobian, measures the rate of change of an infinitesimal phase space volume $V_{ps}(t)$, following an orbit $x(t)$. In this case, Liouville's theorem (Arnold, 1973) states that:

$$V_{ps}(t) = V_{ps}^{i} \cdot \exp\left[\int_0^t div\{\mathbf{F}[\mathbf{x}(\tau)]\}d\tau\right] \tag{21}$$

where:

$$div\{\mathbf{F}[\mathbf{x}(t)]\} = \frac{\partial F_1[\mathbf{x}(t)]}{\partial x_1} + \frac{\partial F_2[\mathbf{x}(t)]}{\partial x_2} + \ldots + \frac{\partial F_d[\mathbf{x}(t)]}{\partial x_d} \tag{22}$$

However, using Eq. (21), it is also possible to write (Strozzi et al., 1999):

$$div = \frac{\dot{V}_{ps}(t)}{V_{ps}(t)} \tag{23}$$

To calculate the phase-space volume and its change, we need to apply embedding theory. The embedding theory is a way to move from a temporal time series of measurements, $s(t)=h[\mathbf{x}(t)]$, which is related to the state variables by a unknown function, h, to a phase space similar -in a topological sense- to that of the underlying dynamical system we are interested in analysing. Techniques of phase space reconstruction were introduced by (Packard et al., 1981; Takens, 1981), who showed it is possible to address this problem using time delay embedding vectors of the original measurements, for example: $\{s(t), s(t-\Delta t), s(t-2\Delta t),\ldots, s(t-(d_E-1)\,\Delta t)\}$.

The extension of this theory for the case of electrical grids is complicated by the dynamic nature (nonstationarity) of the system that implies that embedding parameters, i.e. time delay, Δt (the lag between data when reconstructing the phase space), and embedding dimension, d_E (the dimension of the space required to unfold the dynamics) are changing during the process. However, as it was discussed in Zbilut et al. (2002) an appropriate value for these parameters can be chosen to allow phase space reconstruction. Furthermore, several methods of reconstruction may be used: time delay embedding vectors, derivative coordinates and integral coordinates (Bosch et al., 2004b). However, the more robust reconstruction approach against noise is the one based on delayed vectors of some measured variable, in this case of the speeds of the rotors: ω_1 *and* ω_2 , i.e. $\{\omega_i(t),\omega_i(t-\Delta t),\ldots\}$ (Bosch et al., 2004b) or a combination of both values (Zaldívar et al.,2005) have been chosen as the measured variables. However, it is always possible to

reconstruct the phase space using other representative variables as it has been showed in Bosch et al (2004c).

Numerically, $V_{ps}(t)$ may be calculated, assuming that the time step from one point to another in the time series is short enough that the Jacobian of the system has not substantially changed, using the determinant of the matrix obtained from close points in phase space as (Bosch et al., 2004b):

$$V_{ps}(t) = \left| \det \begin{bmatrix} \omega(t) - \omega(t-\Delta t) & 0 \\ 0 & \omega(t-\Delta t) - \omega(t-2\Delta t) \end{bmatrix} \right| \tag{24}$$

for an embedding dimension of two. $\Delta V_{ps}(t)$ and the derivative may be easily calculated as:

$$\dot{V}_{ps}(t) = \frac{\Delta V_{ps}(t)}{h} = \frac{V_{ps}(t) - V_{ps}(t-h)}{h} \tag{25}$$

where h is a convenient time step. However, other numerical approximations to the derivative can also be chosen (Burden and Faires, 1996).

- Selection of the reconstruction parameters: time delay and embedding dimension

In this work as the system converges to a fixed point (state space dimension 0), we have selected $d_E = 2$, and $\Delta t = 0.15$ for the reconstruction, and $h = 0.06$ for the calculation of ΔV_{ps}.

As an example, Figure 74, 75 and 76 show the values obtained for three different cases. Even though V_{ps} and ΔV_{ps} are dynamically similar to the analytical divergence, there are some numerical problems when calculating $V_{ps} / \dot{V}_{ps}$, Eq. (23). This has been already discussed in Bosch et al. (2004a) as an inherent property of dissipative dynamical systems that tend to contract state space volume like in the simulated cases, where from oscillations (limit cycle of dimension 2) we pass to a fixed point (dimension 0) as the oscillations disappear. In such cases it is advisable to use V_{ps} and ΔV_{ps} separately in the control strategy (Zaldívar et al., 2005b).

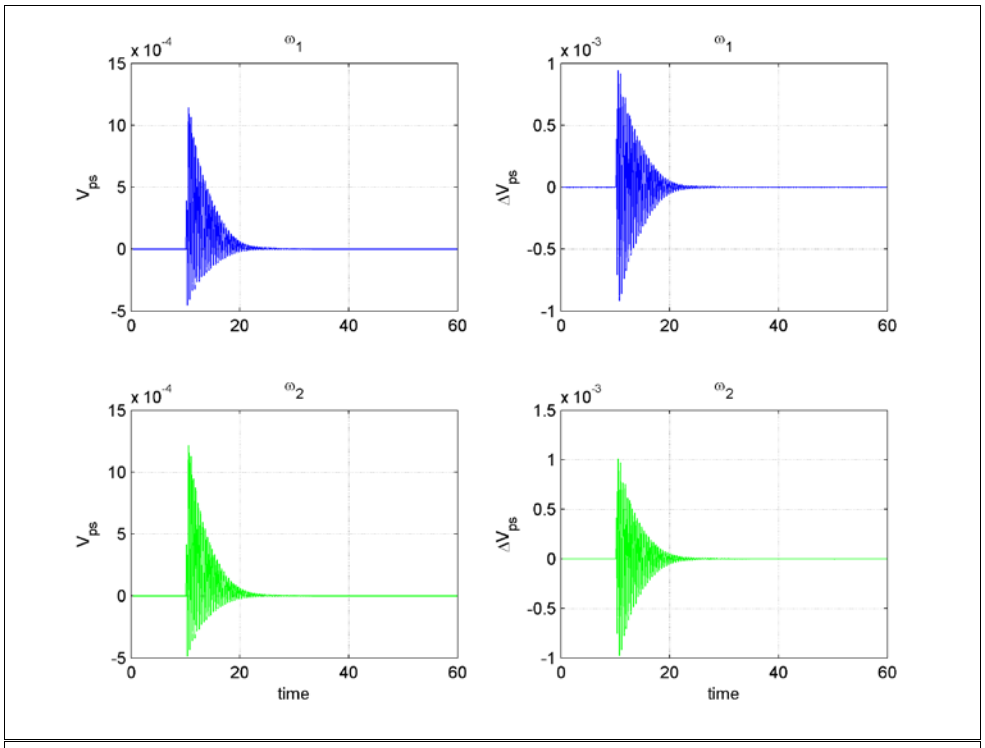

Figure 74

Phase space volume, V_{ps}, and its variation, ΔV_{ps}, as a function of ω_1 and ω_2 for Test 1 without regulation. Notice that *div* may be calculated using Eq. (23).

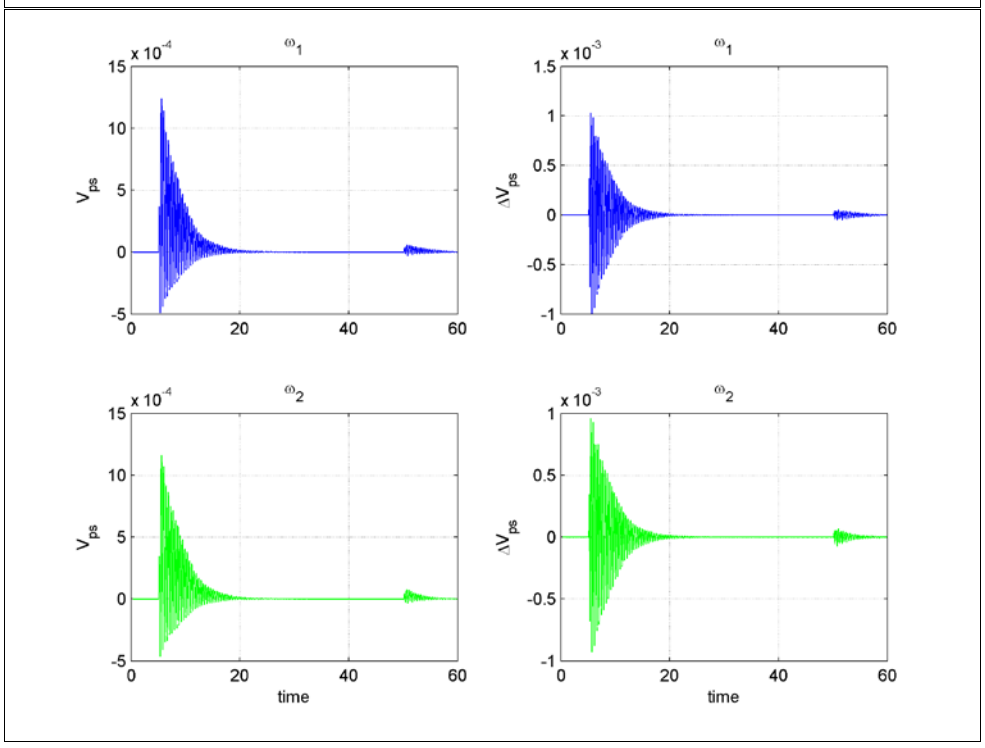

Figure 75

Phase space volume, V_{ps}, and its variation, ΔV_{ps}, as a function of ω_1 and ω_2 for Test 2 without regulation.

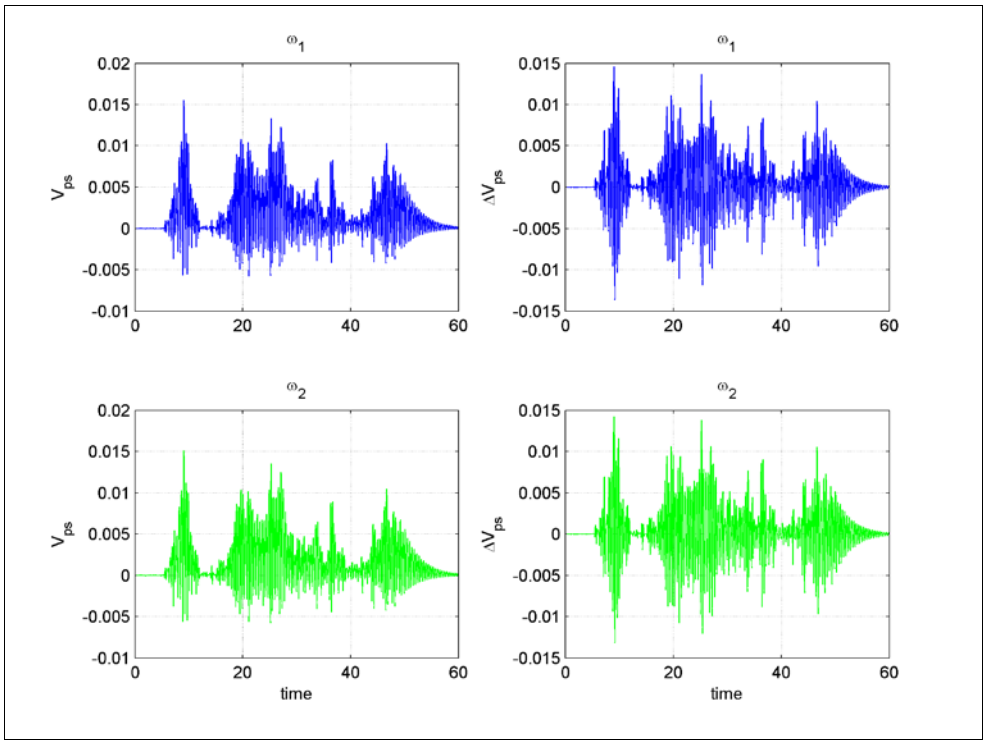

Figure 76
Phase space volume, V_{ps}, and its variation, ΔV_{ps}, as a function of ω_1 and ω_2 for Test 4 described in Appendix A.

13. CONCLUSIONS

In this study a model to represent an electrical system made up of a MV microgrid connected to the HV network, its generators and its utilities, was developed. The model was then used to evaluate the effectiveness of the divergence as indicator of the overall power system's stability, able to assure better performances than the present regulation devices.

The comparison between the regulation based on the divergence and that made by local quantities (rotational speed of a generator) has shown that the use of the divergence ensures significantly better results. The regulators driven by local quantities increase the stability of the machine to which the monitored quantities refer, but they do not possess the knowledge of the effects that their actions have on the rest of the network (i.e. the other generators). Local controllers since they monitor a single quantity of one generator, allow maximizing the benefits on this generator, obtaining, for the machine considered, better results than using the divergence, at the price of worse performance on the whole grid.

Let us consider the situation where a generator is accelerating and the other is slowing due to two torque disturbances of opposite sign. If driven by the engine speed of the accelerating SM, a traditional regulator will tend to absorb electric power, causing damage to the other SM, which will slow down further. The regulator driven by the divergence will instead be able to avoid this phenomenon, not intervening in a situation like this (and then allowing the generators to exchange the electrical energy needed to return to the synchronism speed) or acting only marginally if there is a difference in the rotational speed changes of the two generators.

For the stability purpose the overall power system dynamics are certainly more important than the dynamics of a single machine: the results achieved using the divergence are much preferable that those obtained using local quantities.

Moreover, the reduction of the generators' rotational speed oscillations obtained introducing the storage device are small due to the reduced size of the device itself. In fact, having adopted a storage system with a rated power equal to 5% of the power of each generator, it will have limited performances. It is reasonable to assume that increasing the size will permit a stronger regulation, able to introduce higher benefits for the system. Also, no specific damping function was implemented in the adjusting device, which would certainly improve the performances.

The potential of this study, besides the determination and the assessment of the divergence operator, is also in the realization of the model by the Simulink software. That model, resulting from the coupling of the dynamic equations system of the machines with the dynamic equations of the load flow, can easily be applied to other cases of interest, with different network topology, generators and utilities. It can also be used in simulations where not only the torque applied to the synchronous machines is modified, but also other quantities of the system. In fact, it should be possible to evaluate the electrical system behavior in presence of a rearrangement of the network: in this case it is enough change the admittances matrix used in the load flow by that related to the

network after the rearrangement. Similarly, it is also possible to consider the effect of the load power absorption. That would cause again a modification of the terms on the main diagonal of the admittances matrix. Several others studies are possible with this model: they are all feasible by altering the model built here just in a marginal way.

Finally, the possibility to reconstruct the divergence using simulated variables has been assessed. The fact that it is not necessary to have the model of the system for calculate this value on real-time opens the possibility for the application of this global control strategy to electric grids. This could allow to a reduction of costs and an increase of performance in electrical networks when compared with “traditional” regulators schemes in which there is no a global view of how the system behaves and where the action in one part can compromise the overall performance of the system. Our future work will continue along these lines by trying to develop a real divergence-based controller and trying to assess its performance under more realistic environments.

14. APPENDIX A

This Appendix shows the results of a further series of tests, posted here for a better readability. Besides, only the rotational speeds of the two generators are reported, since they represent the most important quantities for the power system stability.

In the graphs below, to indicate whether or not the regulator is present and how it operates, the following convention is used:

- Blue: absence of the regulator;
- Red: regulator based on the divergence;
- Black: regulator based on the rotational speed of SM 2.

A list of the simulations reported in the appendix, with the relative torque characteristics of both generators and possible notes, is given in Table 2.

	Synchronous machine 1				Synchronous machine 2			
Test number	Type	Amplitude [*p.u.* related to C_n]	Frequency [*Hz*]	Notes	Type	Amplitude [*p.u.* related to C_n]	Frequency [*Hz*]	Notes
1	Normal	0,01	5		Normal	0,01	5	
2	Normal	0,005	5		Normal	0,005	5	
	Sinusoidal	0,05	0,07	Phase: -1,7·π	Sinusoidal	0,05	0,07	Phase: -0,7·π
3	Normal	0,05	0,333		Normal	0,05	0,333	
	Normal	0,005	20		Normal	0,005	20	
4	Normal	0,05	0,333		Normal	0,05	0,333	
5	Sinusoidal	0,05	0,07	Phase: -1,2·π Applied at 8,571 s	Sinusoidal	0,05	0,07	Phase: -0,7·π

Table 2 – Simulations reported in the Appendix A.

TEST 1

Torques applied to the synchronous machines 1 and 2

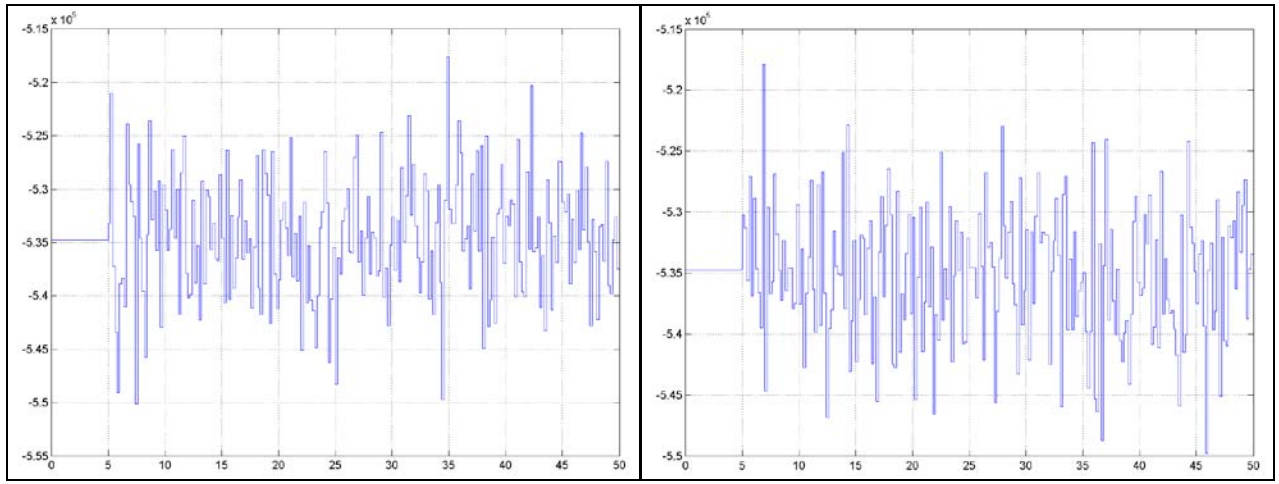

Mechanical speed of the synchronous machine 1

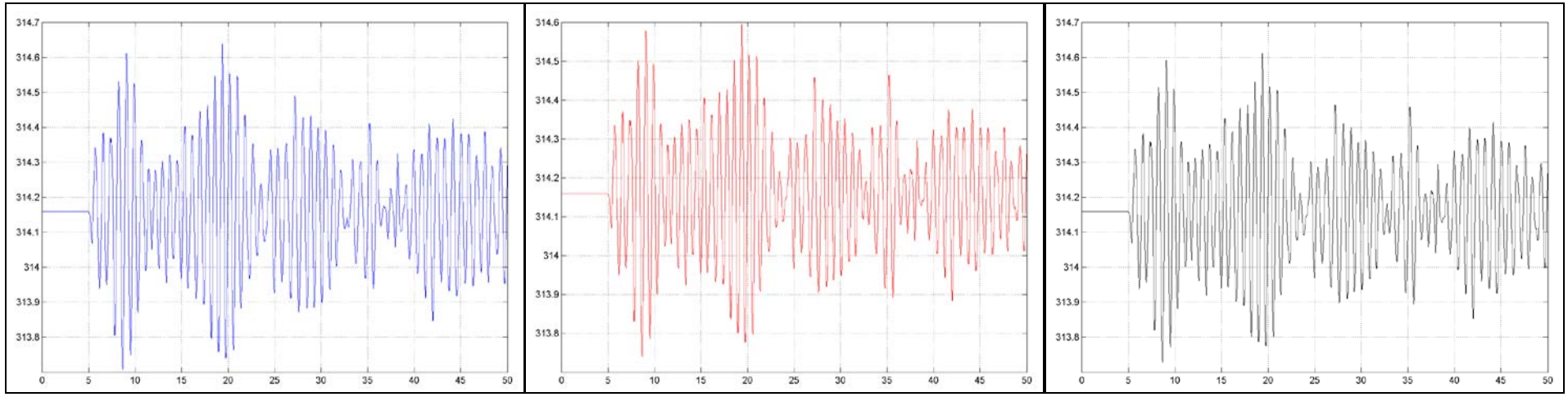

Mechanical speed of the synchronous machine 2

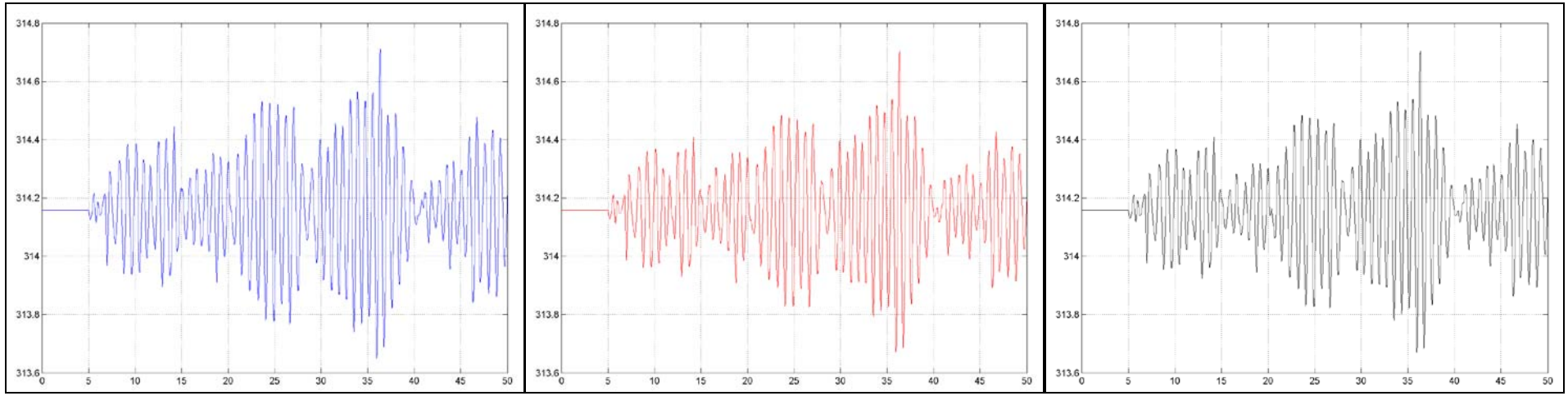

TEST 2

Torques applied to the synchronous machines 1 and 2

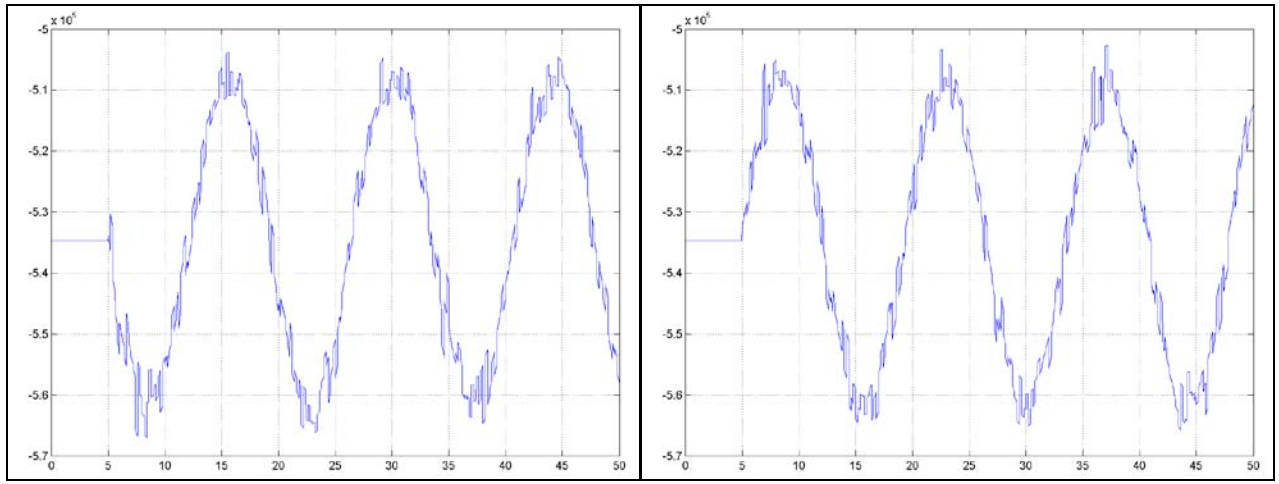

Mechanical speed of the synchronous machine 1

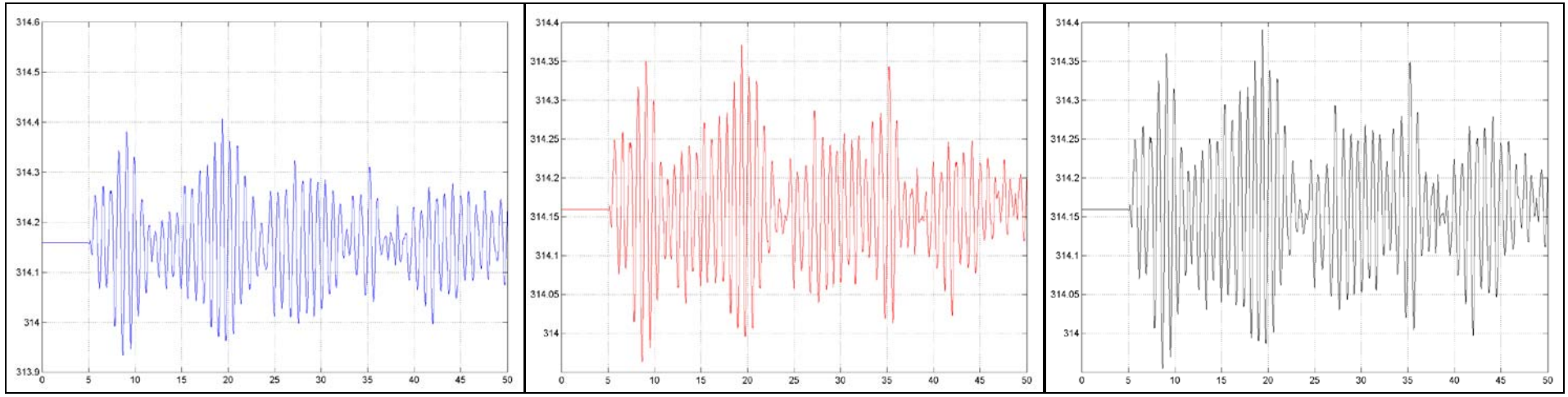

Mechanical speed of the synchronous machine 2

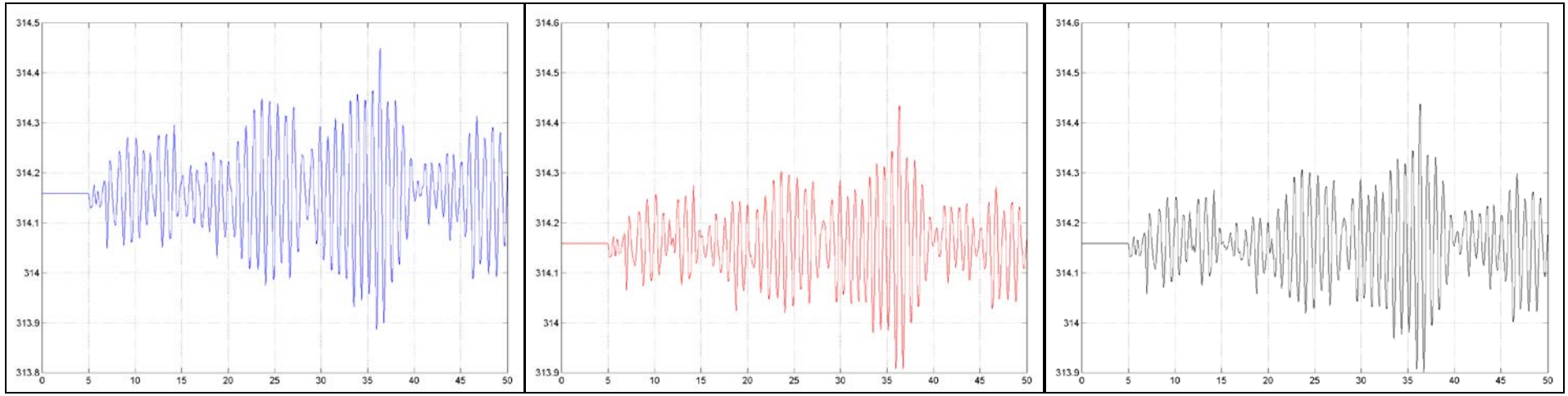

TEST 3

Torques applied to the synchronous machines 1 and 2

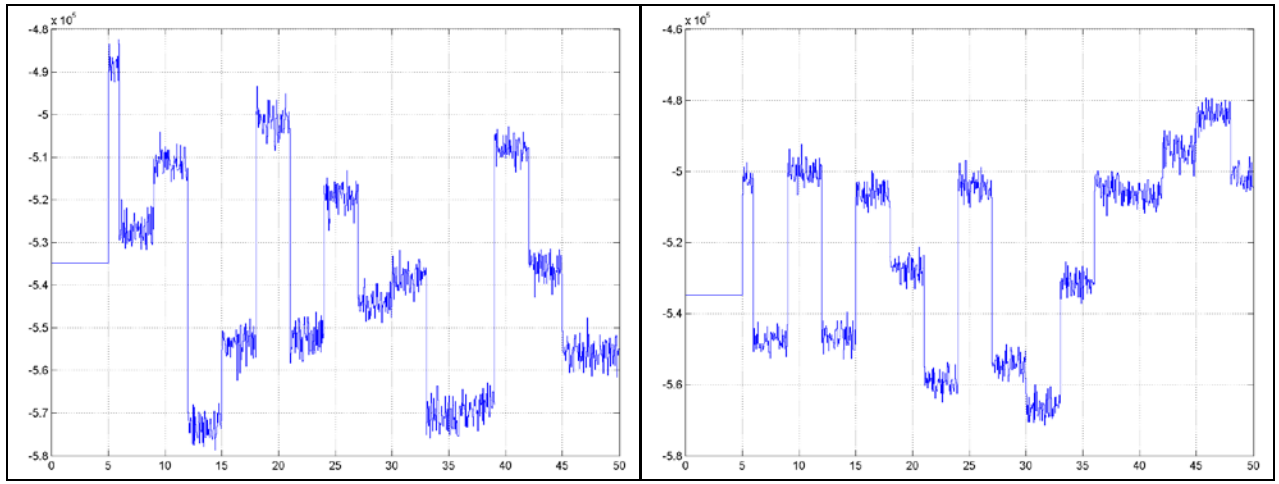

Mechanical speed of the synchronous machine 1

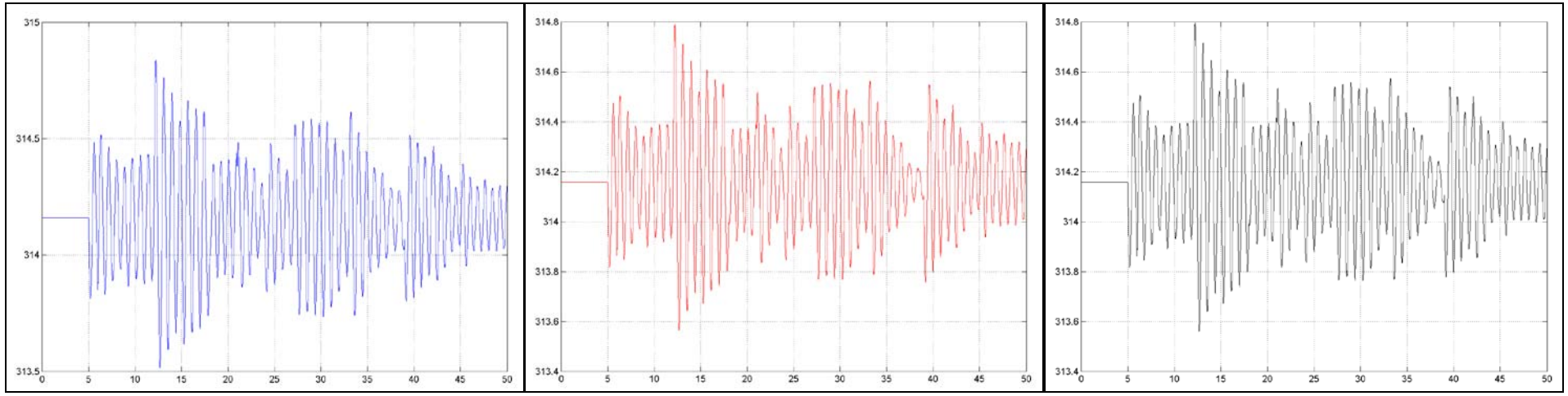

Mechanical speed of the synchronous machine 2

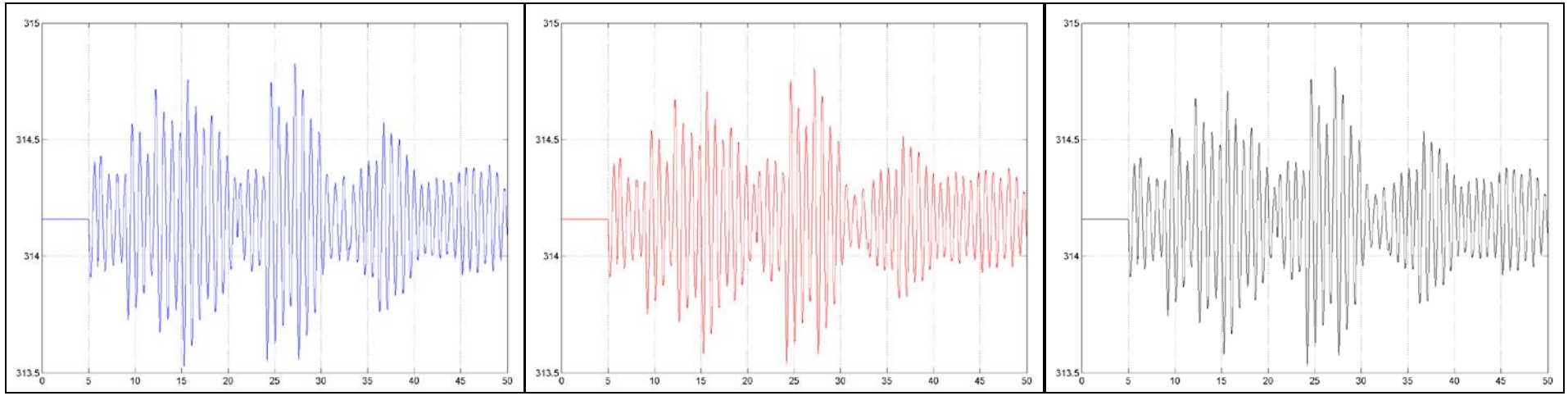

TEST 4

Torques applied to the synchronous machines 1 and 2

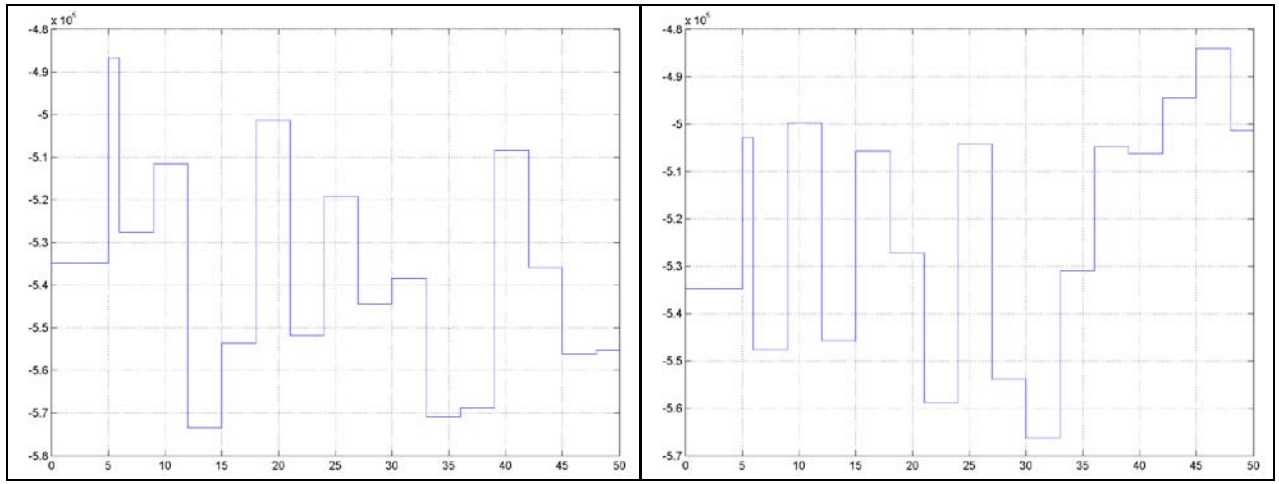

Mechanical speed of the synchronous machine 1

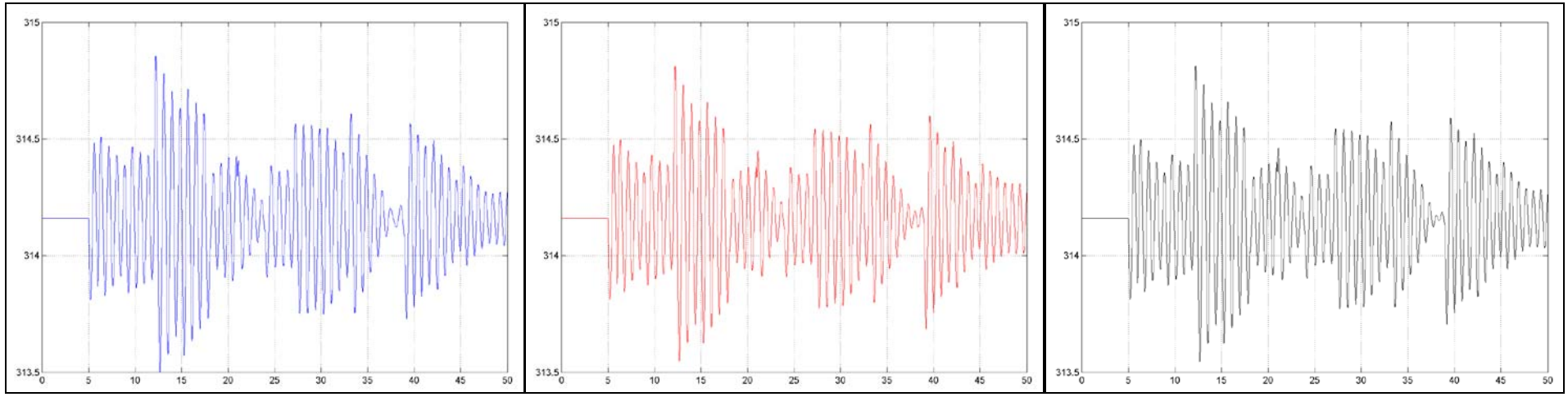

Mechanical speed of the synchronous machine 2

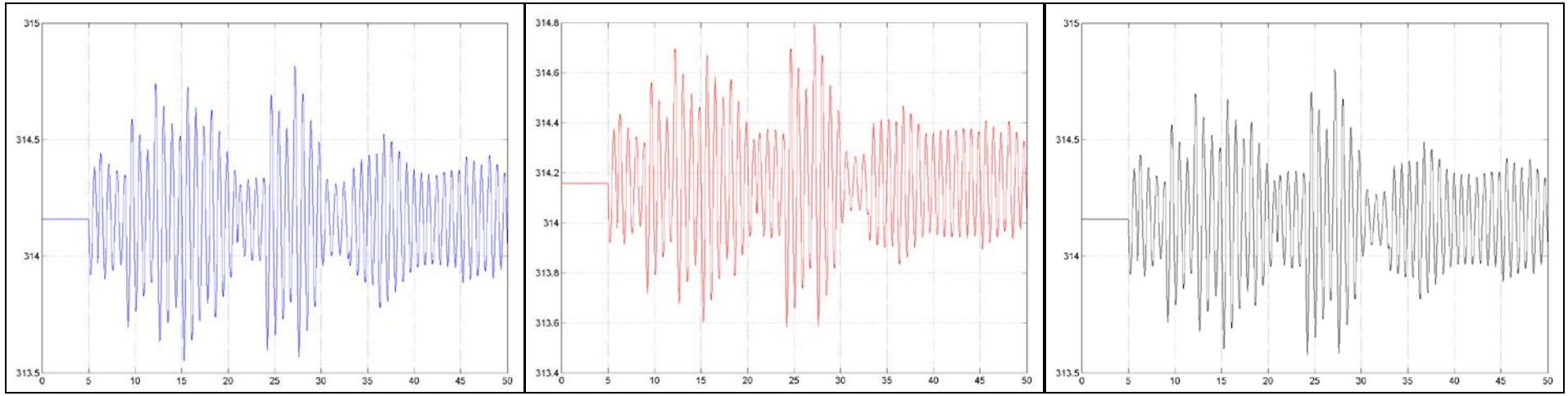

TEST 5

Torques applied to the synchronous machines 1 and 2

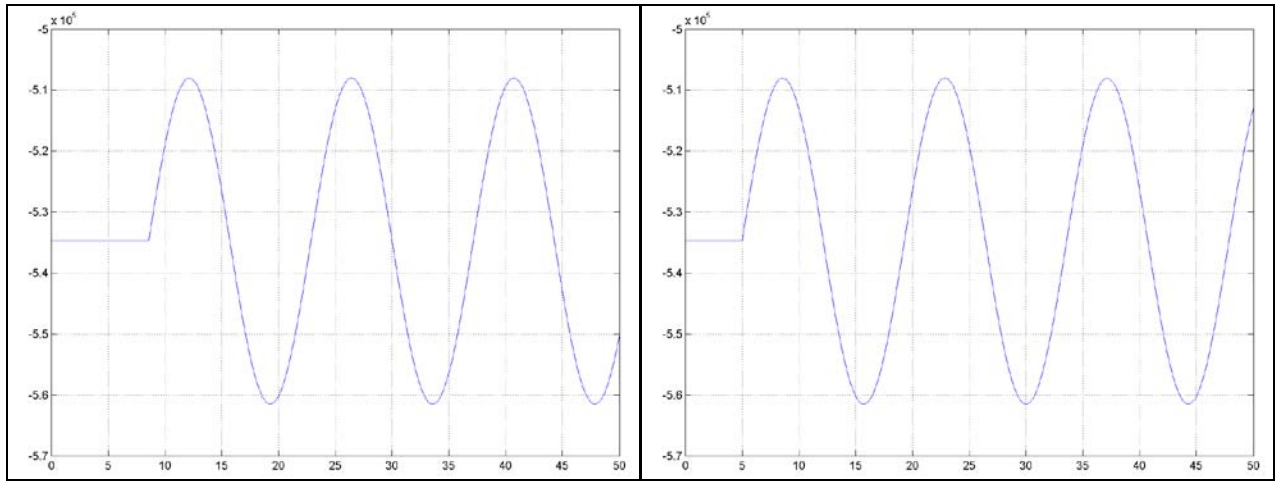

Mechanical speed of the synchronous machine 1

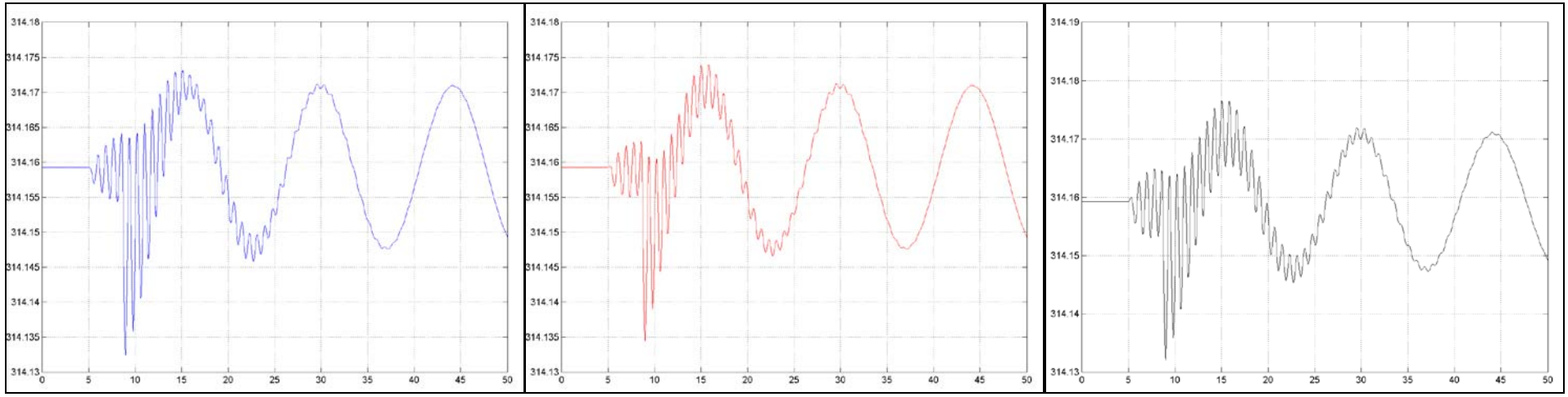

Mechanical speed of the synchronous machine 2

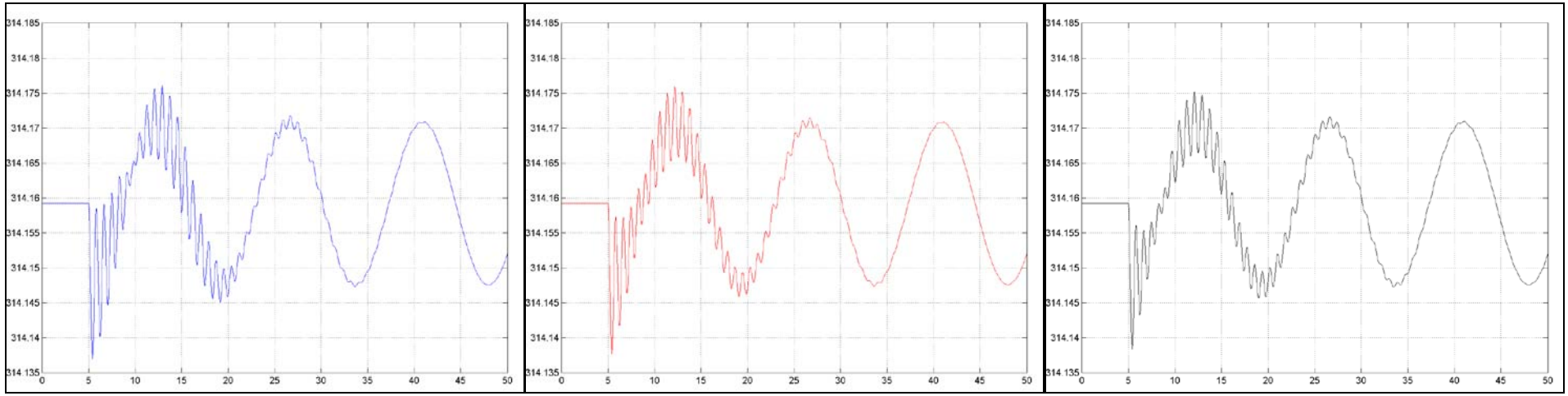

15. BIBLIOGRAPHY

Arnold, V. I., 1973, Ordinary differential equations, MIT Press, Cambridge.

Bosch J., Kerr, D. Snee, T. J., Strozzi, F. and Zaldívar, J. M., 2004a, Runaway detection in a pilot plant facility. Ind. Eng. Chem. Res. 43: 7019-7024.

Bosch, J., Strozzi, F., Zbilut, J. P., Zaldívar, J. M., 2004b, On line application of the divergence criterion for runaway detection in isoperibolic batch reactors: Simulated and experimental results. Computers Chem. Eng., 28: 527-544.

Bosch J., Strozzi, F., Snee, T. J., Hare, J. A. and Zaldívar, J. M., 2004c, A comparative analysis between temperature and pressure measurements for early detection of runaway initiation. J. Loss Prev. Process Ind., 17, 389-395.

Burden, R. L., and Faires, J. D. 1996, Numerical analysis, 3rd ed. Boston, PWS.

Krause, P. C., Wasynczuk, O., & Sudhoff, S. D. (2002). *Analysis of Electric Machinery and Drive Systems* (2nd Edition ed.). Wiley-IEEE Press.

Kundur, P. (1994). *Power system stability and control.* McGraw-Hill.

Marconato, R. (2002). *Electric Power Systems.* CEI.

Packard, N., Crutchfield, J., Farmer, D. and Shaw, R., 1980, Geometry from a time series. Phys. Rev. Lett., 45: 712-715.

Stagg, G. W., & El-Abiad, A. H. (1983). *Computer methods in power system analysis.*

Strozzi, F., Zaldívar, J. M., Kronberg A. and Westerterp, K. R., 1999, On-line runaway prevention in chemical reactors using chaos theory techniques. AIChE J., 45: 2394-2408.

Takens, F., 1981, in Dynamical Systems and Turbulence, Warwick 1980, vol 898 of Lecture Notes in Mathematics, edited by A. Rand and L.S. Young, Springer, Berlin, pp 366-381.

Zaldívar, J. M., Bosch, J., Strozzi, F., and Zbilut, J. P., 2005, Early warning detection of runaway initiation using non-linear approaches. Commun. Nonlinear Sci. Numer. Sim., 10: 299-311.

Zaldívar, J.M., Strozzi, F. and Bosch, J., 2005b.The divergence as a goal function for control and on-line optimization. AIChE J., 51: 678-681.

Zbilut, J.P., Zaldívar, J.M. and Strozzi, F., 2002, Recurrence quantification based-Liapunov exponents for monitoring divergence in experimental data, Phys. Lett. A 297: 173-181.